Supporting information

Boosting PDT with DPA-NI-Bu: High Photocytotoxicity through Redox Homeostasis Perturbation

Jingwen Tu [a], Zhiyuan Wang [a], Mengzhao Zhang [a], Suntao Shi [a], Miao Zhong [a], Zhengyu Ma [a], Haijuan Zhang [a], Jiang Wu [b], Zhongtian Bai [c], Baoxin Zhang [a, *]

[a] State Key Laboratory of Applied Organic Chemistry and College of Chemistry and Chemical Engineering, Lanzhou University, Lanzhou 730000, China

[b] Key Laboratory for Tibet Plateau Phytochemistry of Qinghai Province, College of Pharmacy, Qinghai Minzu University, Xining 810007, Qinghai, P. R. China

[c] Key Laboratory of Biotherapy and Regenerative Medicine, The First Hospital of Lanzhou University, Lanzhou 730000, China.

***Corresponding Authors**

Baoxin Zhang, E-mail: zhangbx@lzu.edu.cn

Contents:

1. Detailed experimental procedures of spectral measurement and biological activity measurements

1.1 Spectral data

DPA-NI-Me. Yield: 39%. ^{1}H NMR (600 MHz, DMSO) δ 8.48 (d, *J* = 8.0 Hz, 1H), 8.44 (d, *J* = 7.2 Hz, 1H), 8.17 (d, *J* = 8.5 Hz, 1H), 7.67 (t, *J* = 7.9 Hz, 1H), 7.44 (d, *J* = 8.0 Hz, 1H), 7.31 (t, *J* = 7.7 Hz, 4H), 7.09 (t, *J* = 7.4 Hz, 2H), 6.99 (d, *J* = 7.9 Hz, 4H), 3.40 (s, 3H); ^{13}C NMR (151 MHz, DMSO) δ 163.62, 163.11, 149.96, 147.92, 131.83, 130.66, 130.47, 129.74, 129.52, 127.64, 126.79, 125.77, 123.51, 123.29, 122.93, 118.63, 26.63; ESI-MS: m/z calcd for $C_{25}H_{18}N_2O_2^+$ 379.1441, found 379.1409; HPLC purity: 96.71% (CH_3CN:H_2O = 90/10, flow rate: 0.4 mL/min, Rt = 9.351 min).

DPA-NI-Et. Yield: 39%. ^{1}H NMR (600 MHz, DMSO) δ 8.46 (d, *J* = 8.0 Hz, 1H), 8.42 (d, *J* = 6.1 Hz, 1H), 8.15 (d, *J* = 7.4 Hz, 1H), 7.67 – 7.63 (m, 1H), 7.42 (d, *J* = 8.0 Hz, 1H), 7.32 – 7.27 (m, 4H), 7.07 (t, *J* = 7.4 Hz, 2H), 6.98 (d, *J* = 7.3 Hz, 4H), 4.07 (q, *J* = 7.0 Hz, 2H), 1.20 (t, *J* = 7.0 Hz, 3H); ^{13}C NMR (151 MHz, DMSO) δ 163.12, 162.61, 150.03, 147.92, 131.91, 130.74, 130.52, 129.74, 129.61, 127.64, 126.81, 125.79, 123.53, 123.31, 122.92, 118.61, 34.65, 13.13; MS: m/z calcd for $C_{26}H_{20}N_2O_2^+$ 393.15975, found 393.1567; HPLC purity: 96.55% (CH_3CN:H_2O = 90/10, flow rate: 0.4 mL/min, Rt = 11.141 min).

DPA-NI-Pro. Yield: 41%. ^{1}H NMR (600 MHz, DMSO) δ 8.46 (d, *J* = 8.0 Hz, 1H), 8.43 (d, *J* = 7.2 Hz, 1H), 8.15 (d, *J* = 8.5 Hz, 1H), 7.66 (t, *J* = 7.9 Hz, 1H), 7.42 (d, *J* = 8.0 Hz, 1H), 7.30 (t, *J* = 7.7 Hz, 4H), 7.08 (t, *J* = 7.4 Hz, 2H), 6.99 (d, *J* = 8.0 Hz, 4H), 4.02 – 3.98 (m, 2H), 1.65 (q, *J* = 7.4 Hz, 2H), 0.92 (t, *J* = 7.5 Hz, 3H); ^{13}C NMR (151 MHz, DMSO) δ 163.34, 162.83, 149.99, 147.89, 131.92, 130.76, 130.49, 129.71, 129.61, 127.63, 126.78, 125.78, 123.50, 123.28, 122.85, 118.54, 41.08, 20.84, 11.33; MS: m/z calcd for $C_{27}H_{22}N_2O_2^+$ 407.1754, found 407.1724; HPLC purity: 96.34% (CH_3CN:H_2O = 90/10, flow rate: 0.4 mL/min, Rt = 12.785 min).

Ph-NI-Me. Yield: 53%. ^{1}H NMR (600 MHz, DMSO) δ 9.39 (s, 1H), 8.82 (d, *J* = 7.4 Hz, 1H), 8.50 (d, *J* = 6.2 Hz, 1H), 8.27 (d, *J* = 8.4 Hz, 1H), 7.81 – 7.77 (m, 1H), 7.48 – 7.42 (m, 2H), 7.40 (d, *J* = 7.1 Hz, 2H), 7.24 (d, *J* = 8.5 Hz, 1H), 7.19 (t, *J* = 7.3 Hz, 1H), 3.37 (s, 3H);

^{13}C NMR (151 MHz, DMSO) δ 163.98, 163.14, 147.92, 140.36, 133.38, 130.97, 129.58, 129.41, 129.00, 125.12, 124.25, 122.74, 122.07, 121.62, 111.11, 107.70, 26.48; MS: m/z calcd for $C_{19}H_{14}N_2O_2^+$ 303.1128, found 303.1109; HPLC purity: 95.35% (CH_3CN:H_2O = 90/10, flow rate: 0.4 mL/min, Rt = 6.464 min).

Ph-NI-Et. Yield: 57%. ^{1}H NMR (600 MHz, DMSO) δ 9.38 (s, 1H), 8.82 (d, *J* = 8.5 Hz, 1H), 8.50 (d, *J* = 6.2 Hz, 1H), 8.27 (d, *J* = 8.4 Hz, 1H), 7.81 – 7.76 (m, 1H), 7.48 – 7.43 (m, 2H), 7.40 (d, *J* = 7.2 Hz, 2H), 7.24 (d, *J* = 8.5 Hz, 1H), 7.19 (t, *J* = 7.3 Hz, 1H), 4.06 (q, *J* = 7.0 Hz, 2H), 1.19 (t, *J* = 7.1 Hz, 3H); ^{13}C NMR (151 MHz, DMSO) δ 163.48, 162.64, 147.91, 140.36, 140.11, 133.41, 131.01, 129.57, 129.48, 129.01, 125.12, 124.24, 122.71, 122.11, 121.61, 111.11, 107.72, 34.41, 13.28; MS: m/z calcd for $C_{20}H_{16}N_2O_2^+$ 317.12845, found 317.1261; HPLC purity: 95.44% (CH_3CN:H_2O = 90/10, flow rate: 0.4 mL/min, Rt = 7.027 min).

Ph-NI-Pro. Yield: 53%. ^{1}H NMR (600 MHz, DMSO) δ 9.37 (s, 1H), 8.80 (d, *J* = 7.5 Hz, 1H), 8.48 (d, *J* = 6.2 Hz, 1H), 8.25 (d, *J* = 8.5 Hz, 1H), 7.79 – 7.75 (m, 1H), 7.47 – 7.43 (m, 2H), 7.39 (d, *J* = 7.1 Hz, 2H), 7.23 (d, *J* = 8.5 Hz, 1H), 7.19 (t, *J* = 7.3 Hz, 1H), 4.00 – 3.95 (m, 2H), 1.63 (h, *J* = 7.5 Hz, 2H), 0.90 (t, *J* = 7.4 Hz, 3H); ^{13}C NMR (151 MHz, DMSO) δ 163.67, 162.84, 147.87, 140.36, 133.42, 131.02, 129.56, 129.47, 128.98, 125.09, 124.22, 122.70, 122.03, 121.58, 111.04, 107.70, 40.86, 20.95, 11.40; MS: m/z calcd for $C_{21}H_{18}N_2O_2^+$ 331.1441, found 331.1451; HPLC purity: 96.08% (CH_3CN:H_2O = 90/10, flow rate: 0.4 mL/min, Rt = 7.630 min).

Ph-NI-Bu. Yield: 55%. ^{1}H NMR (600 MHz, DMSO) δ 9.37 (s, 1H), 8.80 (d, *J* = 7.4 Hz, 1H), 8.48 (d, *J* = 6.2 Hz, 1H), 8.25 (d, *J* = 8.4 Hz, 1H), 7.80 – 7.75 (m, 1H), 7.48 – 7.42 (m, 2H), 7.40 (d, *J* = 7.2 Hz, 2H), 4.03 – 3.99 (m, 2H), 1.59 (t, *J* = 7.5 Hz, 2H), 1.33 (q, *J* = 7.4 Hz, 2H), 0.92 (t, *J* = 7.4 Hz, 3H); ^{13}C NMR (151 MHz, DMSO) δ 163.65, 162.81, 147.86, 140.36, 133.41, 131.01, 129.55, 129.47, 128.98, 125.09, 124.21, 122.69, 122.04, 121.58, 111.06, 107.71, 29.78, 19.83, 13.75; MS: m/z calcd for $C_{22}H_{20}N_2O_2^+$ 345.15975, found 345.1606; HPLC purity: 95.49% (CH_3CN:H_2O = 90/10, flow rate: 0.4 mL/min, Rt = 8.083 min).

Ph-NI-Ph. Yield: 47%. ^{1}H NMR (600 MHz, DMSO) δ 9.45 (s, 1H), 8.88 (d, *J* = 7.3 Hz, 1H), 8.51 (d, *J* = 6.2 Hz, 1H), 8.28 (d, *J* = 8.5 Hz, 1H), 7.84 (dd, *J* = 8.5, 7.3 Hz, 1H), 7.51

(t, *J* = 7.5 Hz, 2H), 7.46 (q, *J* = 7.8, 7.2 Hz, 3H), 7.42 (d, *J* = 7.1 Hz, 2H), 7.36 – 7.32 (m, 2H), 7.29 (d, *J* = 8.4 Hz, 1H), 7.20 (t, *J* = 7.3 Hz, 1H); ^{13}C NMR (151 MHz, DMSO) δ 163.94, 163.10, 148.02, 140.37, 136.39, 133.51, 131.16, 130.02, 129.68, 129.59, 129.20, 128.78, 127.95, 125.17, 124.26, 123.48, 122.68, 122.57, 121.78, 111.42, 107.82; MS: m/z calcd for $C_{24}H_{16}N_2O_2^+$ 365.12845, found 365.1293; HPLC purity: 97.13% (CH_3CN:H_2O = 90/10, flow rate: 0.4 mL/min, Rt = 6.208 min).

Mor-NI-Me. Yield: 72%. ^{1}H NMR (600 MHz, DMSO) δ 8.50 – 8.43 (m, 2H), 8.39 (d, *J* = 8.0 Hz, 1H), 7.80 (t, *J* = 7.8 Hz, 1H), 7.34 (d, *J* = 8.1 Hz, 1H), 3.91 (t, *J* = 4.5 Hz, 4H), 3.37 (s, 3H), 3.22 (t, *J* = 4.5 Hz, 4H); ^{13}C NMR (151 MHz, DMSO) δ 163.78, 163.27, 155.36, 132.03, 130.52, 130.44, 128.98, 126.06, 125.28, 122.60, 115.92, 115.05, 66.18, 53.02, 26.52; MS: m/z calcd for $C_{17}H_{16}N_2O_3^+$ 297.12337, found 297.1216; HPLC purity: 99.01% (CH_3CN:H_2O = 90/10, flow rate: 0.4 mL/min, Rt = 6.194 min).

Mor-NI-Et. Yield: 74%. ^{1}H NMR (600 MHz, DMSO) δ 8.51 – 8.47 (m, 2H), 8.42 (d, *J* = 8.1 Hz, 1H), 7.83 – 7.79 (m, 1H), 7.36 (d, *J* = 8.1 Hz, 1H), 4.07 (q, *J* = 7.1 Hz, 2H), 3.93 – 3.89 (m, 4H), 3.24 – 3.19 (m, 4H), 1.20 (t, *J* = 7.1 Hz, 3H); ^{13}C NMR (151 MHz, DMSO) δ 163.33, 162.82, 155.44, 132.15, 130.64, 130.54, 129.11, 126.13, 125.30, 122.67, 115.96, 115.10, 66.19, 53.04, 34.56, 13.20; MS: m/z calcd for $C_{18}H_{18}N_2O_3^+$ 311.13902, found 311.1371; HPLC purity: 99.46% (CH_3CN:H_2O = 90/10, flow rate: 0.4 mL/min, Rt = 6.768 min).

Mor-NI-Pro. Yield: 77%. ^{1}H NMR (600 MHz, DMSO) δ 8.50 (t, *J* = 8.0 Hz, 2H), 8.42 (d, *J* = 8.0 Hz, 1H), 7.84 – 7.80 (m, 1H), 7.37 (d, *J* = 8.1 Hz, 1H), 4.02 – 3.98 (m, 2H), 3.91 (t, *J* = 4.5 Hz, 4H), 3.23 (t, *J* = 4.5 Hz, 4H), 1.64 (q, *J* = 7.4 Hz, 2H), 0.91 (t, *J* = 7.4 Hz, 3H); ^{13}C NMR (151 MHz, DMSO) δ 163.55, 163.04, 132.17, 130.66, 130.51, 129.12, 126.11, 125.30, 122.61, 115.88, 115.10, 66.16, 54.87, 53.01, 20.86, 11.32; MS: m/z calcd for $C_{19}H_{20}N_2O_3^+$ 325.15467, found 325.1527; HPLC purity: 99.51% (CH_3CN:H_2O = 90/10, flow rate: 0.4 mL/min, Rt = 7.356 min).

Mor-NI-Bu. Yield: 84%. ^{1}H NMR (600 MHz, DMSO) δ 8.49 (t, *J* = 7.9 Hz, 2H), 8.41 (d, *J* = 8.1 Hz, 1H), 7.84 – 7.79 (m, 1H), 7.36 (d, *J* = 8.1 Hz, 1H), 4.06 – 4.00 (m, 2H), 3.93 – 3.88 (m, 4H), 3.25 – 3.19 (m, 4H), 1.60 (p, *J* = 7.5 Hz, 2H), 1.34 (p, *J* = 7.5 Hz, 2H), 0.92 (t, *J* = 7.4 Hz, 3H); ^{13}C NMR (151 MHz, DMSO) δ 163.51, 163.00, 155.41, 132.15, 130.64,

130.50, 129.10, 126.10, 125.29, 122.61, 115.89, 115.09, 66.16, 53.01, 29.68, 19.76, 13.68; MS: m/z calcd for $C_{20}H_{22}N_2O_3^+$ 339.17032, found 339.1705; HPLC purity: 99.34% (CH_3CN:H_2O = 90/10, flow rate: 0.4 mL/min, Rt = 8.117 min).

Mor-NI-Ph. Yield: 58%. ^{1}H NMR (600 MHz, DMSO) δ 8.56 (d, *J* = 8.4 Hz, 1H), 8.49 (d, *J* = 7.2 Hz, 1H), 8.42 (d, *J* = 8.0 Hz, 1H), 7.85 (t, *J* = 7.8 Hz, 1H), 7.52 (t, *J* = 7.6 Hz, 2H), 7.45 (t, *J* = 7.5 Hz, 1H), 7.40 (d, *J* = 8.1 Hz, 1H), 7.35 (d, *J* = 7.6 Hz, 2H), 3.93 (s, 4H), 3.25 (t, *J* = 4.5 Hz, 4H); ^{13}C NMR (151 MHz, DMSO) δ 163.81, 163.30, 155.59, 136.16, 132.21, 130.74, 130.72, 129.63, 129.15, 128.82, 128.09, 126.16, 125.43, 123.16, 116.36, 115.11, 66.19, 53.07; MS: m/z calcd for $C_{22}H_{18}N_2O_3^+$ 359.13902, found 359.1556; HPLC purity: 99.70% (MeOH:H_2O = 50/50, flow rate: 0.4 mL/min, Rt = 9.280 min).

Pip-NI-Me. Yield: 65%. ^{1}H NMR (400 MHz, $CDCl_3$) δ 8.57 (d, *J* = 8.6 Hz, 1H), 8.51 (d, *J* = 8.0 Hz, 1H), 8.41 (d, *J* = 8.7 Hz, 1H), 7.68 (t, *J* = 7.8 Hz, 1H), 7.20 (d, *J* = 8.0 Hz, 1H), 3.53 (s, 3H), 3.24 (d, *J* = 5.1 Hz, 4H), 3.20 (d, *J* = 4.8 Hz, 4H), 1.77 (s, 1H); ^{13}C NMR (101 MHz, $CDCl_3$) δ 164.93, 164.45, 156.56, 132.72, 131.21, 130.49, 129.93, 126.34, 125.74, 123.28, 116.71, 115.07, 54.57, 46.39, 29.83, 27.02; MS: m/z calcd for $C_{17}H_{17}N_3O_2^+$ 296.13935, found 296.1376; HPLC purity: 99.75% (MeOH:H_2O = 50/50, flow rate: 0.4 mL/min, Rt = 7.457 min).

Pip-NI-Et. Yield: 69%. ^{1}H NMR (600 MHz, DMSO) δ 8.45 (d, *J* = 7.3 Hz, 1H), 8.43 (d, *J* = 8.3 Hz, 1H), 8.38 (d, *J* = 8.0 Hz, 1H), 7.79 (t, *J* = 7.8 Hz, 1H), 7.30 (d, *J* = 8.1 Hz, 1H), 4.06 (q, *J* = 7.1 Hz, 2H), 3.16 (t, *J* = 4.8 Hz, 4H), 3.05 – 3.01 (m, 4H), 1.19 (t, *J* = 7.1 Hz, 3H); ^{13}C NMR (151 MHz, DMSO) δ 163.34, 162.81, 156.15, 132.19, 130.58, 130.56, 129.14, 125.91, 125.31, 122.60, 115.42, 114.94, 53.75, 45.47, 34.53, 13.20; MS: m/z calcd for $C_{18}H_{19}N_3O_2^+$ 310.155, found 310.1529; HPLC purity: 96.07% (MeOH:H_2O = 50/50, flow rate: 0.4 mL/min, Rt = 10.105 min).

Pip-NI-Pro. Yield: 66%. ^{1}H NMR (400 MHz, $CDCl_3$) δ 8.58 (d, *J* = 7.2 Hz, 1H), 8.52 (d, *J* = 8.0 Hz, 1H), 8.41 (d, *J* = 8.4 Hz, 1H), 7.69 (t, *J* = 7.9 Hz, 1H), 7.22 (d, *J* = 8.1 Hz, 1H), 4.17 – 4.09 (m, 2H), 3.25 (s, 4H), 3.22 (s, 4H), 1.95 (s, 1H), 1.75 (q, *J* = 7.5 Hz, 2H), 1.00 (t, *J* = 7.4 Hz, 3H); ^{13}C NMR (101 MHz, $CDCl_3$) δ 164.67, 164.20, 156.31, 132.68, 131.24, 130.31, 130.06, 126.37, 125.83, 123.51, 117.07, 115.16, 54.33, 46.27, 41.94, 29.84, 21.58, 11.68; MS: m/z calcd for $C_{19}H_{21}N_3O_2^+$ 324.17065, found 324.1685; HPLC purity:

99.91% (MeOH:H_2O = 50/50, flow rate: 0.4 mL/min, Rt = 14.930 min).

Pip-NI-Bu. Yield: 73%. ^{1}H NMR (400 MHz, $CDCl_3$) δ 8.57 (d, *J* = 7.3 Hz, 1H), 8.51 (d, *J* = 8.1 Hz, 1H), 8.41 (d, *J* = 8.4 Hz, 1H), 7.68 (t, *J* = 7.9 Hz, 1H), 7.20 (d, *J* = 8.1 Hz, 1H), 4.16 (t, *J* = 7.6 Hz, 2H), 3.23 (s, 4H), 3.20 (s, 4H), 1.77 (s, 1H), 1.70 (t, *J* = 7.8 Hz, 2H), 1.44 (d, *J* = 7.7 Hz, 2H), 0.96 (t, *J* = 7.3 Hz, 3H); ^{13}C NMR (101 MHz, $CDCl_3$) δ 164.65, 164.19, 156.45, 132.67, 131.18, 130.36, 130.04, 126.35, 125.75, 123.48, 116.94, 115.08, 54.57, 46.39, 40.23, 30.41, 29.83, 20.54, 14.25, 14.00; MS: m/z calcd for $C_{20}H_{23}N_3O_2^+$ 338.1863, found 338.1842.; HPLC purity: 99.72% (CH_3CN:H_2O = 90/10, flow rate: 0.4 mL/min, Rt = 9.426 min).

Pip-NI-Ph. Yield: 58%. ^{1}H NMR (600 MHz, DMSO) δ 8.51 (d, *J* = 8.5 Hz, 1H), 8.47 (d, *J* = 7.2 Hz, 1H), 8.40 (d, *J* = 8.0 Hz, 1H), 7.84 (t, *J* = 7.8 Hz, 1H), 7.52 (t, *J* = 7.6 Hz, 2H), 7.45 (t, *J* = 7.4 Hz, 1H), 7.35 (dd, *J* = 7.9, 4.7 Hz, 3H), 3.20 (s, 4H), 3.06 (s, 4H), 1.23 (s, 1H); ^{13}C NMR (151 MHz, DMSO) δ 163.83, 163.30, 156.31, 136.19, 132.28, 130.78, 130.69, 129.68, 129.16, 128.81, 128.07, 125.97, 125.45, 123.10, 115.84, 114.98, 53.73, 45.43; MS: m/z calcd for $C_{22}H_{19}N_3O_2^+$ 358.155, found 358.1573; HPLC purity: 99.13% (CH_3CN:H_2O = 90/10, flow rate: 0.4 mL/min, Rt = 5.859 min).

1.2 Ultraviolet and fluorescence spectroscopy tests measurements

The 19 photosensitizer molecules obtained were dissolved in DMSO to prepare the solution with a concentration of 10 mM, and then diluted to 10 μM in PBS for optical testing. Subsequently, each compound was subjected to 2 mL of diluted PBS solution in a 1 cm quartz cuvette. Spectral data were obtained by fluorescence spectrophotometer and UV-Vis spectrophotometer. The excitation wavelength was set to 428 nm, and the excitation and emission slits were adjusted to 10.0 nm.

1.3 Photophysical measurement

The absolute photoluminescence quantum yield (Φ_F) was determined according to the following equation:

$$\Phi_F = \frac{E_c[(1-A)\cdot E_b]}{L_a \cdot A}, \quad A = 1-\left(\frac{L_c}{L_b}\right)$$

where the E_b denote the total number of photons emitted by the reflected light, the

L_b denote the total number of photons absorbed by the reflected light and A denote the absorption of the sample within the integrating sphere.

1.4 ROS generation measurements

Calculation of relative singlet oxygen quantum yields (Φ_Δ) was performed by following the literature [1]. Relative singlet oxygen quantum yields were calculated and compared to $Ru(bpy)_3$ (Φ_Δ = 0.66 in DMSO). The absorption of DPBF at 414 nm was recorded every 30 seconds to obtain the photosensitizing process' decay rate. Measurements were performed using a blue LED light source (25 $mW.cm^{-2}$). DPBF and photosensitizers were placed in a cuvette containing air-saturated organic solvents, and the solutions were kept in the dark until the absorbance reading was stable, followed by continuous light irradiation. The $^1O_2$ quantum yields of the dyes were calculated according to the following equation:

$$\Phi_{\Delta,\,sam} = \Phi_{\Delta,\,std} \times \frac{k_{sam}}{k_{std}} \times \frac{F_{sam}}{F_{std}}$$

where sam and std for test and reference, respectively. *k* is the slope of the change in absorbance of DPBF at absorbance maxima with the irradiation time. F is the absorption correction factor, which is given as $F = 1\text{-}10^{-OD}$.

1.5 Computational calculation

All quantum-chemical calculations were performed with the Gaussian 09 package (Revision D.01). The ground-state geometry of photosensitizers was fully optimized in the gas phase using density functional theory (DFT) at the B3LYP/6-31G(d) level, without imposing any symmetry constraints. Harmonic vibrational frequency analyses were carried out at the same level to verify that each optimized structure corresponds to a true minimum (i.e., no imaginary frequencies). Vertical excitation energies (singlet and triplet) and oscillator strengths were obtained via time-dependent DFT (TD-DFT) using B3LYP/6-31G(d). For each optimized geometry, 20 excited states (including both singlet-A and triplet-A manifolds) were requested.

1.6 Biological activity measurement

In all biological activity assays, compounds were prepared as stock solutions in DMSO

and diluted for experiments so that the final DMSO concentration did not exceed 1%.

Cell lines and culture conditions [2].

Human cervical cancer (HeLa) and hepatocellular carcinoma (HepG2) cell lines were acquired from the Shanghai Institute of Biochemistry and Cell Biology, Chinese Academy of Sciences. The TrxR1 knockdown cell line (HeLa-sh*TrxR1*) and its negative control (HeLa-sh*NT*) were constructed according to the previous method of our research group, and puromycin (1 μg/mL) was employed for screening target cells. All cell lines mentioned above were cultured in an incubator with DMEM containing 10% FBS and 100 units/mL penicillin-streptomycin antibiotic mixture, incubated under standard cell culture conditions (37 °C, 5% CO_2).

Cell Counting Kit-8 (CCK-8) assay [3].

A certain number of different cells were planted in 96-well plates. After the cells were attached to the plate, various concentrations of compounds were added. The control group treated cells with the maximum introduced amount of DMSO, while the blank group was only treated with DMEM. After dark treatment or light exposure, the basic culture medium containing 10 μL CCK-8 solution was added by medium replacement and continued incubation for 2 h. Finally, the 450 nm absorbance values were conducted utilizing a full-range microplate scanning spectrophotometer, and the cell viability was calculated by [($OD_{\text{experiment group}}$-$OD_{\text{blank group}}$)/($OD_{\text{control group}}$-$OD_{\text{blank group}}$)]×100. When exploring the effects of NAC and BSO on cells, cells were incubated with designated concentrations of BSO and NAC for 24 h before adding compounds to plates, but subsequent processing was unchanged.

Cellular TrxR activity assay [4].

5×10^5 HeLa cells were planted in 60 mm dishes. After the cells were attached to the dish, different concentrations of **DPA-NI-Bu** were added, and the cells were treated with dark or light for the specified time. Cell pellets obtained through centrifugation were processed with two PBS washing steps and lysed in RIPA buffer solution. Following protein concentration determination (2 mg/mL) using Bradford's method, intracellular TrxR activity was determined using the end-point insulin reduction assay.

Determination of cellular total glutathione and GSH/GSSG ration [5].

2×10^6 HeLa cells were planted in 100 mm dishes. After the cells were attached to the dish, different concentrations of **DPA-NI-Bu** were added, and the cells were treated with dark or light for the specified time. After washing and counting, the cells were collected and resuspended with 1 mL PBS. 300 μL of cell suspension was taken as the total GSH group and 600 μL as the GSGG group. Subsequently, the supernatant was discarded and subjected to lysis using a phosphate-based buffer system containing 0.5% sulfosalicylic acid. The intracellular GSH and GSSG contents of different treatments were finally determined using the enzyme recycling method, and the GSH/GSSG ratio was calculated.

Determination of cellular caspase 3 activity [6].

5×10^5 HeLa cells were planted in 60 mm dishes. After the cells were attached to the dish, different concentrations of **DPA-NI-Bu** were added, and the cells were treated with dark or light for the specified time. T Cell pellets obtained through centrifugation were processed with two PBS washing steps and lysed in RIPA buffer solution. Sample protein concentrations were standardized to 4 mg/mL using the Bradford method. Subsequently, caspase-3 activity was measured by incubating 10 μL of cell extract with 90 μL of assay buffer containing 0.2 mM Ac-DEVD-pNA tetrapeptide substrate at 37 °C for one hour.

Cell proliferation assay [7].

2×10^3 HeLa cells were planted in 6 well plates. After the cells were attached to the dish, different concentrations of **DPA-NI-Bu** were added, and the cells were treated with dark or light for the specified time. Then, the complete medium was added by replacement and continued for 9 days, when a white cell mass could be seen at the bottom of the 6-well plate. Subsequently, the medium was aspirated and rinsed with PBS, and the cells were fixed with 1 mL of 70% ethanol for 1 h. Then, the PBS buffer containing 0.5% crystal violet was absorbed into the plate to dye cells for 2 h. Finally, the plates were dried at room temperature after rinsing with PBS and photographed.

Electron paramagnetic resonance (EPR) measurements for detection of ROS [8].

EPR spectroscopy was utilized to validate the generation of $O_2^{\bullet-}$ and $^1O_2$. DMPO (5,5-dimethyl-1-pyrroline N-oxide) was used as a spin-trapping reagent for $O_2^{\bullet-}$, while

TEMP (4-amino-2,2,6,6-tetramethylpiperidine) served as a spin-trapping reagent for $^1O_2$. EPR signals were measured in two groups of samples. In the first group, **DPA-NI-Bu** (50 mM) was dispersed in 3 mL of methanol containing 25 mM of DMPO or 3 mL of water containing 25 mM of TEMP, and the samples were incubated in the dark. In the second group, the same mixtures were irradiated with blue light (472 nm) at an intensity of 25 mM/cm^2. Subsequently, the EPR signals were recorded using the Bruker E500 instrument.

1.7 Statistics

Statistical analysis was performed using Origin version 2018. The data for each experiment were obtained by three parallel experiments and expressed as mean±SE. Comparative statistical analysis between the dark and light groups was performed using Student's *t*-test analysis. The threshold for statistical significance was established at $P < 0.05$.

2. Experiment results

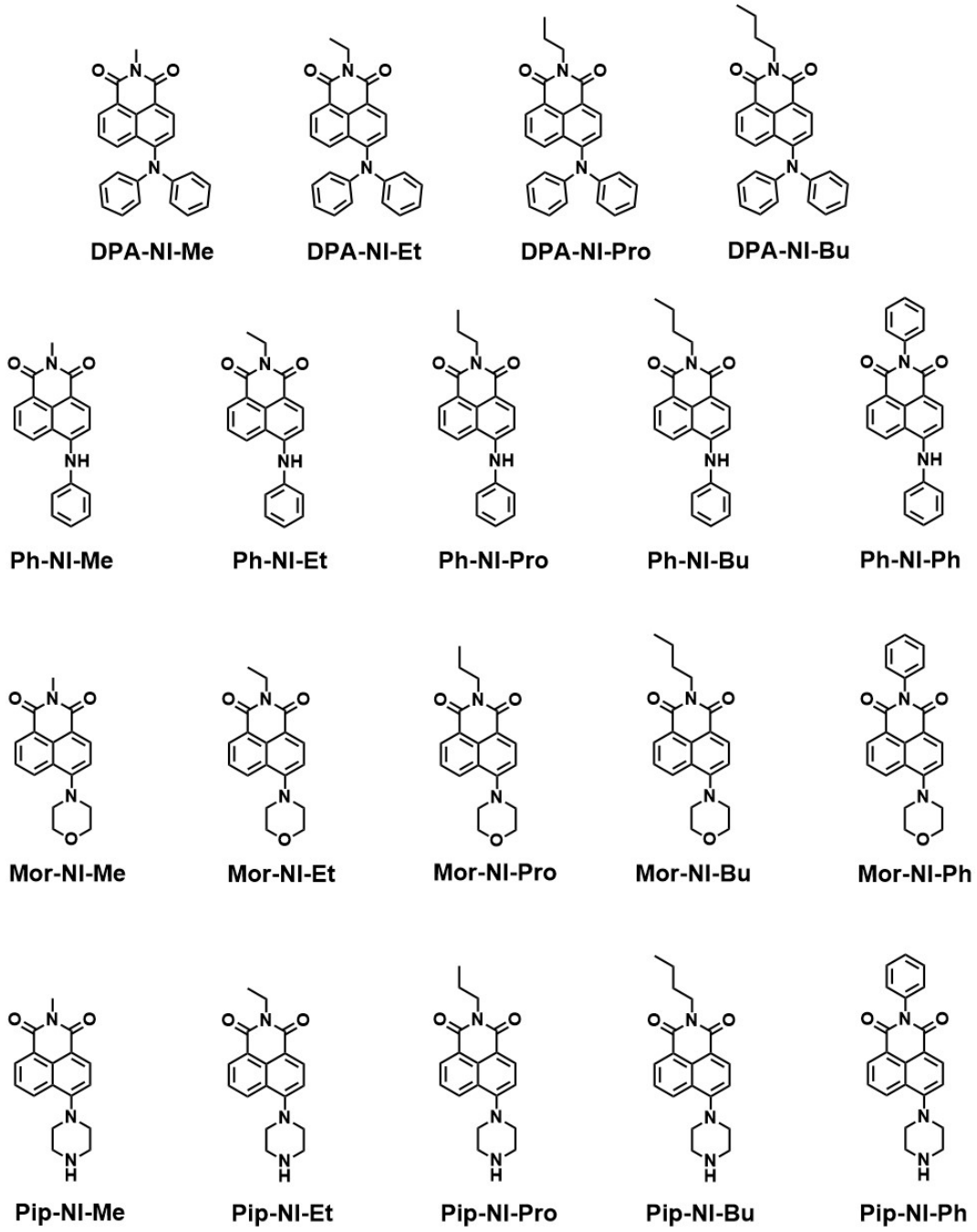

Figure S1. Chemical structure of naphthalimide photosensitizers.

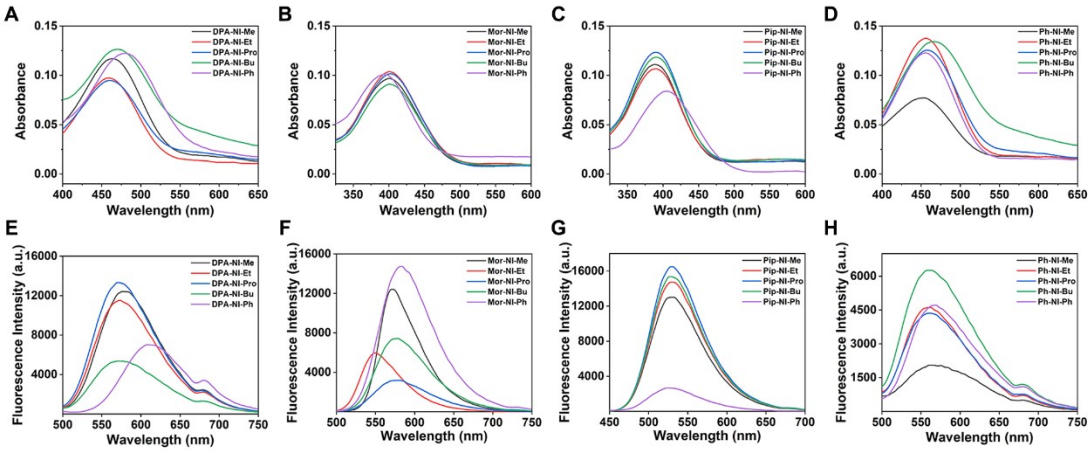

Figure S2. Response of naphthalimide photosensitizers in PBS (10 mM, pH 7.4) at 37℃. Absorbance spectra of naphthalimide photosensitizers (10 μM) (A-D). Emission spectra (λ_{ex} = 470, 426, 422 or 470 nm) of naphthalimide photosensitizers (10 μM) (E-H).

A

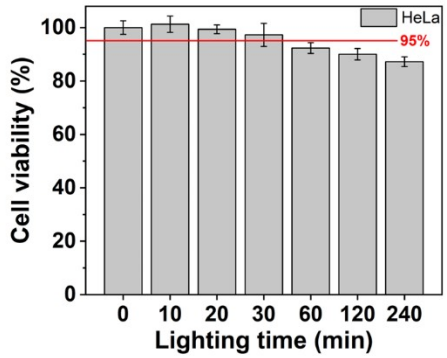

B

Compd.	IC_{50} (μM) HeLa		
	Dark[a]	Light[b]	Phototoxicity Index[c]
DPA-NI-Bu	>100	10.18 (10 min)	>9.82
		4.99 (20 min)	>20.04
		1.70 (30 min)	>58.82
		0.76 (60 min)	>131.58
		0. 14 (120 min)	>714.29
		0.11 (240 min)	>909.09

Figure S3. (A) Cell viability of HeLa cells under light irradiation without photosensitizers at different exposure times. (B) Cytotoxicity of **DPA-NI-Bu** under light irradiation at different exposure times.

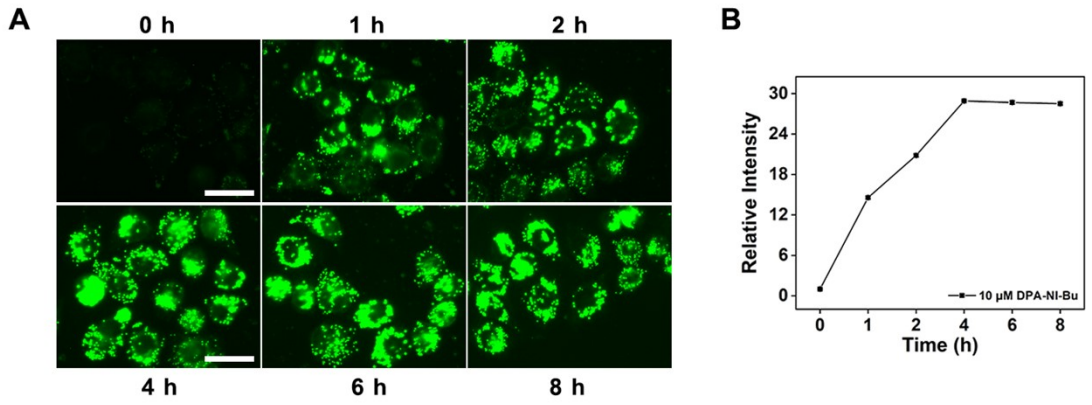

Figure S4. The concentration of **DPA-NI-Bu** in HeLa cells following treatment with 10 μM **DPA-NI-Bu** for different times was assessed using a fluorescence microscopy (A). The analysis of fluorescence intensity in single cells was conducted with Image J, as shown in (B). Data were expressed as mean±SE from triplicates. Scale bar: 25 μm.

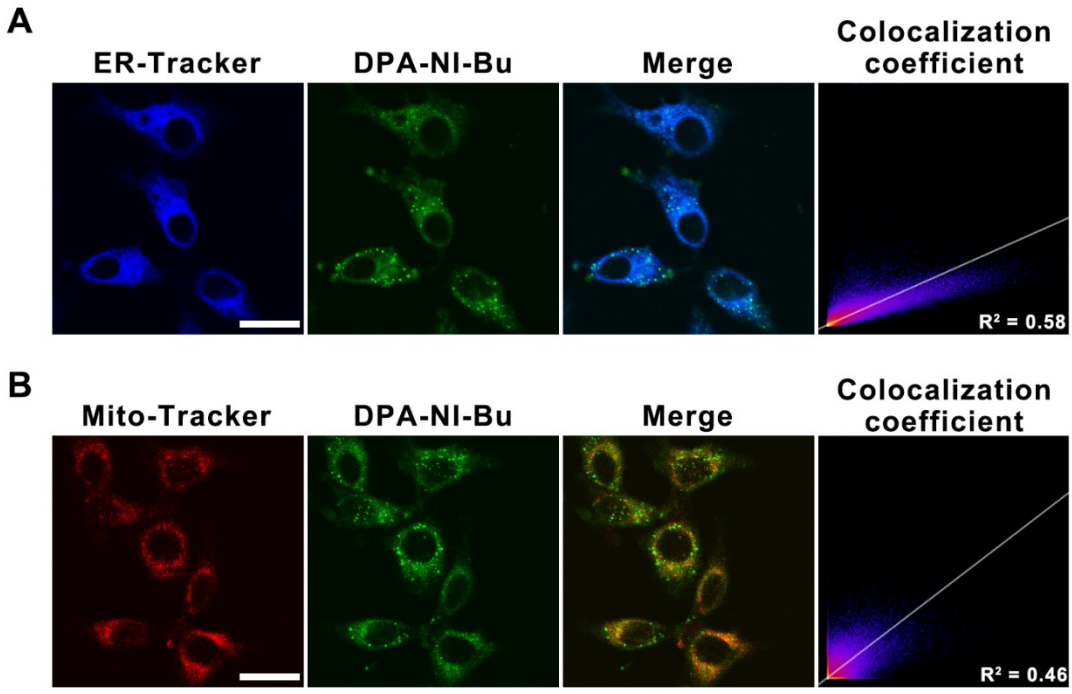

Figure S5. Confocal microscopy imaging of HeLa cells employed with DPA-NI-Bu (10 μM, 4 h, λ_{ex} = 472 nm, λ_{em} = 530-650 nm) and its co-localization with Mito-Tracker (150 nM, λ_{ex} = 644 nm, λ_{em} = 650-750 nm) (A) and ER-Tracker (150 nM, λ_{ex} = 374 nm, λ_{em} = 430-640 nm) (B). The colocalization coefficient graph indicates Pearson's coefficient. Scale bar: 25 μm.

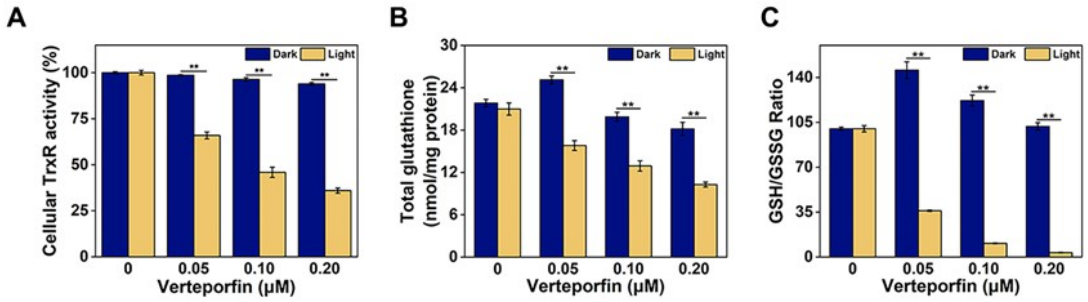

Figure S6. Disruption of redox homeostasis induced by Verteporfin. (A) Cellular TrxR activity in HeLa cells following treatment with Verteporfin was assessed by the method of the insulin endpoint. The intracellular GSH levels (B) and the GSH/GSSG ratio (C) in HeLa cells after treatment with Verteporfin was detected by the enzymatic assay. Cells were incubated in continuous darkness for 10.5 h, or under a combined regimen of 4 h in the dark, 0.5 h of light exposure, and a further 6 h in the dark. Data were expressed as mean ± SE from triplicates. **, $P < 0.01$, the light groups vs. the dark groups in (A) (B) (C).

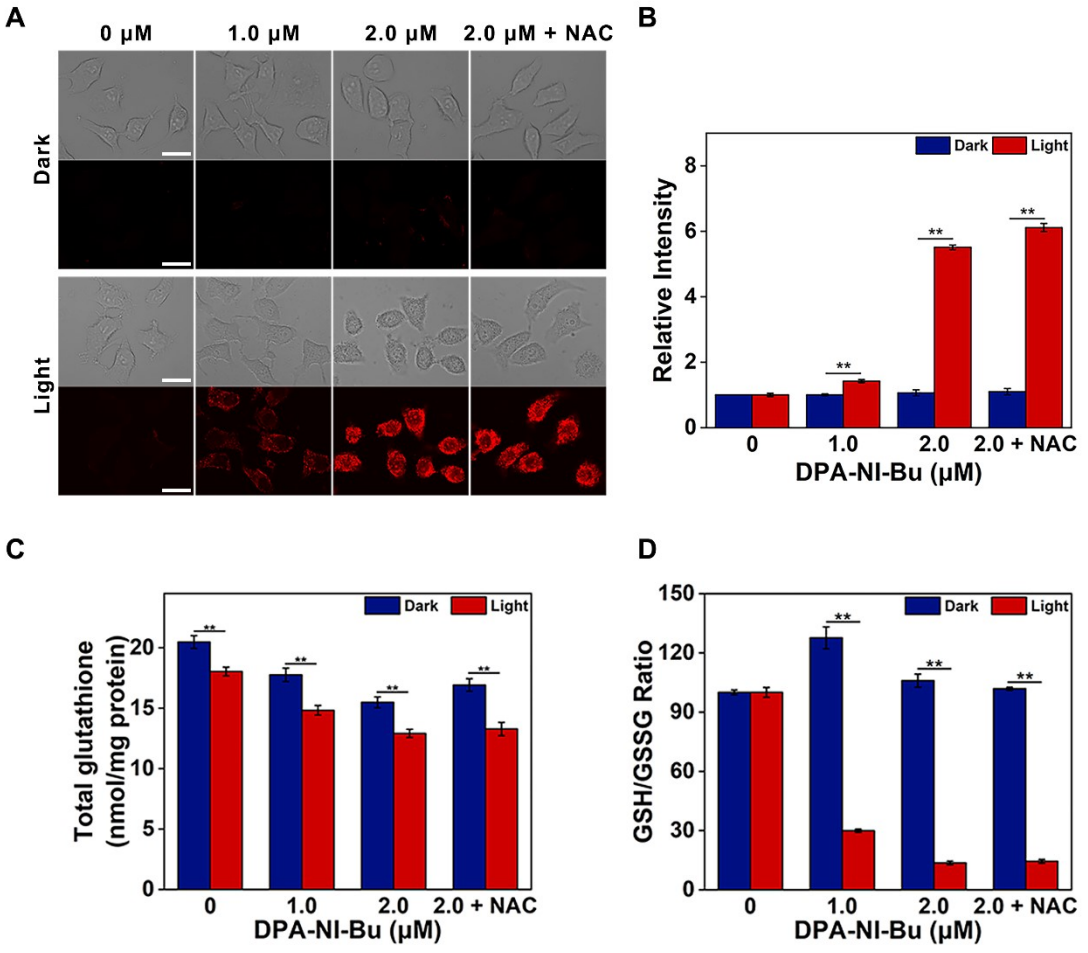

Figure S7. (A) Cellular ROS accumulation was assessed using DHE after **DPA-NI-Bu** treatment (pretreated with NAC for 12 h or not, and continuous dark incubation for 4.5 h or combined treatment involving 4 h of dark exposure followed by 0.5 h of light exposure) towards HeLa cells. Single-cell fluorescence quantification was performed using Image J, as shown in (B). The intracellular GSH levels (A) and the GSH/GSSG ratio (B) in HeLa cells after treatment with **DPA-NI-Bu** (pretreated with NAC for 12 h or not, and continuous dark incubation for 10.5 h or combined treatment involving 4 h of dark exposure followed by 0.5 h of light exposure and another 6 h of dark exposure) was detected by the enzymatic assay. Data were expressed as mean ± SE from triplicates. **, $P < 0.01$, the light groups vs. the dark groups in (B) (C) (D). Scale bar: 25 μm.

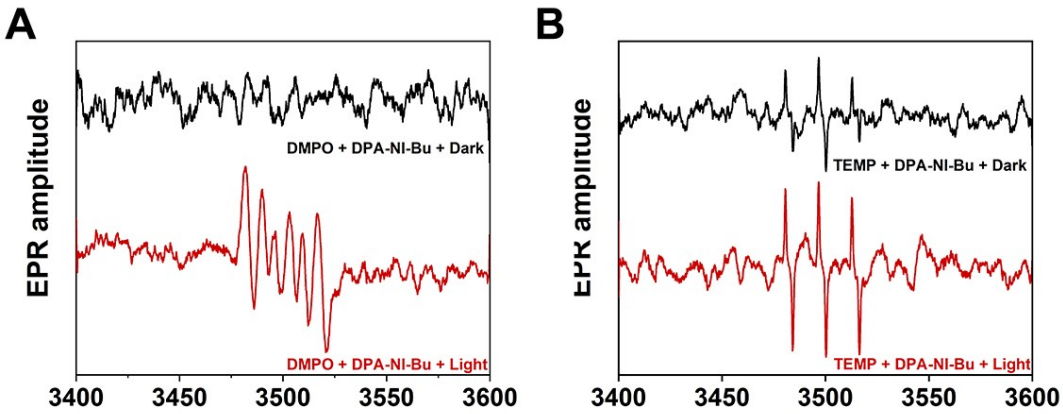

Figure S8. EPR spectroscopy of DMPO for $O_2^{\bullet -}$ characterization (A) and TEMP for $^1O_2$ detection (B) in the presence of **DPA-NI-Bu** (50 mM) with or without light irradiation.

Table S1. Cytotoxicity of DPA-NI-Bu and Verteporfin under light or dark conditions.

	IC_{50} (μM)

Compd.	HeLa			HepG2		
	Dark [a]	Light [b]	Phototoxicity Index [c]	Dark	Light [b]	Phototoxicity Index [c]
DPA-NI-Bu	>100	1.68 ± 0.18	>59.5	>100	1.87 ± 0.24	>53.5
Verteporfin	>100	0.09 ± 0.03	>1111.1	>100	0.11 ± 0.02	>909.1

[a]The data was obtained by the CCK-8 assay after incubating with photosensitizers for 24 h. [b]Cells were incubated with the indicated photosensitizers for 4 h in the dark, activated with a 470 nm light source for 0.5 h, and then incubated in the dark for 19.5 h. Cell viability was measured by the CCK-8 assay after all processing. [c]Phototoxicity Index = $IC_{50,\ dark}/IC_{50,\ light}$. Data were expressed as mean ± SE from triplicates.

Table S2. Calculated electronic transition with significant oscillator strengths (*f*) of **DPA-NI-R**.

	DPA-NI-Me	**DPA-NI-Et**	**DPA-NI-Pro**	**DPA-NI-Bu**
S_1	2.5728 eV f = 0.1837	2.6337 eV f=0.2034	2.6008 eV f = 0.2027	2.6070 eV f = 0.2068
S_2	3.7627 eV f = 0.1047	3.7827 eV f=0.1029	3.7655 eV f = 0.1115	3.7673 eV f = 0.1130
S_3	4.1842 eV f = 0.1644	4.2127 eV f=0.1816	4.1957 eV f = 0.1715	4.1997 eV f = 0.1775
S_4	4.5300 eV f = 0.1022	4.2518 eV f=0.1241	4.2369 eV f = 0.0885	4.2365 eV f = 0.0955
T_1	1.9792 eV	1.9964 eV	1.9834 eV	1.9852 eV
T_2	2.7580 eV	2.8044 eV	2.7775 eV	2.7827 eV
T_3	3.2730 eV	3.2865 eV	3.2779 eV	3.2791 eV
T_4	3.3127 eV	3.3528 eV	3.3119 eV	3.3116 eV
T_5	3.3702 eV	3.3940 eV	3.3557 eV	3.3548 eV
T_6	3.5333 eV	3.5454 eV	3.5261 eV	3.5261 eV

Table S3. Calculated electronic transition with significant oscillator strengths (*f*) of **Ph-**

NI-R.

	Ph-NI-Me	Ph-NI-Et	Ph-NI-Pro	Ph-NI-Bu	Ph-NI-Ph
S_1	2.9728 eV	2.9018 eV	2.8977 eV	2.8970 eV	2.8970 eV
	f = 0.2112	f = 0.2298	f = 0.2309	f = 0.2356	f = 0.2545
S_2	3.8344 eV	3.8122 eV	3.8062 eV	3.8080 eV	3.3165 eV
	f = 0.0923	f = 0.0920	f = 0.0977	f = 0.0987	f = 0.0108
S_3	4.5408 eV	4.4762 eV	4.4742 eV	4.4737 eV	3.8177 eV
	f = 0.1956	f = 0.2260	f = 0.2349	f = 0.2396	f = 0.0945
S_4	5.5633 eV	5.6261 eV	5.6267 eV	5.6269 eV	4.3088 eV
	f = 0.2001	f = 0.1295	f = 0.1328	f = 0.1319	f = 0.2697
T_1	2.1291 eV	2.0770 eV	2.0780 eV	2.0771 eV	2.0722 eV
T_2	2.9859 eV	2.9403 eV	2.9347 eV	2.9356 eV	2.9395 eV
T_3	3.4148 eV	3.3361 eV	3.3342 eV	3.3335 eV	3.0738 eV
T_4	3.4886 eV	3.4174 eV	3.4051 eV	3.4022 eV	3.3839 eV
T_5	3.6333 eV	3.5903 eV	3.5843 eV	3.5832 eV	3.4865 eV
T_6	3.8503 eV	3.6441 eV	3.6427 eV	3.6428 eV	3.5376 eV

Table S4. Calculated electronic transition with significant oscillator strengths (*f*) of **Mor-NI-R**.

	Mor-NI-Me	Mor-NI-Et	Mor-NI-Pro	Mor-NI-Bu	Mor-NI-Ph
S_1	3.0390 eV	3.0317 eV	3.0322 eV	3.0304 eV	3.0175 eV
	f = 0.2304	f = 0.2361	f = 0.2410	f = 0.2426	f = 0.2549
S_2	4.0732 eV	3.6379 eV	3.6351 eV	3.6330 eV	3.3464 eV
	f = 0.0270	f = 0.0004	f = 0.0004	f = 0.0004	f = 0.0100
S_3	4.5648 eV	3.9870 eV	3.9790 eV	3.9758 eV	3.6313 eV
	f = 0.1496	f = 0.0016	f = 0.0027	f = 0.0039	f = 0.0006
S_4	4.7494 eV	4.0387 eV	4.0369 eV	4.0338 eV	3.7382 eV
	f = 0.1682	f = 0.0166	f = 0.0172	f = 0.0190	f = 0.0023
T_1	2.0641 eV	2.0605 eV	2.0623 eV	2.0647 eV	2.0569 eV
T_2	3.1465 eV	3.1458 eV	3.1451 eV	3.1394 eV	3.0969 eV
T_3	3.3637 eV	3.3616 eV	3.3592 eV	3.3571 eV	3.1340 eV
T_4	3.4850 eV	3.4534 eV	3.4399 eV	3.4335 eV	3.4186 eV
T_5	3.6594 eV	3.6425 eV	3.6371 eV	3.6343 eV	3.5189 eV
T_6	3.7723 eV	3.7696 eV	3.7727 eV	3.7810 eV	3.5934 eV

Table S5. Calculated electronic transition with significant oscillator strengths (*f*) of **Pip-NI-R**.

	Pip-NI-Me	Pip-NI-Et	Pip-NI-Pro	Pip-NI-Bu	Pip-NI-Ph
S_1	3.0085 eV f = 0.2297	3.0564 eV f = 0.2366	3.1043 eV f = 0.2435	3.1522 eV f = 0.2504	3.1351 eV f = 0.2626
S_2	3.6574 eV f = 0.0003	3.6501 eV f = 0.00027	3.6428 eV f = 0.00023	3.6355 eV f = 0.0002	3.3562 eV f = 0.0143
S_3	3.8675 eV f = 0.0155	3.8237 eV f = 0.0122	3.7799 eV f = 0.0089	3.7362 eV f = 0.0056	3.6408 eV f = 0.0005
S_4	4.0069 eV f = 0.0006	4.0005 eV f = 0.0013	3.9941 eV f = 0.0020	3.9877 eV f = 0.0027	3.7283 eV f = 0.0037
T_1	2.0464 eV	2.0769 eV	2.1074 eV	2.1380 eV	2.1276 eV
T_2	3.1487 eV	3.1679 eV	3.1871 eV	3.2062 eV	3.1050 eV
T_3	3.3830 eV	3.3740 eV	3.3650 eV	3.3560 eV	3.1939 eV
T_4	3.4893 eV	3.4693 eV	3.4493 eV	3.4294 eV	3.4207 eV
T_5	3.6615 eV	3.6471 eV	3.6327 eV	3.6182 eV	3.5207 eV
T_6	3.7488 eV	3.7400 eV	3.7312 eV	3.7224 eV	3.5657 eV

3. ^{1}H NMR, ^{13}C NMR spectra, MS analysis and HPLC analysis

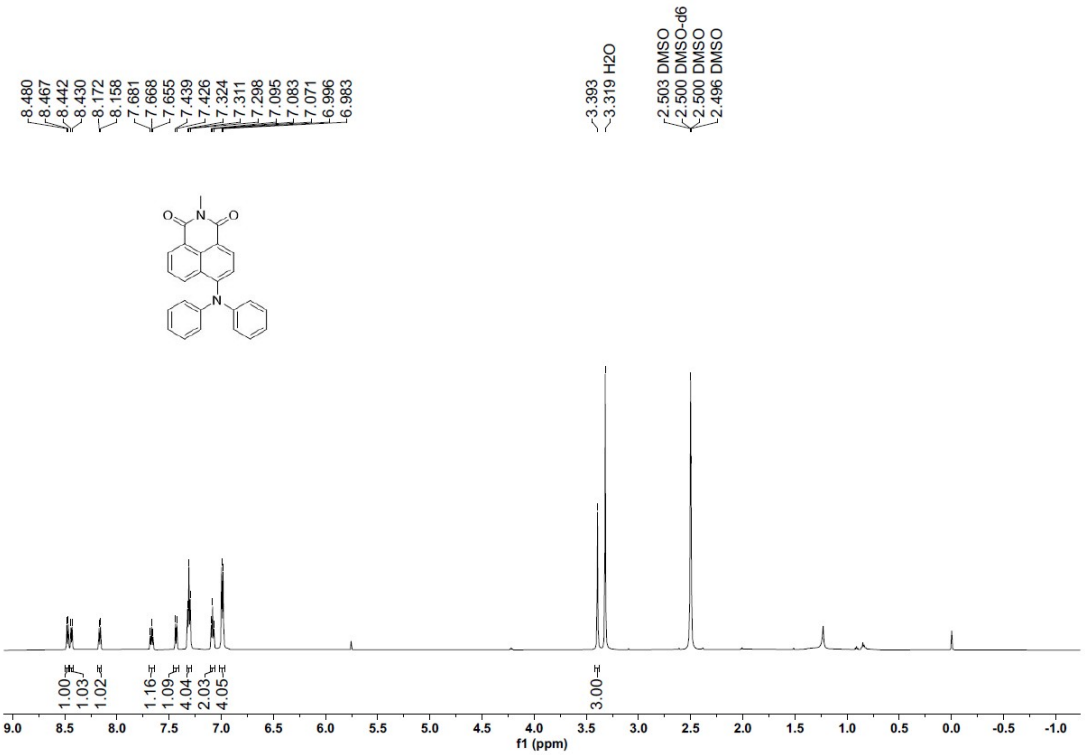

Figure S9. ^{1}H NMR Spectra of **DPA-NI-Me** (600 MHz).

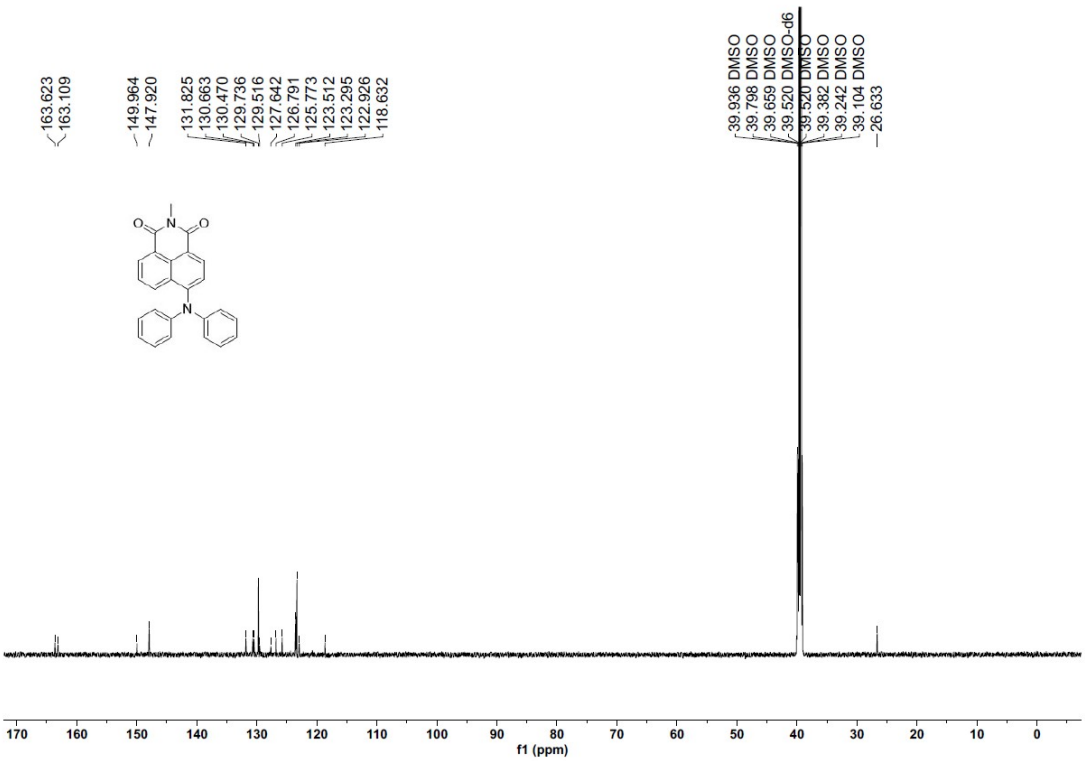

Figure S10. ^{13}C NMR Spectra of **DPA-NI-Me** (151 MHz).

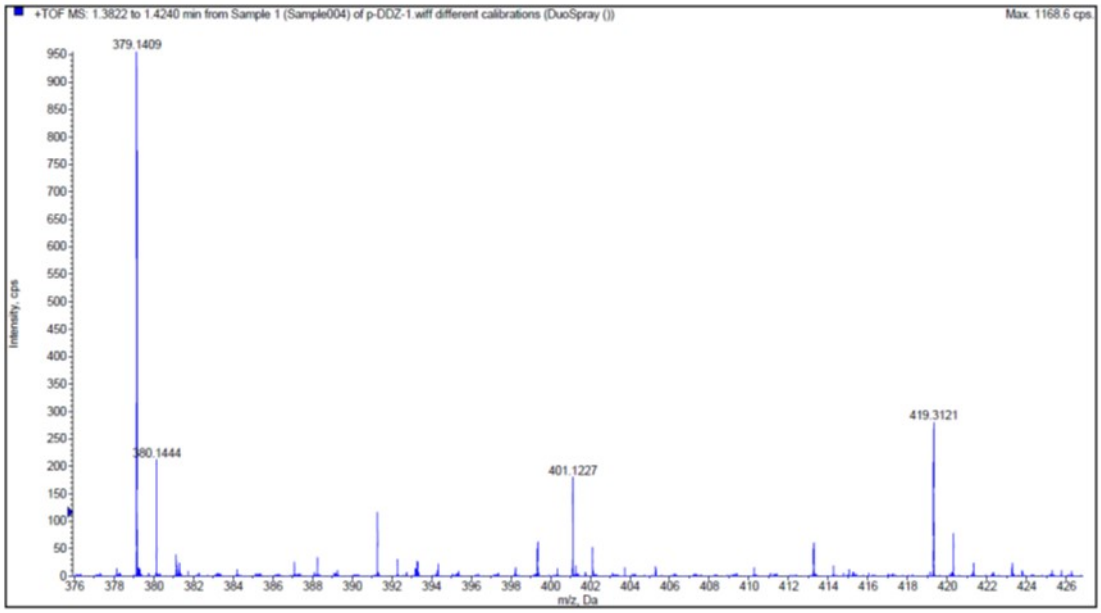

Figure S11. MS spectra of **DPA-NI-Me**.

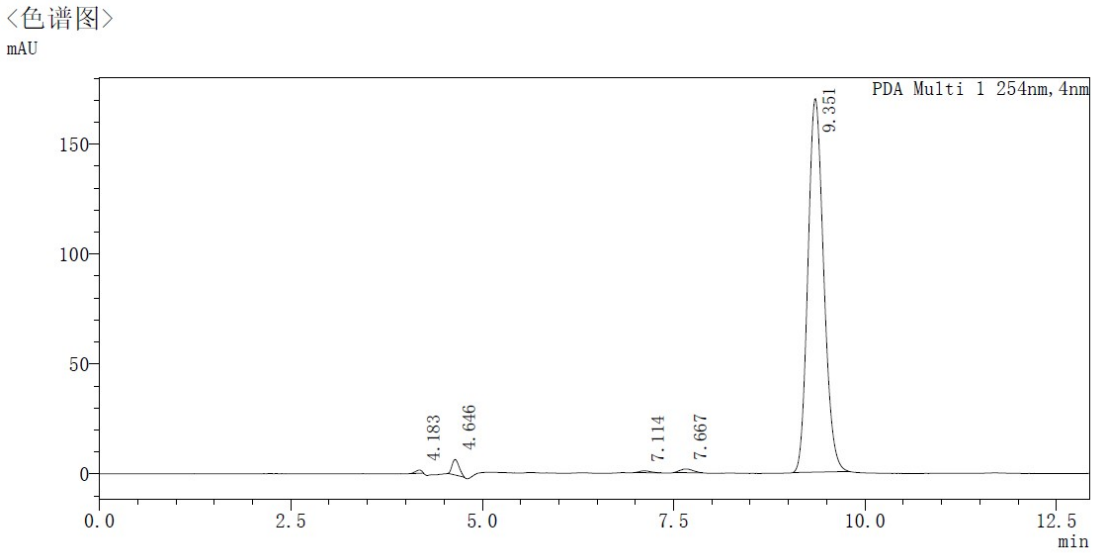

峰表

PDA Ch1 254nm

峰号	保留时间	面积	面积%
1	4.183	8539	0.339
2	4.646	44873	1.782
3	7.114	8956	0.356
4	7.667	20559	0.817
5	9.351	2434643	96.706
总计		2517569	100.000

Figure S12. HPLC analysis of **DPA-NI-Me**.

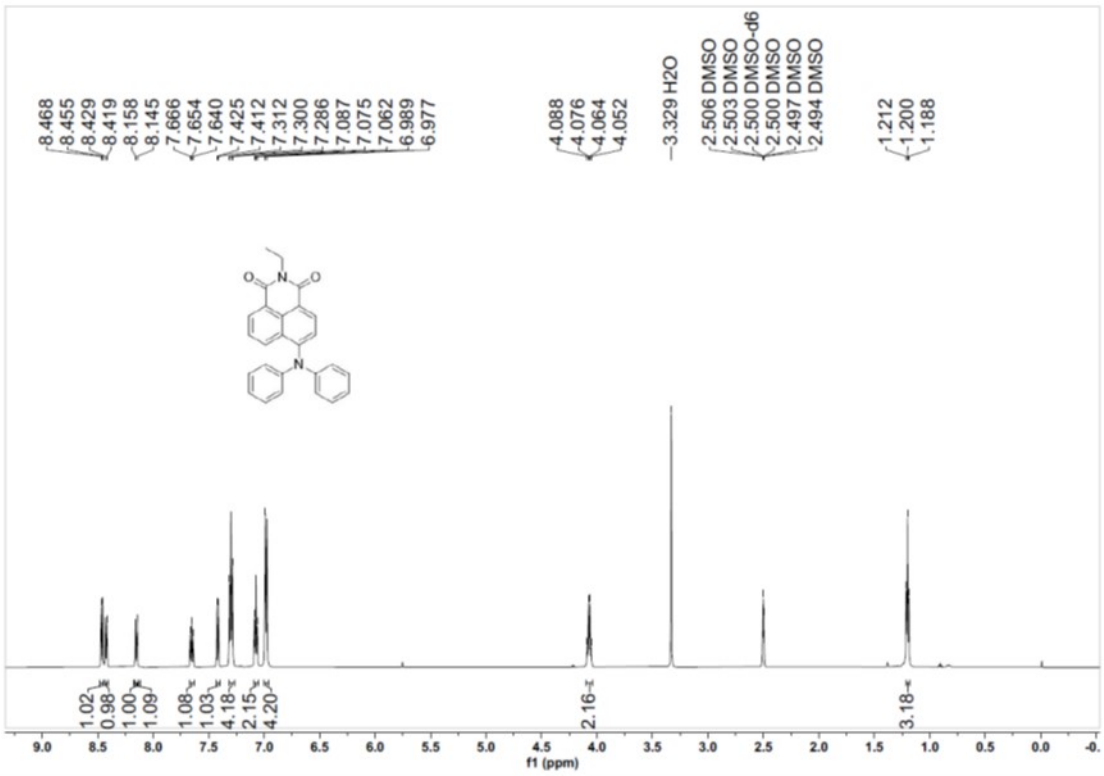

Figure S13. ^{1}H NMR Spectra of **DPA-NI-Et** (600 MHz)

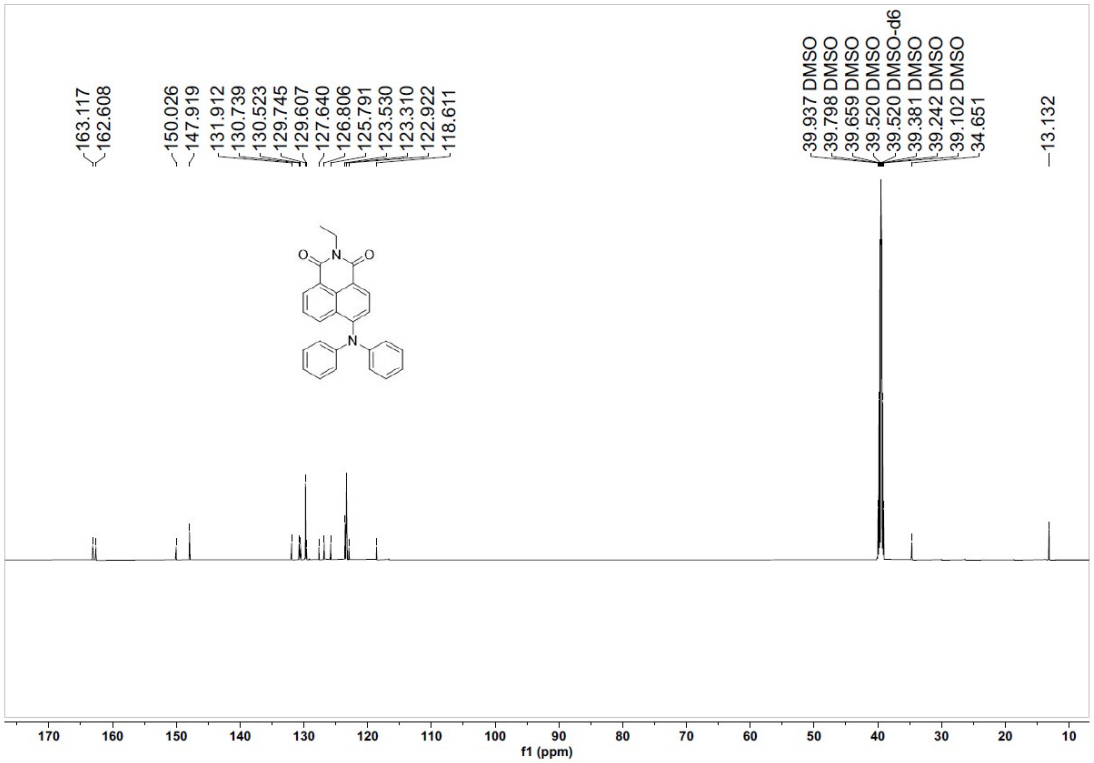

Figure S14. ^{13}C NMR Spectra of **DPA-NI-Et** (151 MHz).

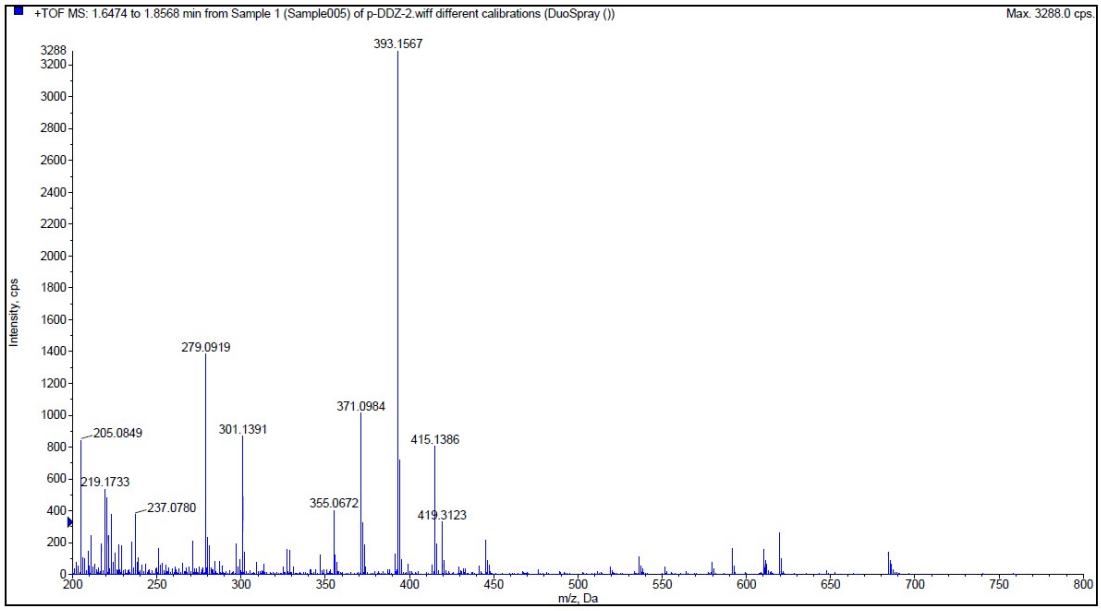

Figure S15. MS spectra of **DPA-NI-Et**.

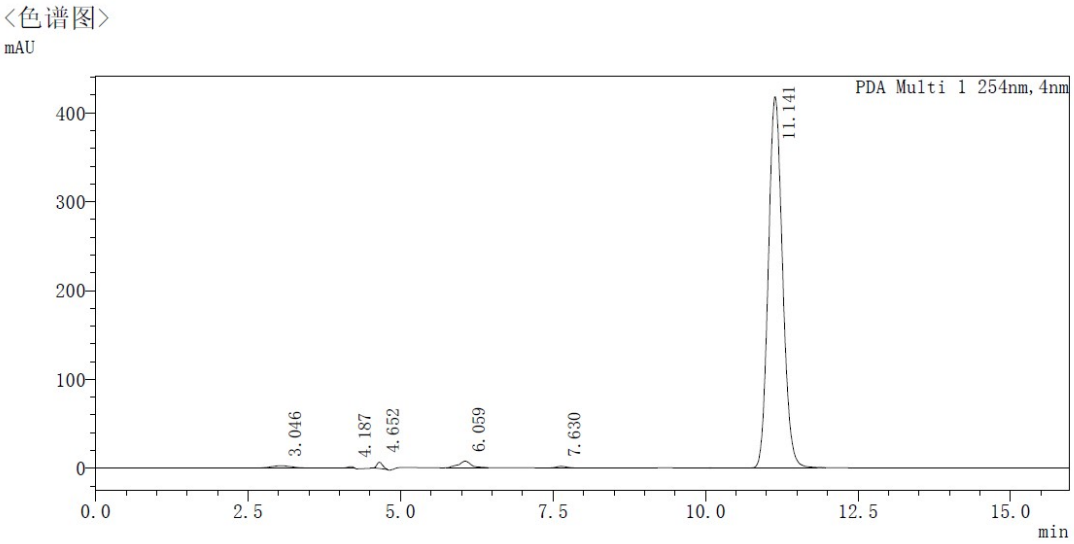

峰表

PDA Ch1 254nm

峰号	保留时间	面积	面积%
1	3.046	56650	0.806
2	4.187	9474	0.135
3	4.652	45888	0.653
4	6.059	108053	1.538
5	7.630	22716	0.323
6	11.141	6783956	96.545
总计		7026737	100.000

Figure S16. HPLC analysis of **DPA-NI-Et**.

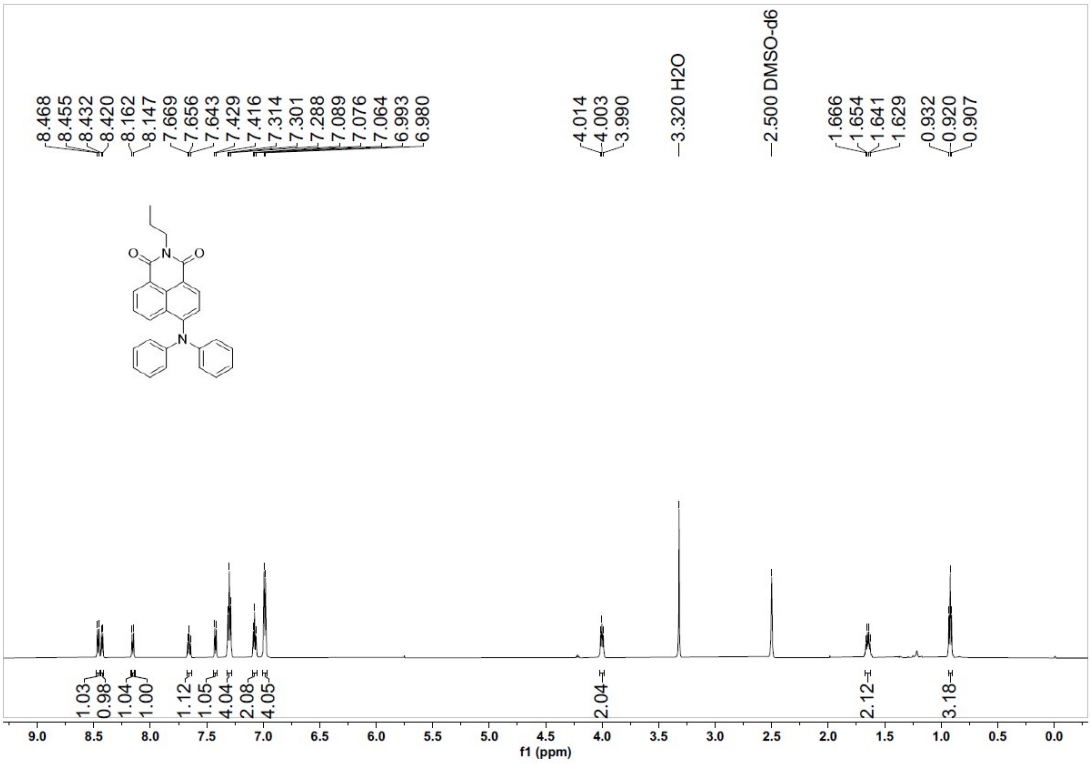

Figure S17. ^{1}H NMR Spectra of **DPA-NI-Pro** (600 MHz).

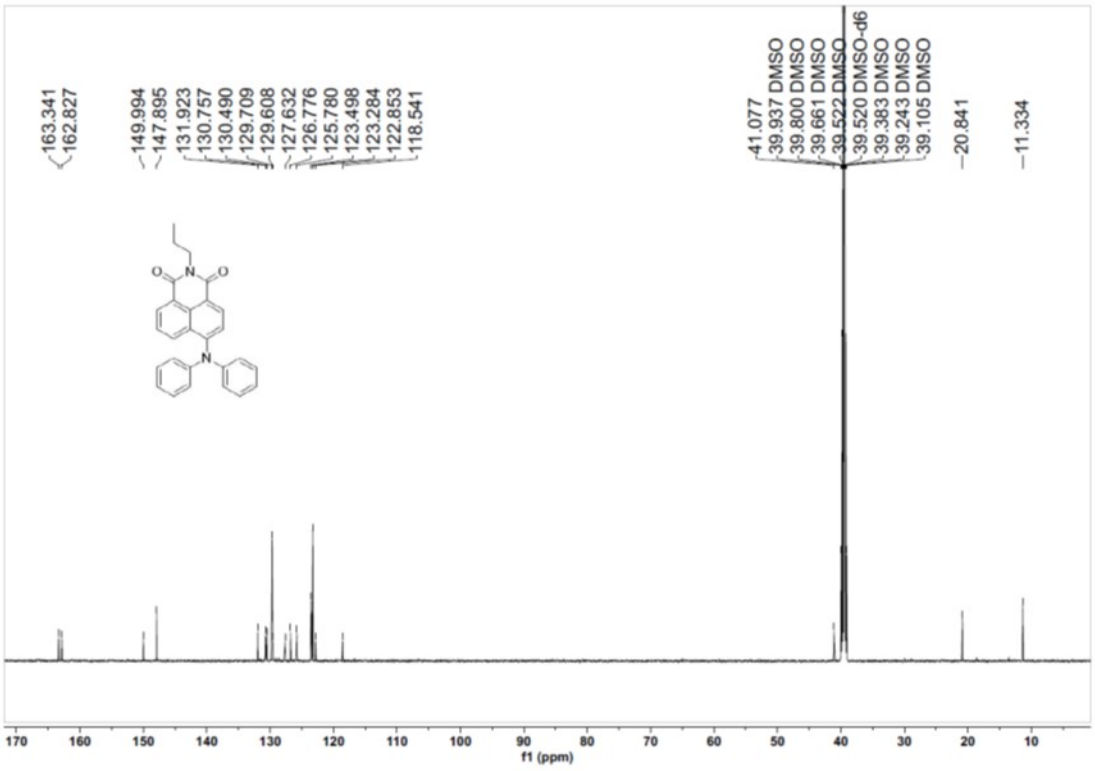

Figure S18. ^{13}C NMR Spectra of **DPA-NI-Pro** (151 MHz).

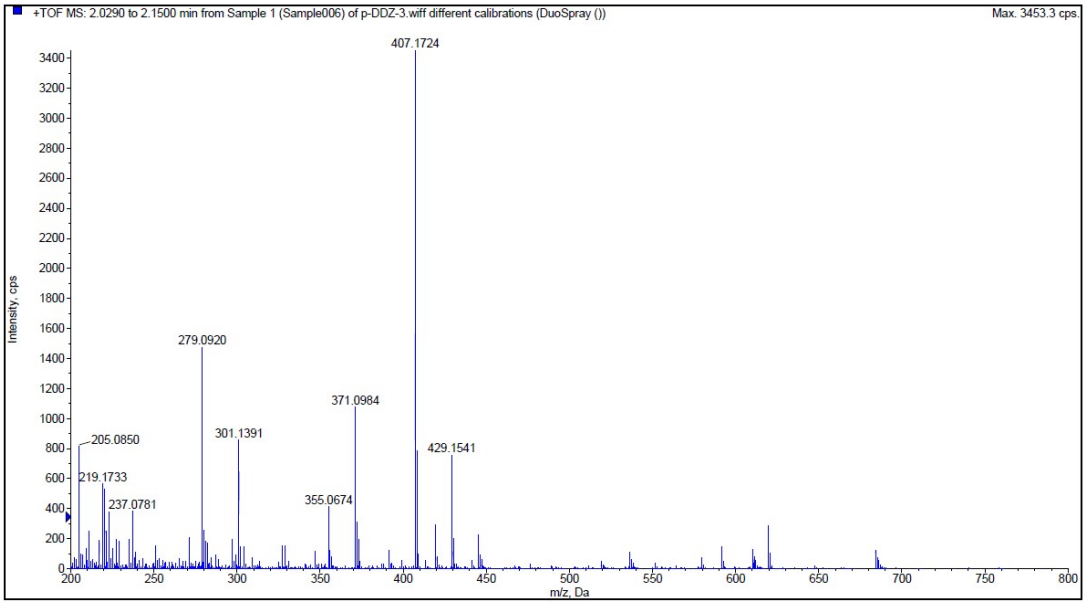

Figure S19. MS spectra of **DPA-NI-Pro**.

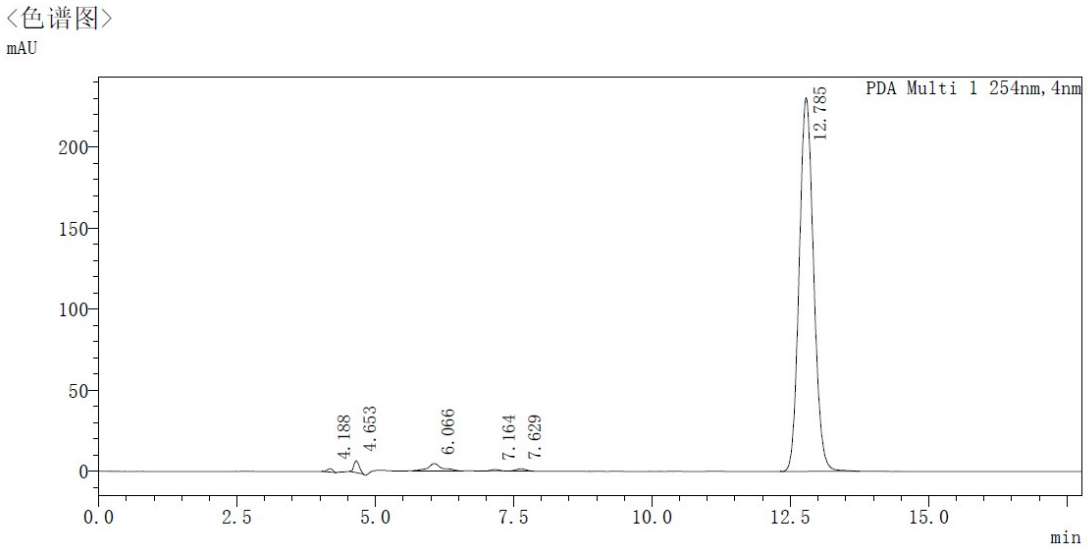

峰表

PDA Ch1 254nm

峰号	保留时间	面积	面积%
1	4.188	14203	0.328
2	4.653	48510	1.122
3	6.066	73746	1.705
4	7.164	6191	0.143
5	7.629	15681	0.363
6	12.785	4166178	96.339
总计		4324508	100.000

Figure S20. HPLC analysis of **DPA-NI-Pro**.

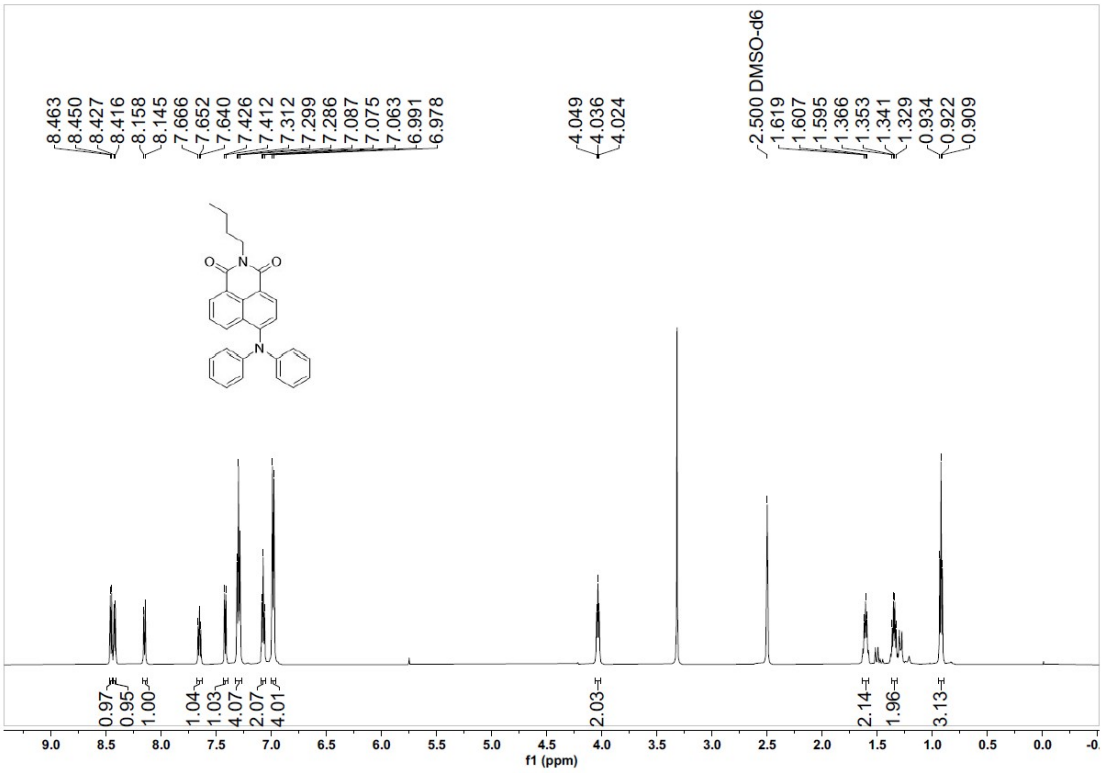

Figure S21. ^{1}H NMR Spectra of **DPA-NI-Bu** (600 MHz).

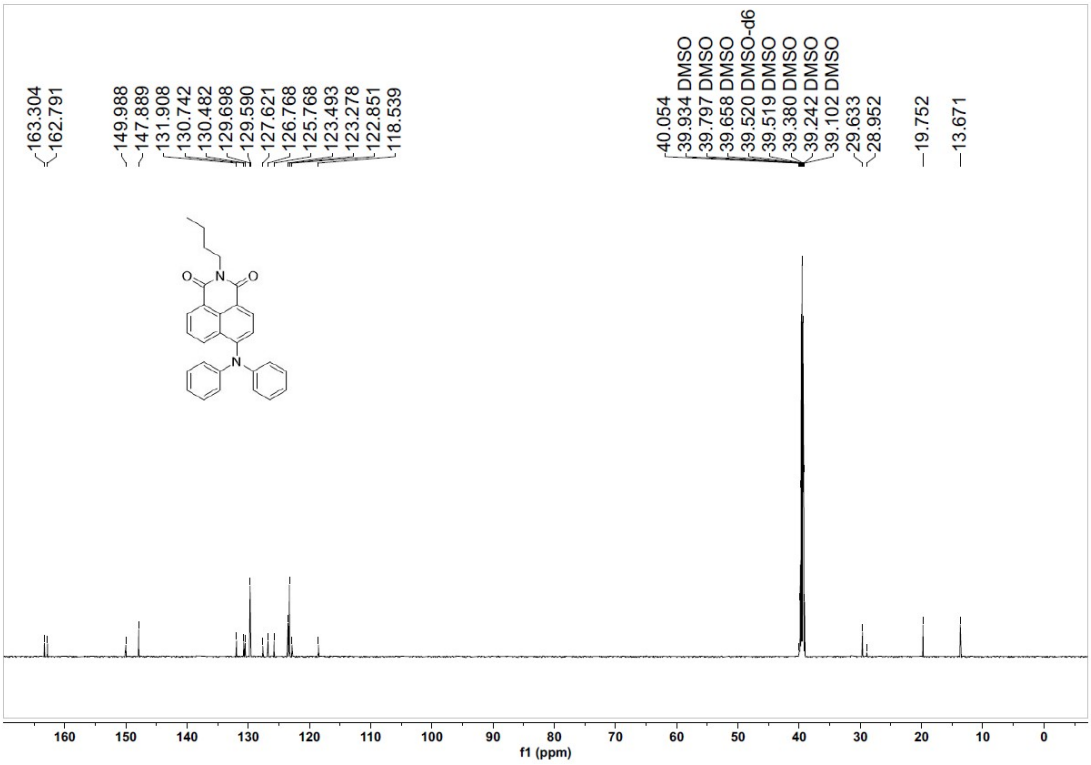

Figure S22. ^{13}C NMR Spectra of **DPA-NI-Bu** (151 MHz).

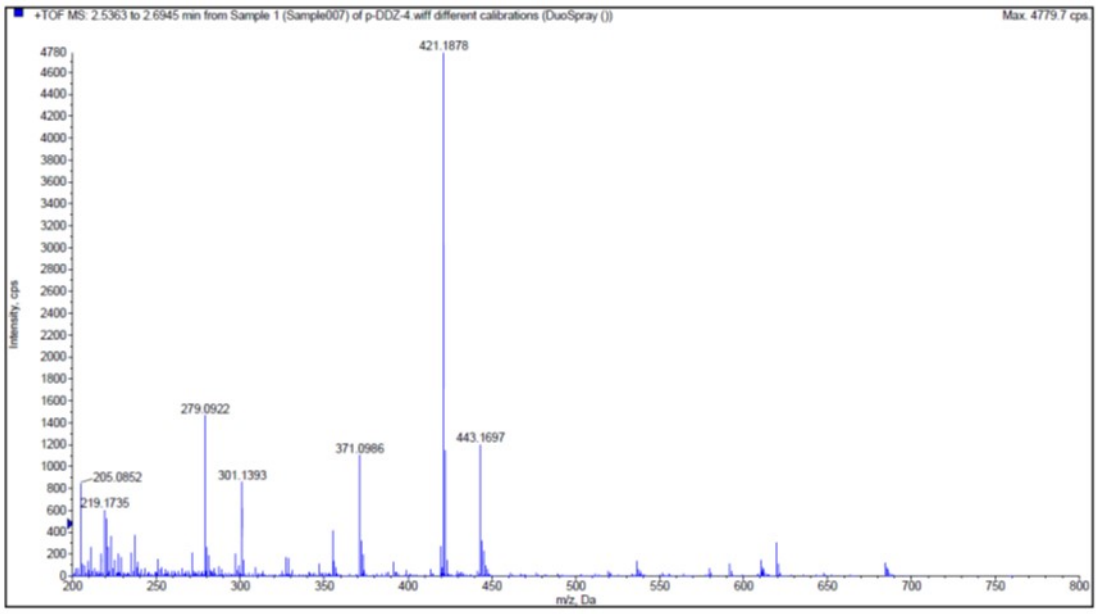

Figure S23. MS spectra of **DPA-NI-Bu**.

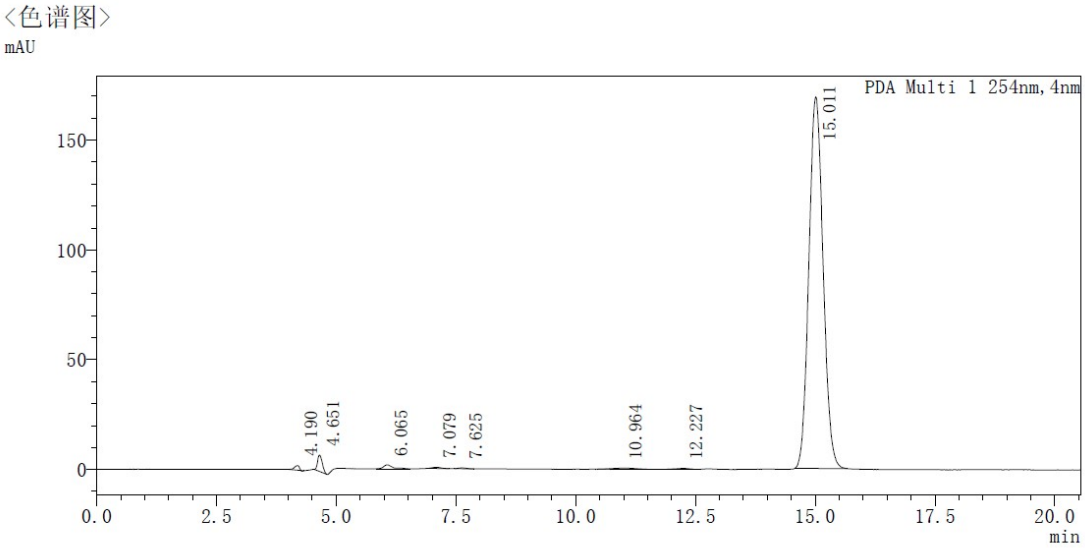

峰表

PDA Ch1 254nm

峰号	保留时间	面积	面积%
1	4.190	13146	0.363
2	4.651	50363	1.389
3	6.065	23522	0.649
4	7.079	8135	0.224
5	7.625	5044	0.139
6	10.964	20181	0.557
7	12.227	8502	0.235
8	15.011	3495758	96.444
总计		3624649	100.000

Figure S24. HPLC analysis of **DPA-NI-Bu**.

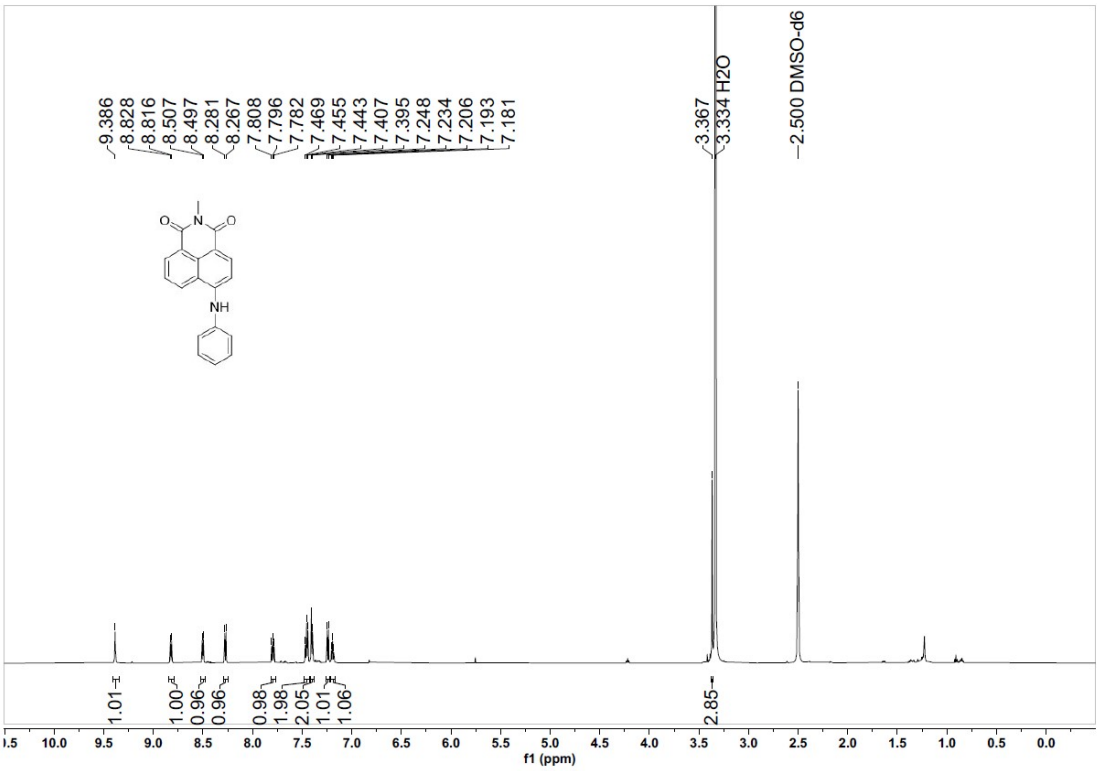

Figure S25. ^{1}H NMR Spectra of **Ph-NI-Me** (600 MHz).

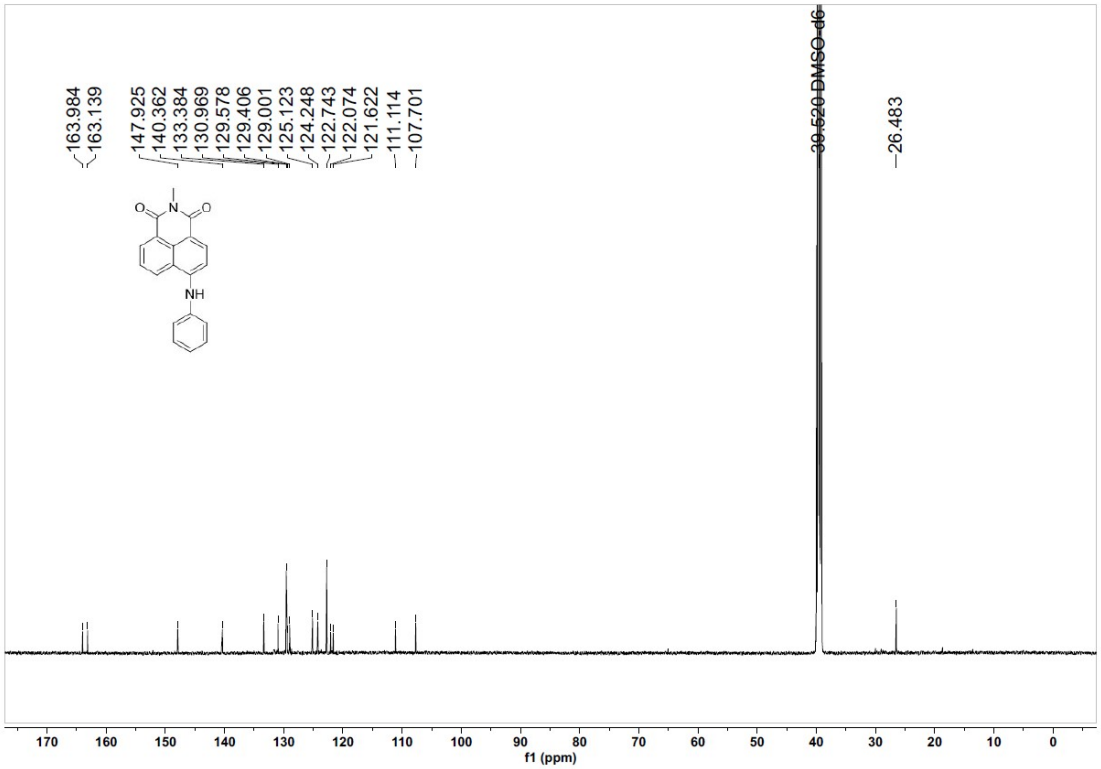

Figure S26. ^{13}C NMR Spectra of **Ph-NI-Me** (151 MHz).

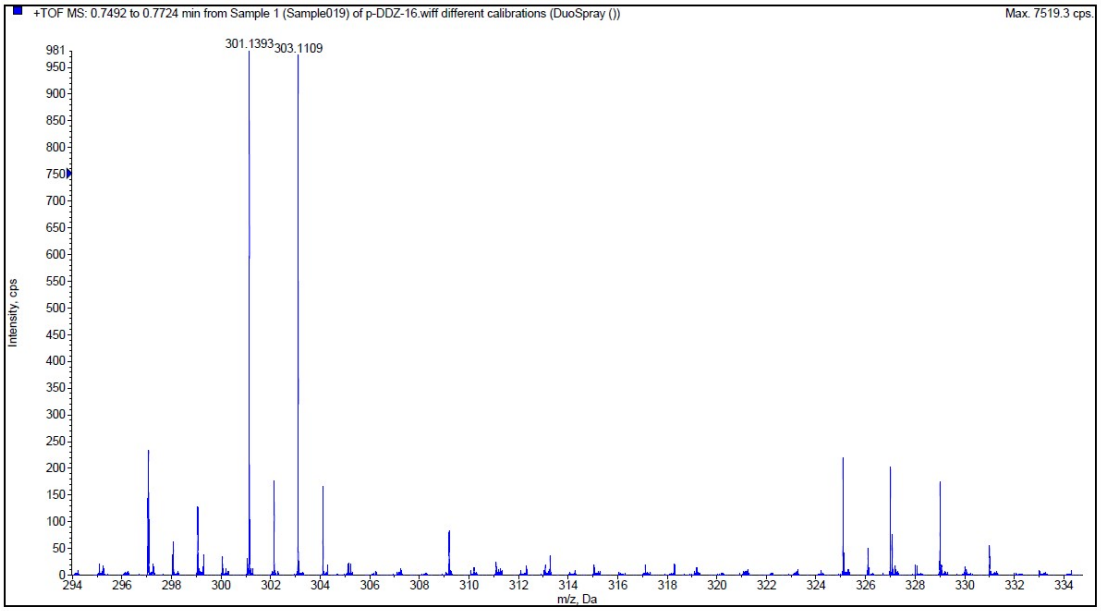

Figure S27. MS Spectra of **Ph-NI-Me**.

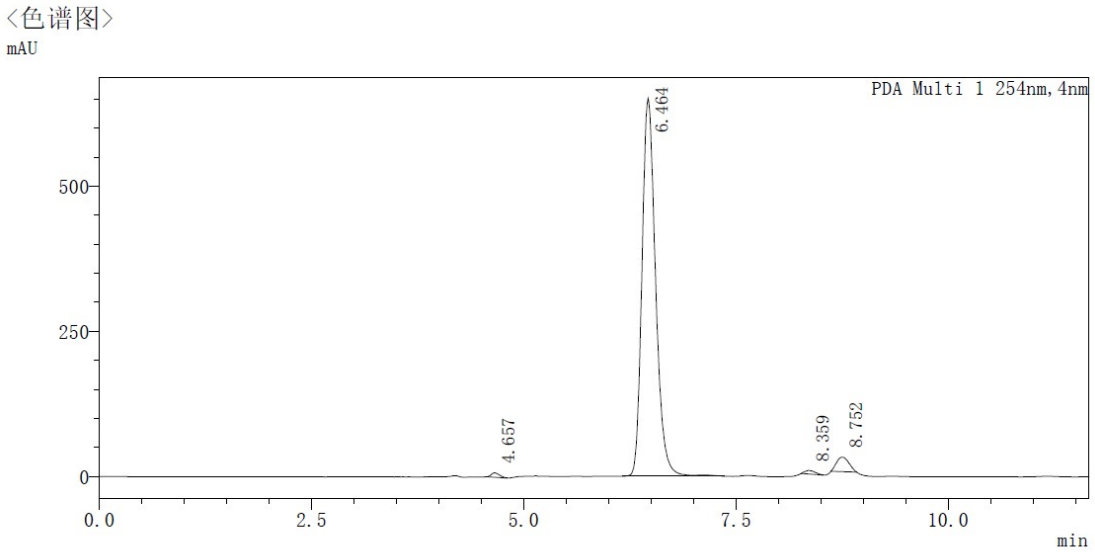

峰表

PDA Ch1 254nm

峰号	保留时间	面积	面积%
1	4.657	50148	0.658
2	6.464	7264350	95.346
3	8.359	50843	0.667
4	8.752	253574	3.328
总计		7618916	100.000

Figure S28. HPLC analysis of **Ph-NI-Me**.

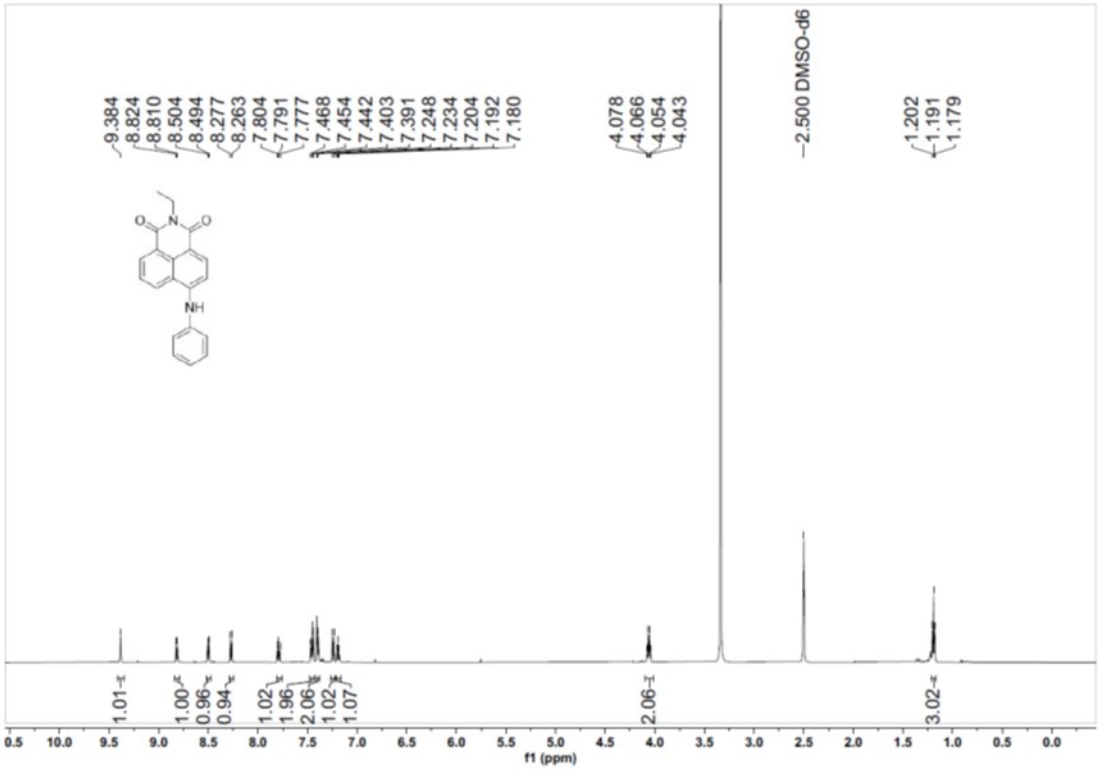

Figure S29. ^{1}H NMR Spectra of **Ph-NI-Et** (600 MHz).

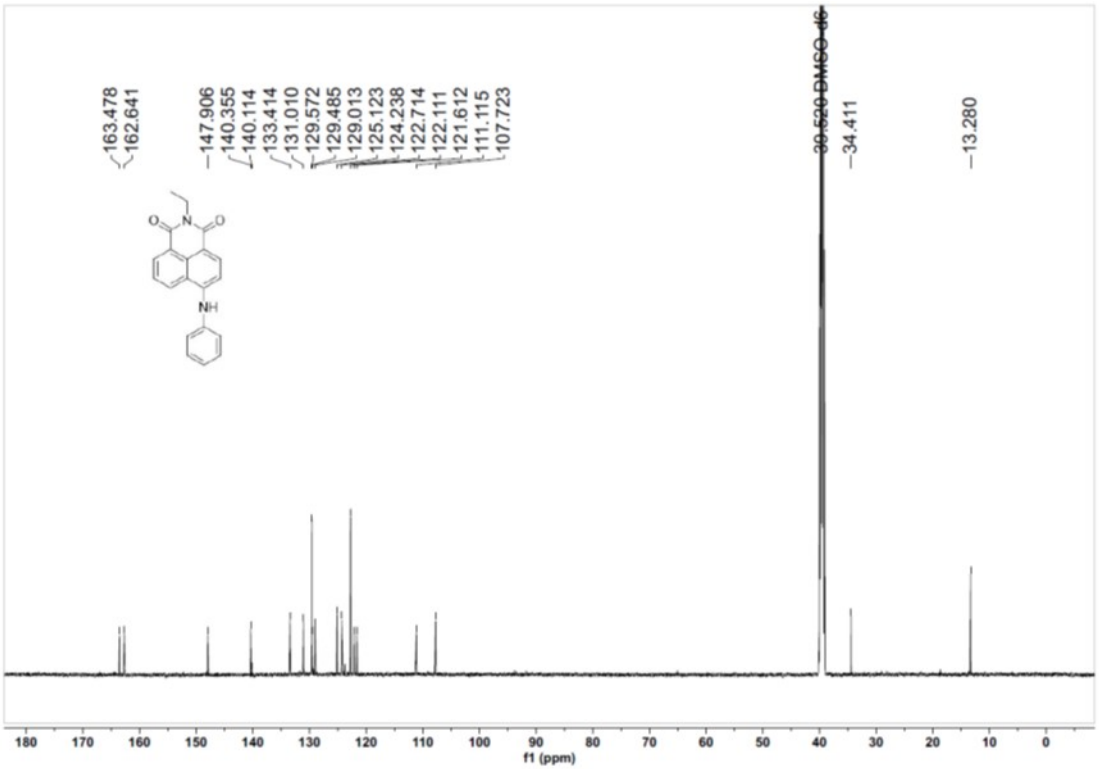

Figure S30. ^{13}C NMR Spectra of **Ph-NI-Et** (151 MHz).

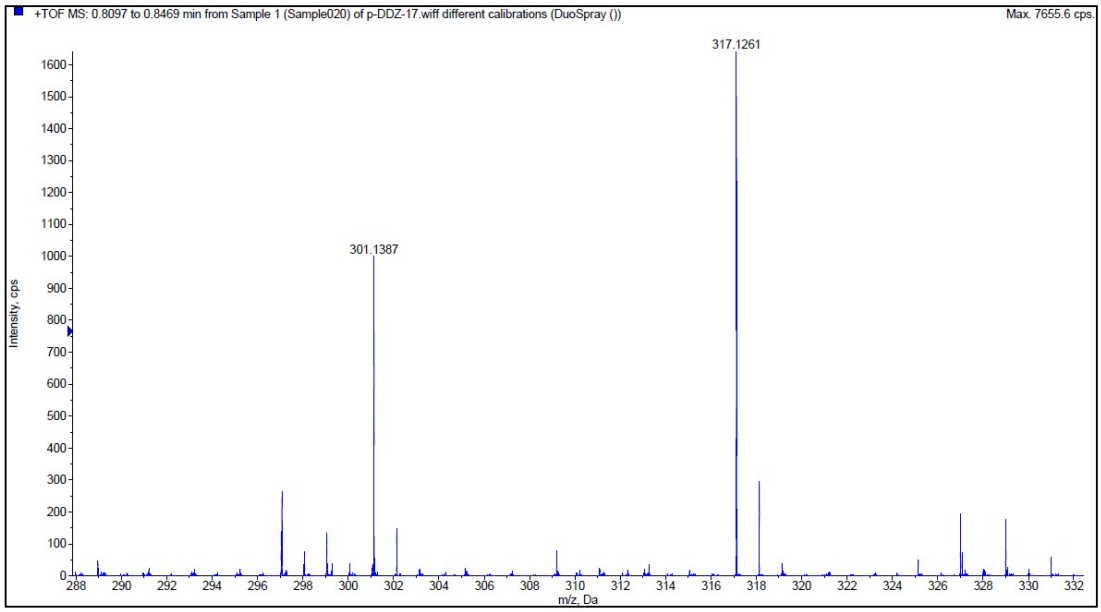

Figure S31. MS Spectra of **Ph-NI-Et**.

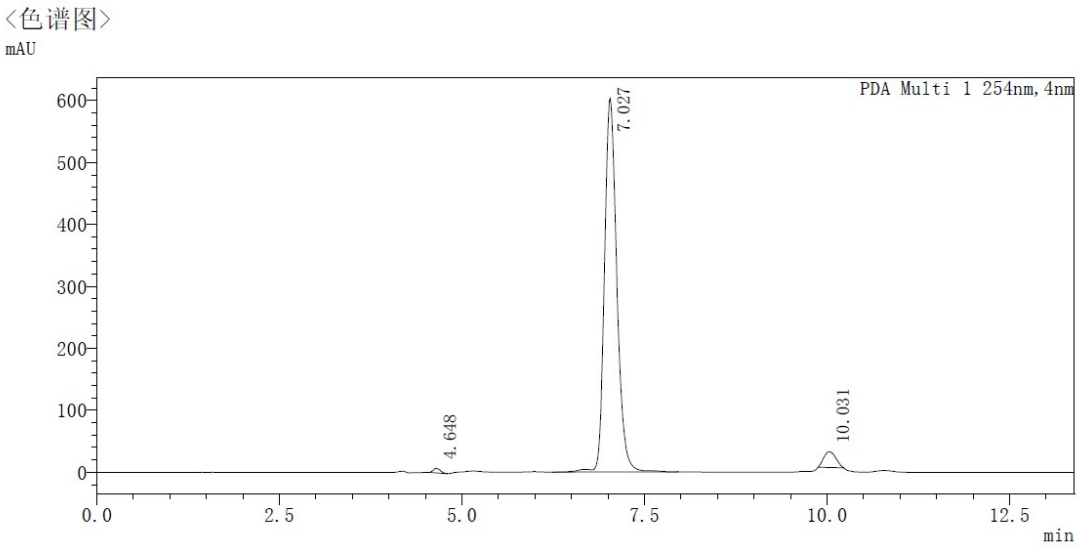

峰表

PDA Ch1 254nm

峰号	保留时间	面积	面积%
1	4.648	47533	0.639
2	7.027	7104632	95.442
3	10.031	291752	3.919
总计		7443917	100.000

Figure S32. HPLC analysis of **Ph-NI-Et**.

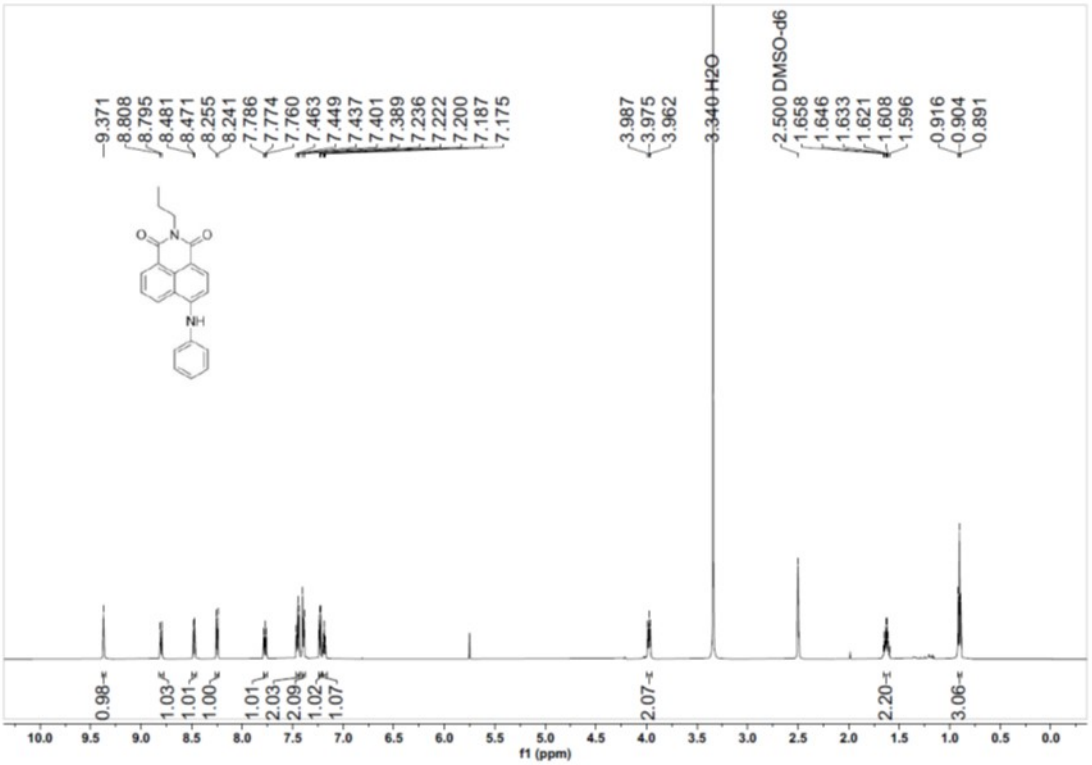

Figure S33. ^{1}H NMR Spectra of **Ph-NI-Pro** (600 MHz).

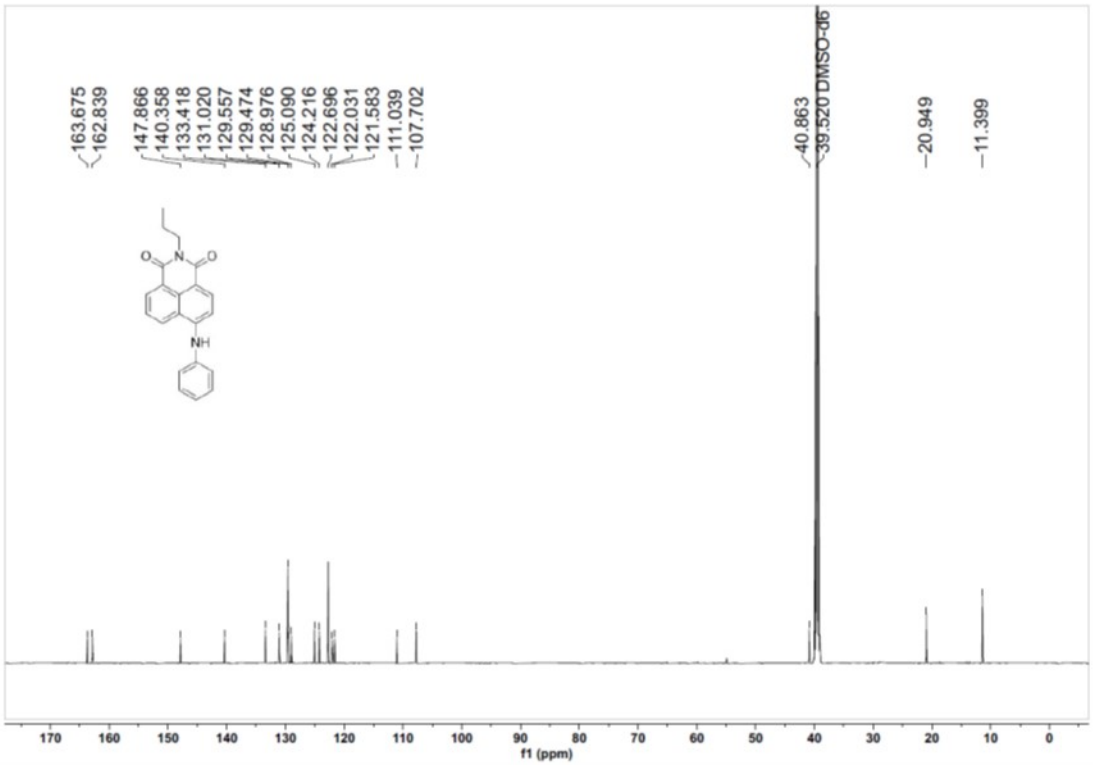

Figure S34. ^{13}C NMR Spectra of **Ph-NI-Pro** (151 MHz).

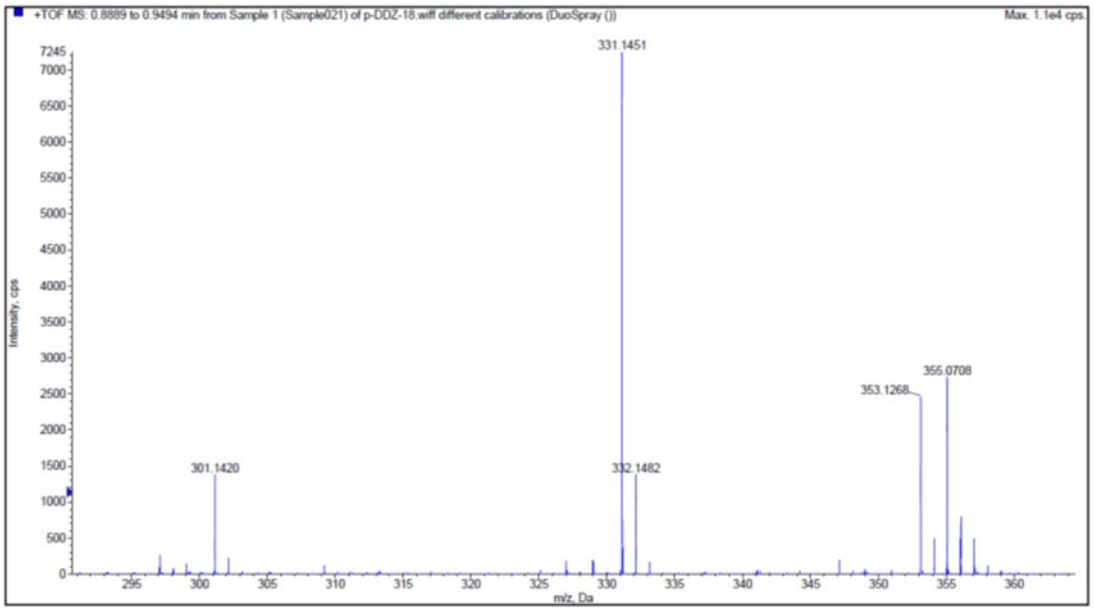

Figure S35. MS Spectra of **Ph-NI-Pro**.

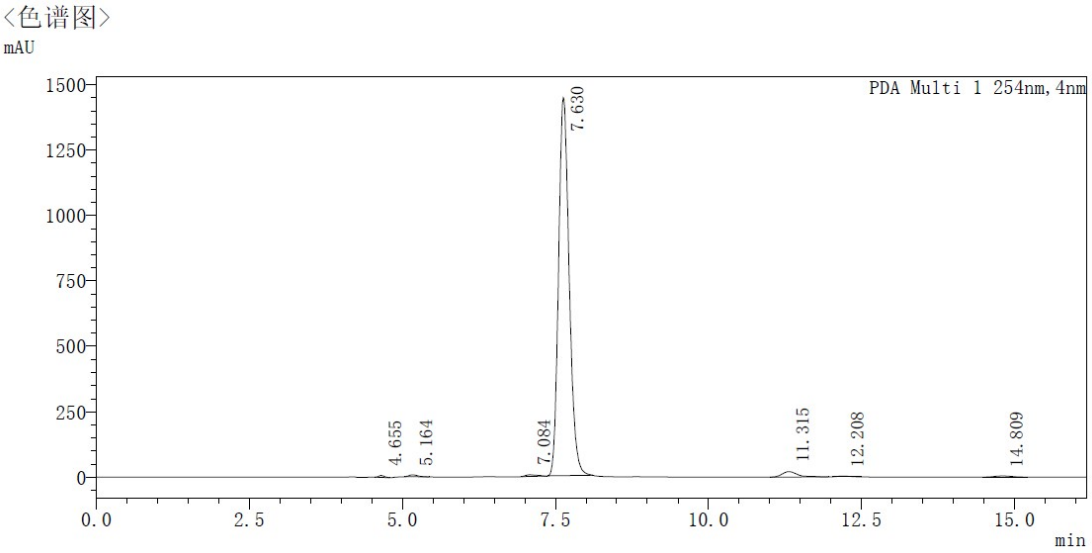

峰表

PDA Ch1 254nm

峰号	保留时间	面积	面积%
1	4.655	45097	0.249
2	5.164	75644	0.417
3	7.084	82247	0.453
4	7.630	17435046	96.077
5	11.315	370868	2.044
6	12.208	41252	0.227
7	14.809	96835	0.534
总计		18146989	100.000

Figure S36. HPLC analysis of **Ph-NI-Pro**.

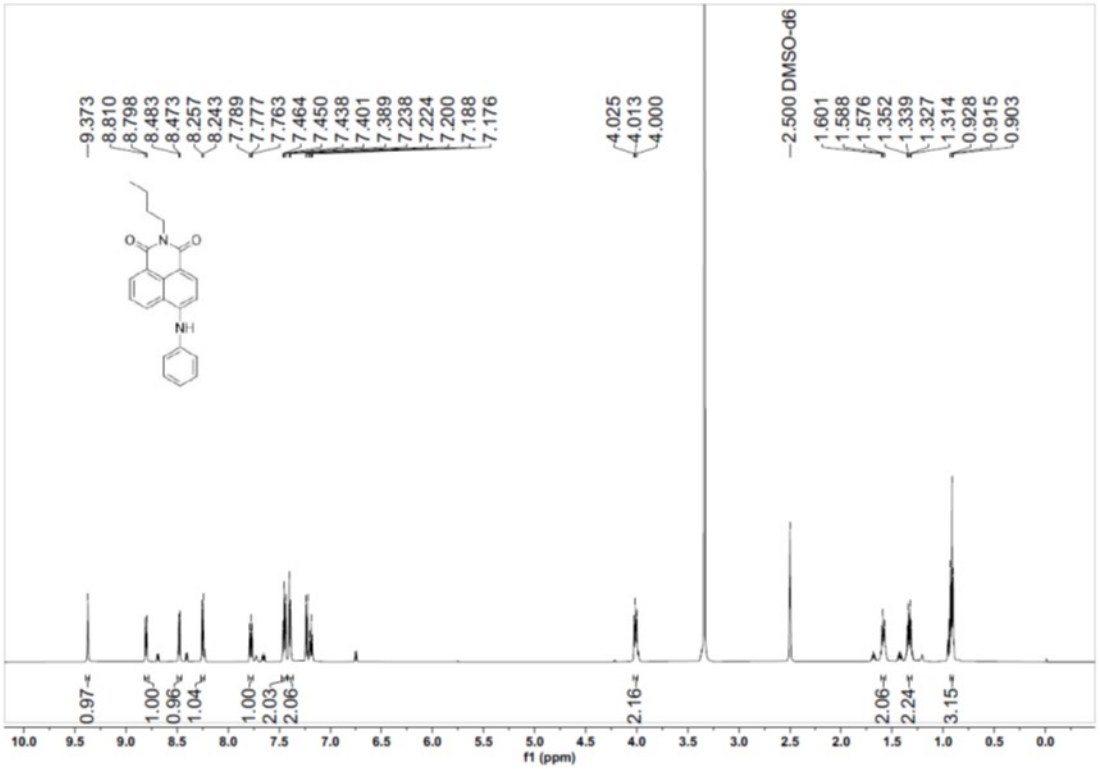

Figure S37. ^{1}H NMR Spectra of **Ph-NI-Bu** (600 MHz).

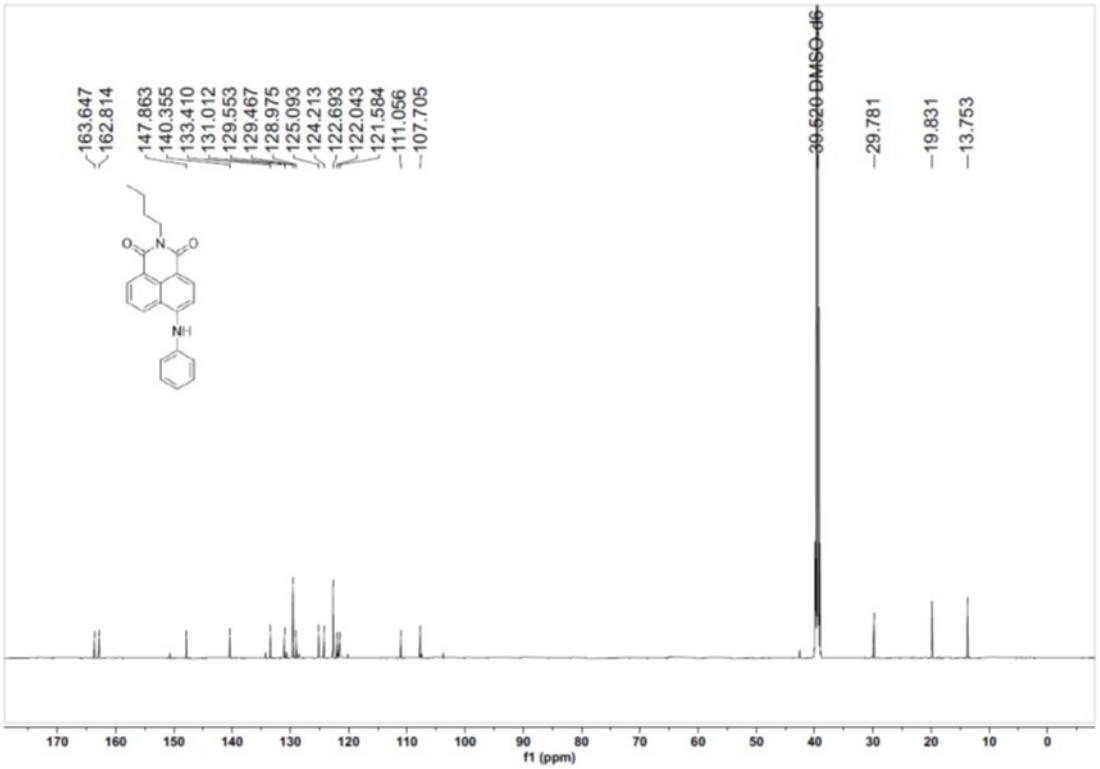

Figure S38. ^{13}C NMR Spectra of **Ph-NI-Bu** (151 MHz).

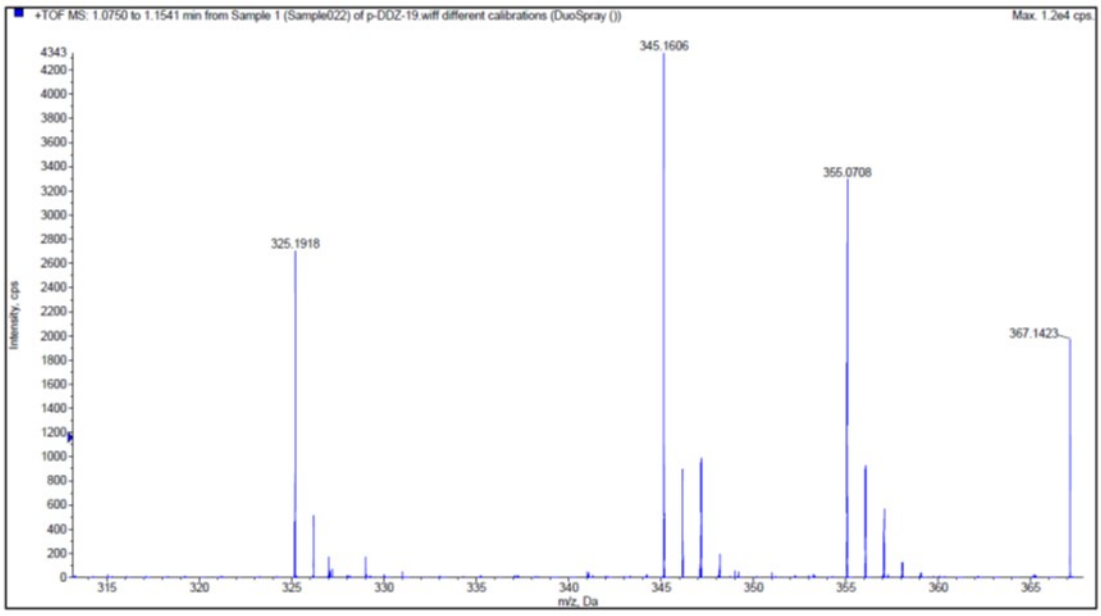

Figure S39. MS Spectra of **Ph-NI-Bu**.

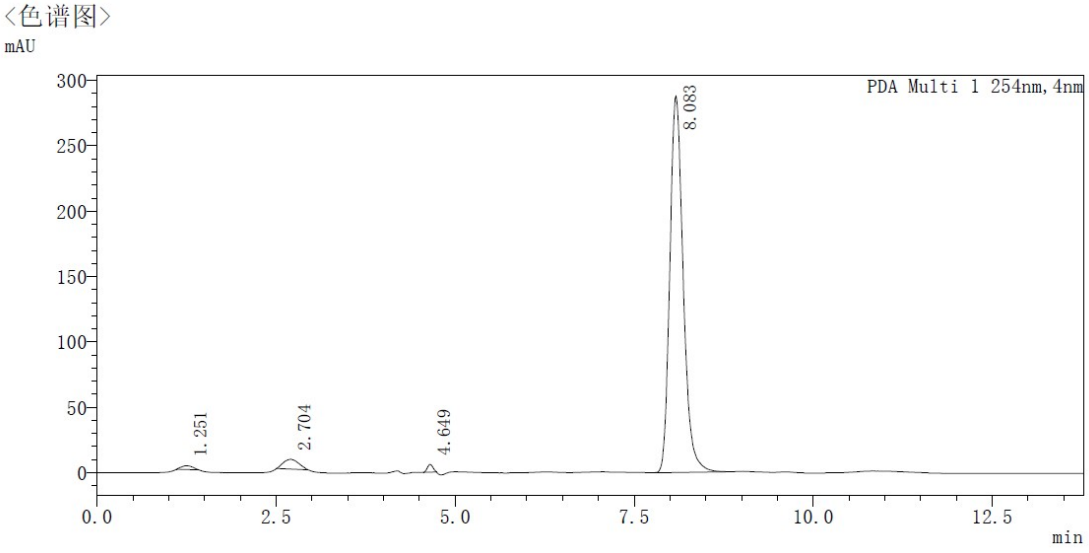

峰表

PDA Ch1 254nm

峰号	保留时间	面积	面积%
1	1.251	32523	0.831
2	2.704	111976	2.861
3	4.649	31895	0.815
4	8.083	3737085	95.493
总计		3913479	100.000

Figure S40. HPLC analysis of **Ph-NI-Bu**.

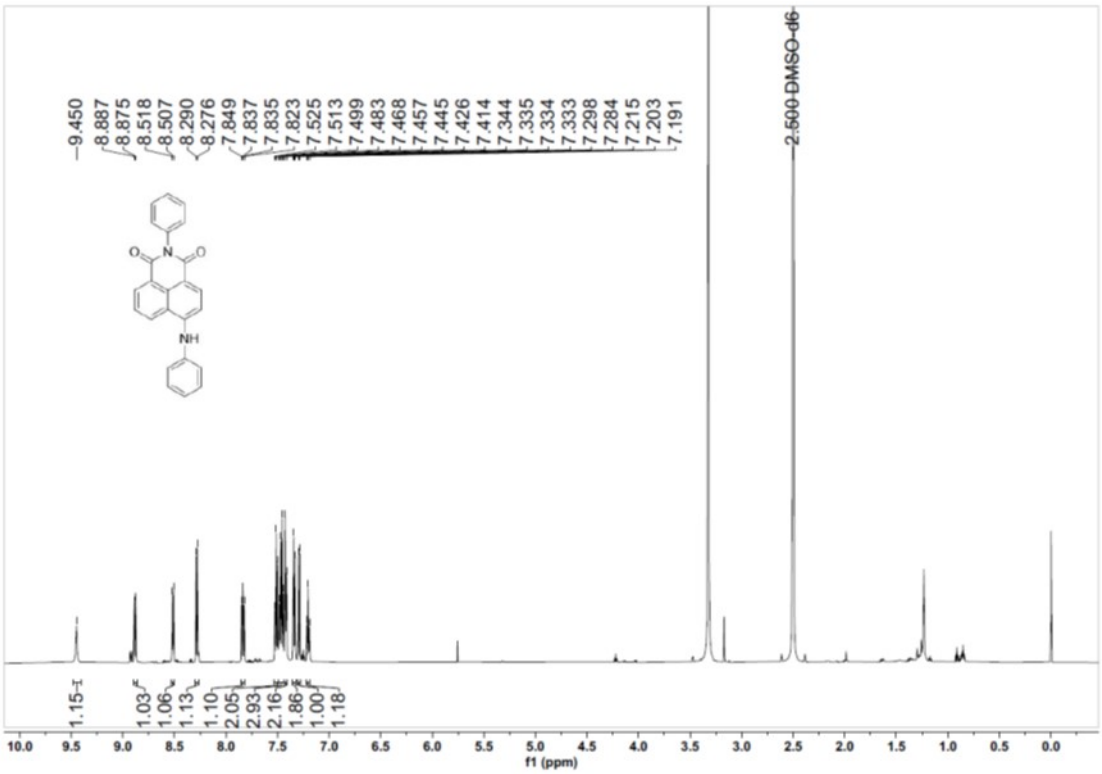

Figure S41. ^{1}H NMR Spectra of **Ph-NI-Pro** (600 MHz).

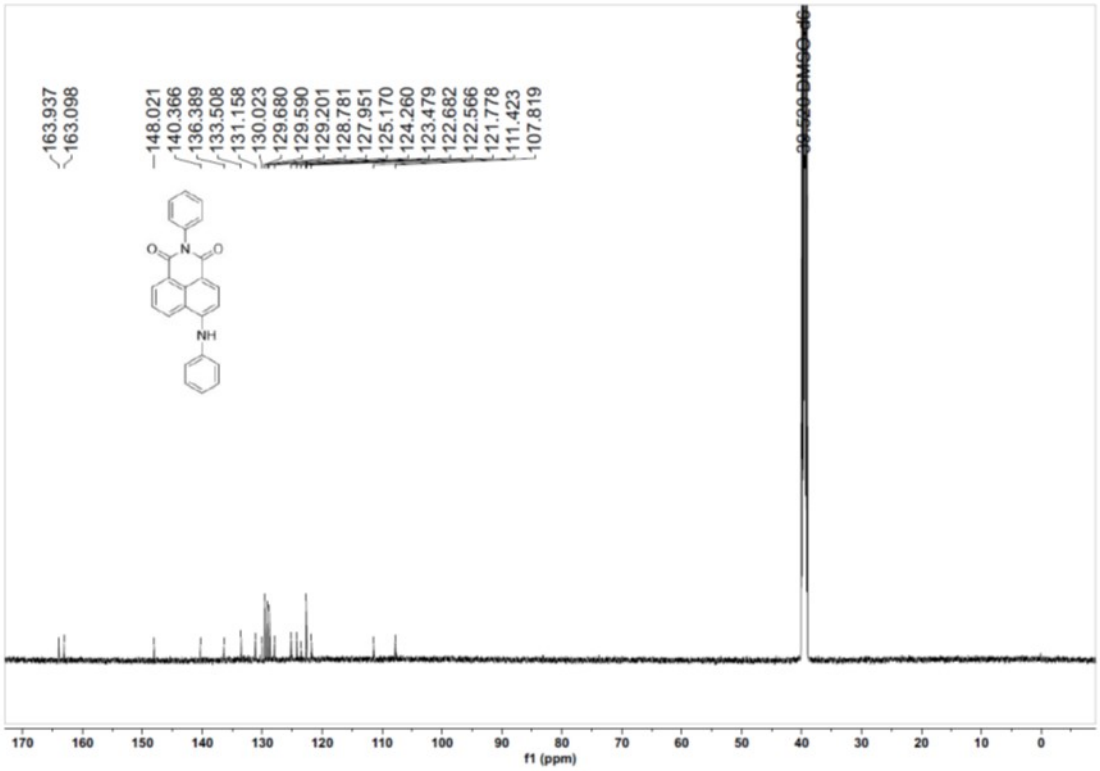

Figure S42. ^{13}C NMR Spectra of **Ph-NI-Pro** (151 MHz).

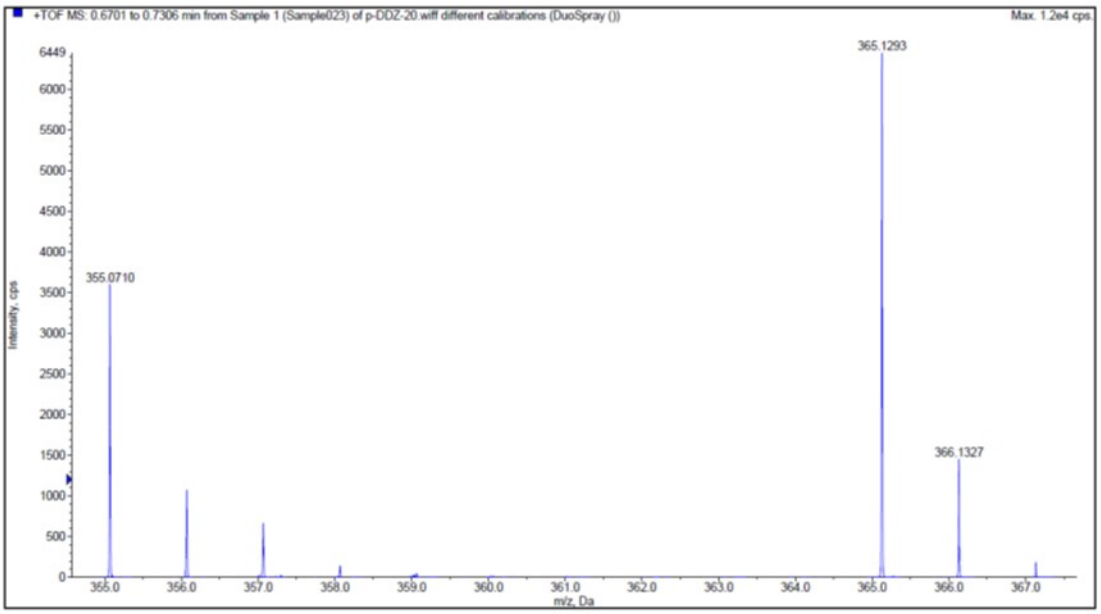

Figure S43. MS Spectra of **Ph-NI-Pro**.

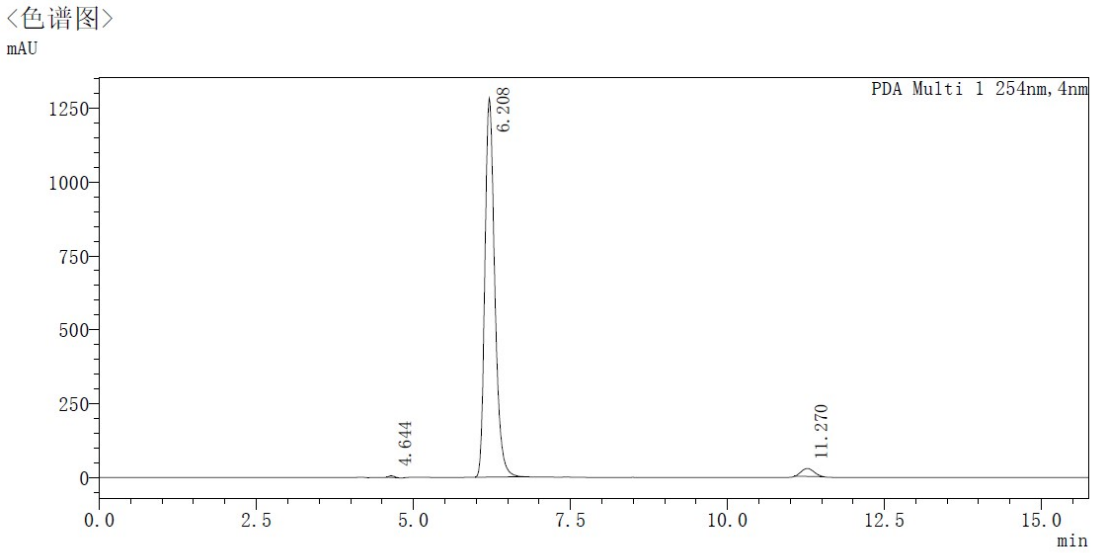

峰表

PDA Ch1 254nm

峰号	保留时间	面积	面积%
1	4.644	34369	0.239
2	6.208	13985421	97.127
3	11.270	379343	2.634
总计		14399133	100.000

Figure S44. HPLC analysis of **Ph-NI-Pro**.

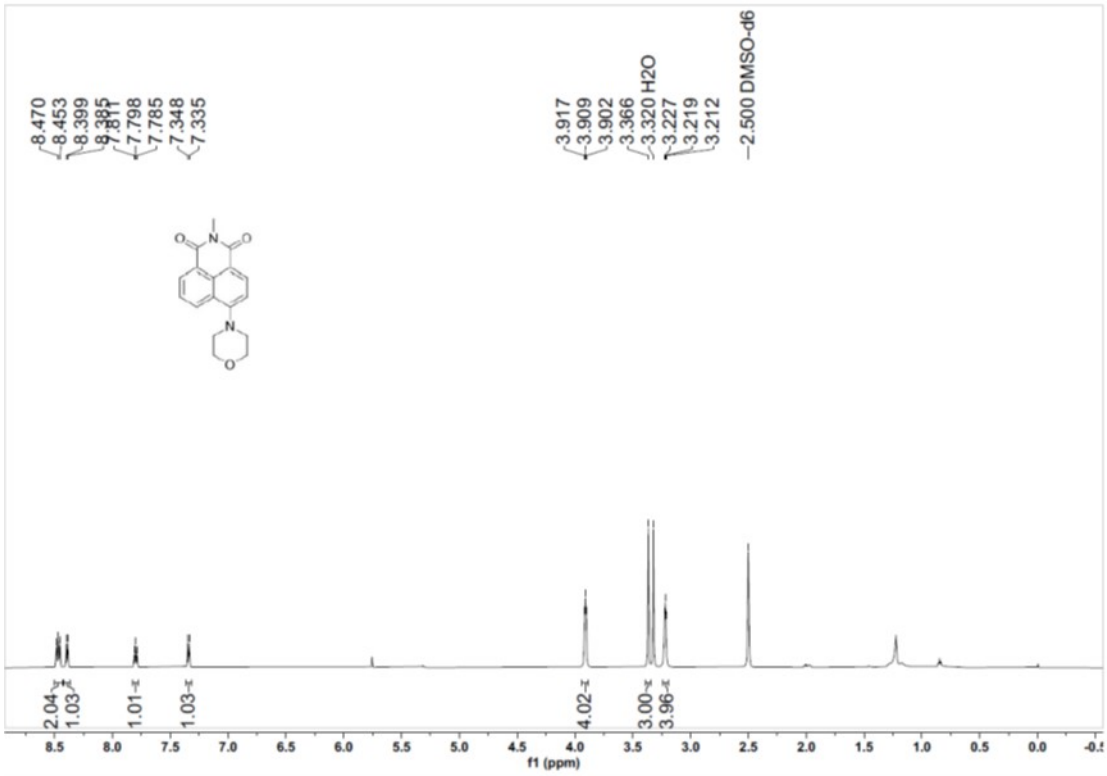

Figure S45. ^{1}H NMR Spectra of **Mor-NI-Me** (600 MHz).

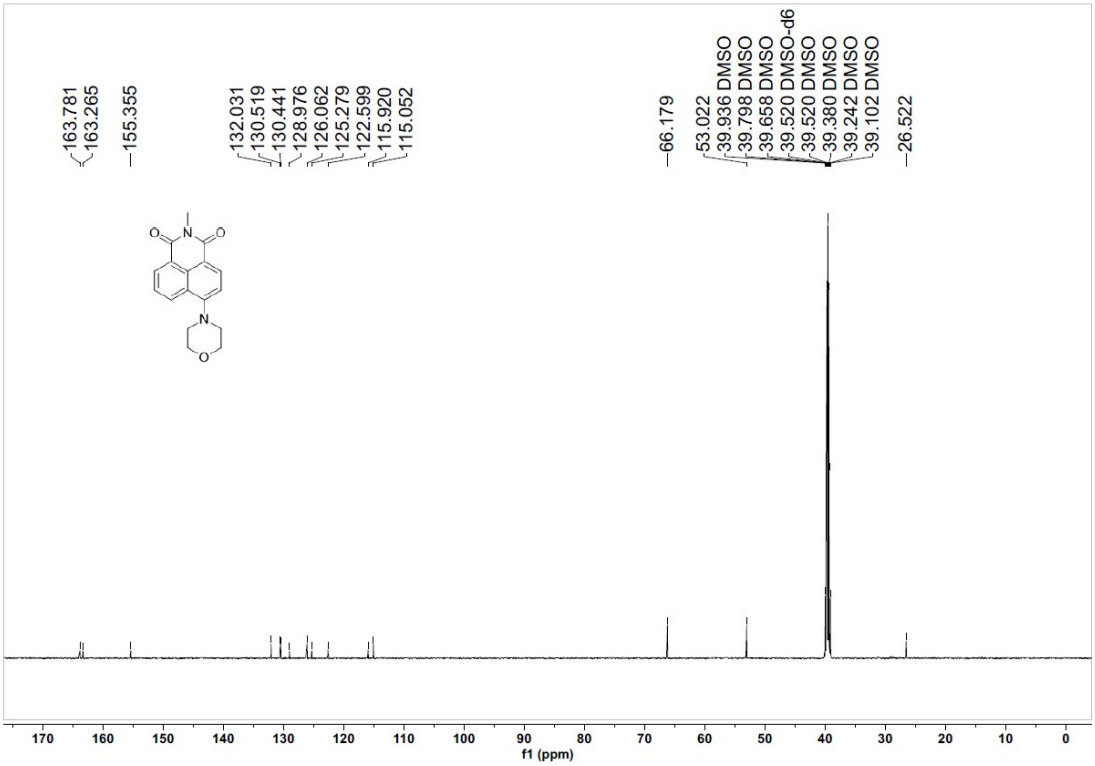

Figure S46. ^{13}C NMR Spectra of **Mor-NI-Me** (151 MHz).

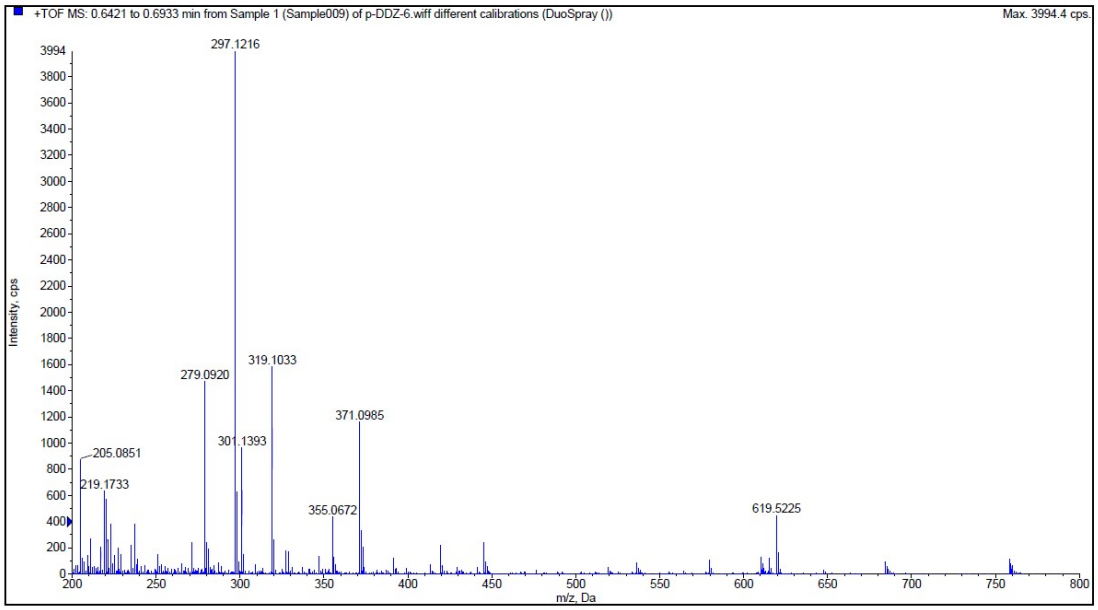

Figure S47. MS spectra of **Mor-NI-Me**.

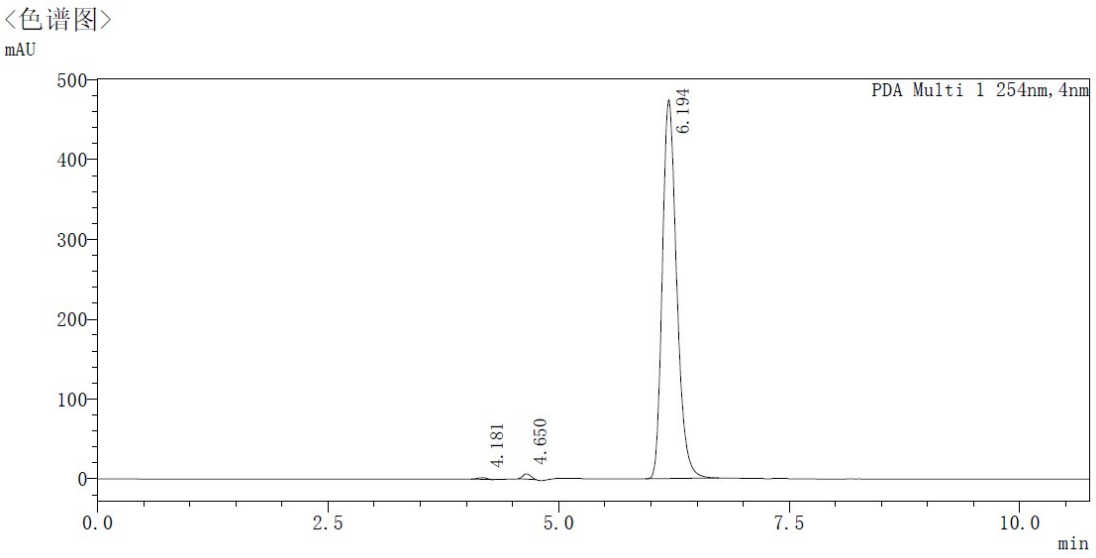

峰表

PDA Ch1 254nm

峰号	保留时间	面积	面积%
1	4.181	11832	0.228
2	4.650	39696	0.766
3	6.194	5127846	99.005
总计		5179374	100.000

Figure S48. HPLC analysis of **Mor-NI-Me**.

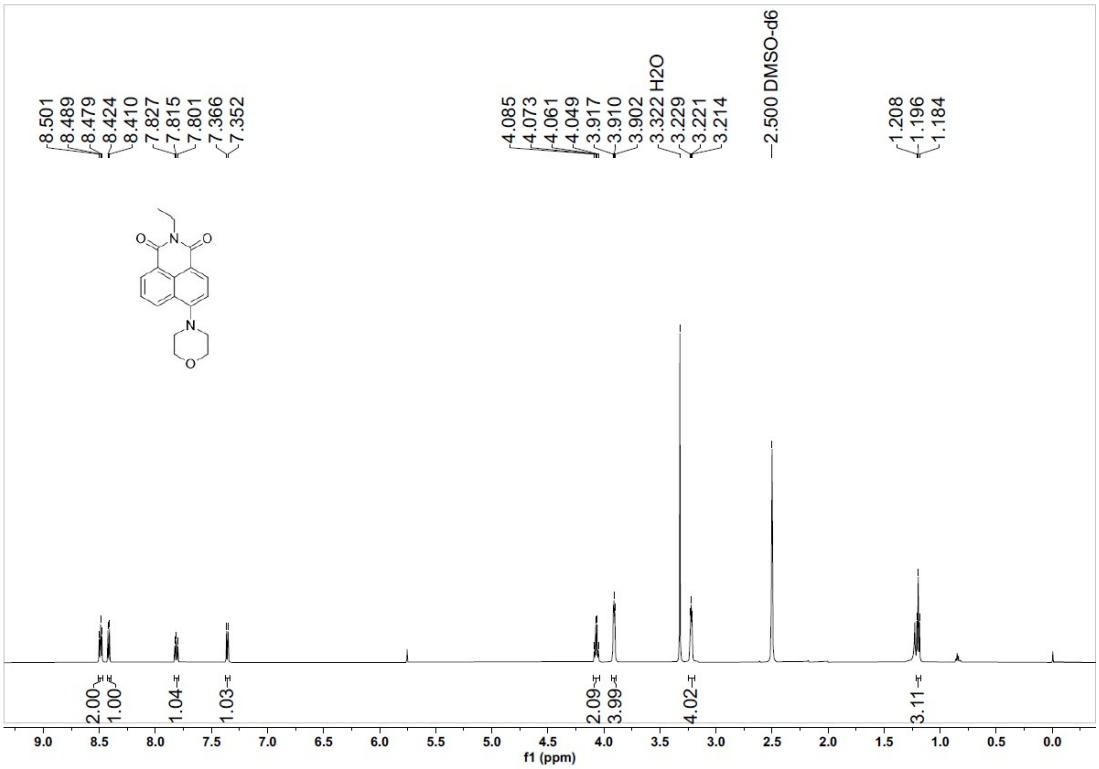

Figure S49. ^{1}H NMR Spectra of **Mor-NI-Et** (600 MHz).

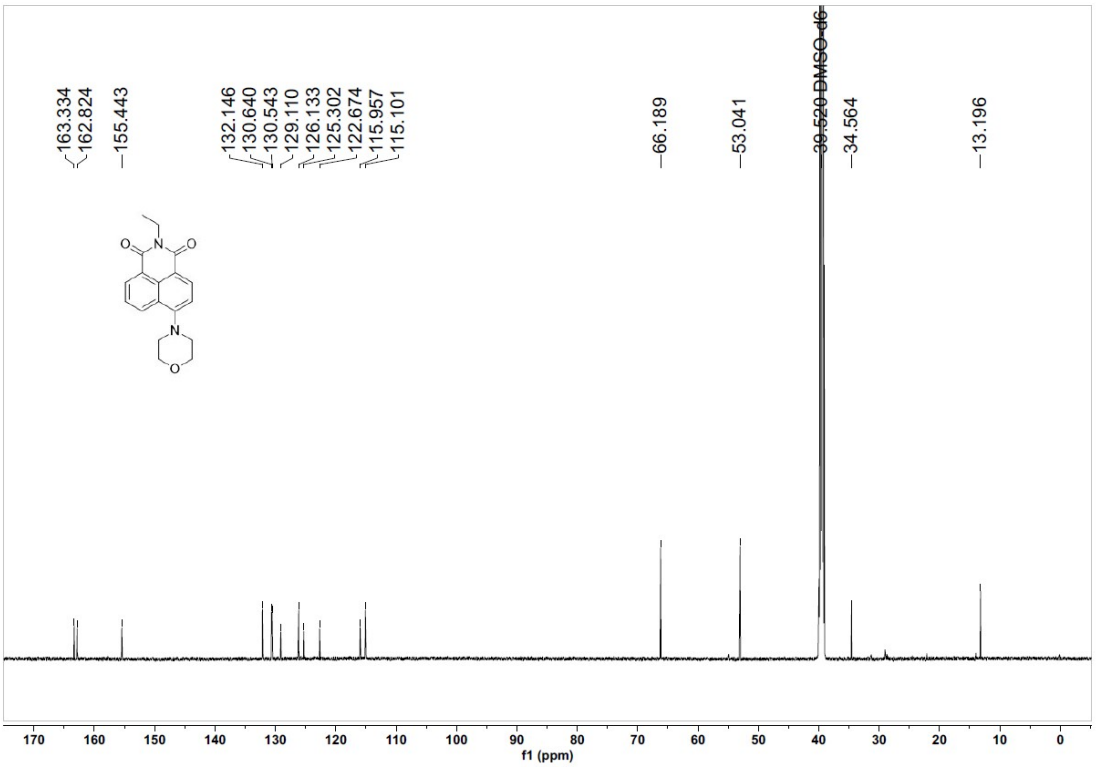

Figure S50. ^{13}C NMR Spectra of **Mor-NI-Et** (151 MHz).

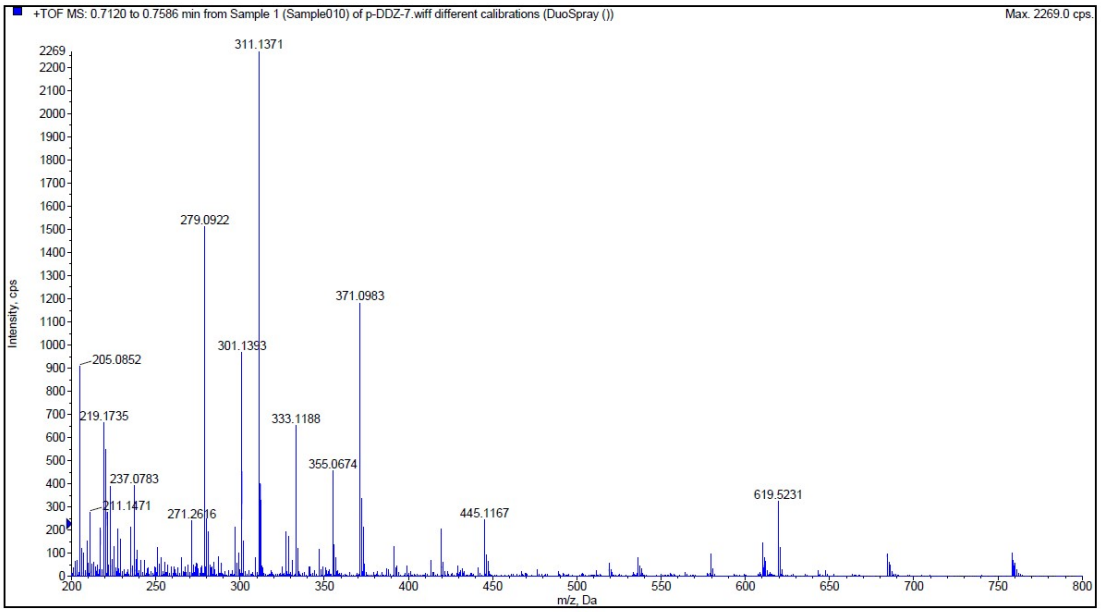

Figure S51. MS spectra of **Mor-NI-Et**.

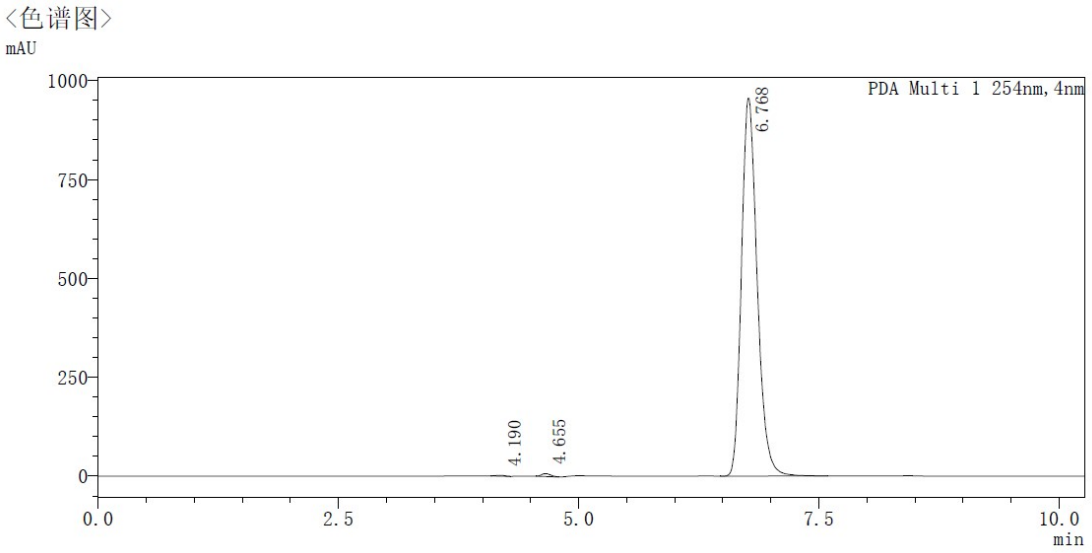

峰表

PDA Ch1 254nm

峰号	保留时间	面积	面积%
1	4.190	12478	0.114
2	4.655	46546	0.426
3	6.768	10860182	99.459
总计		10919206	100.000

Figure S52. HPLC analysis of **Mor-NI-Et**.

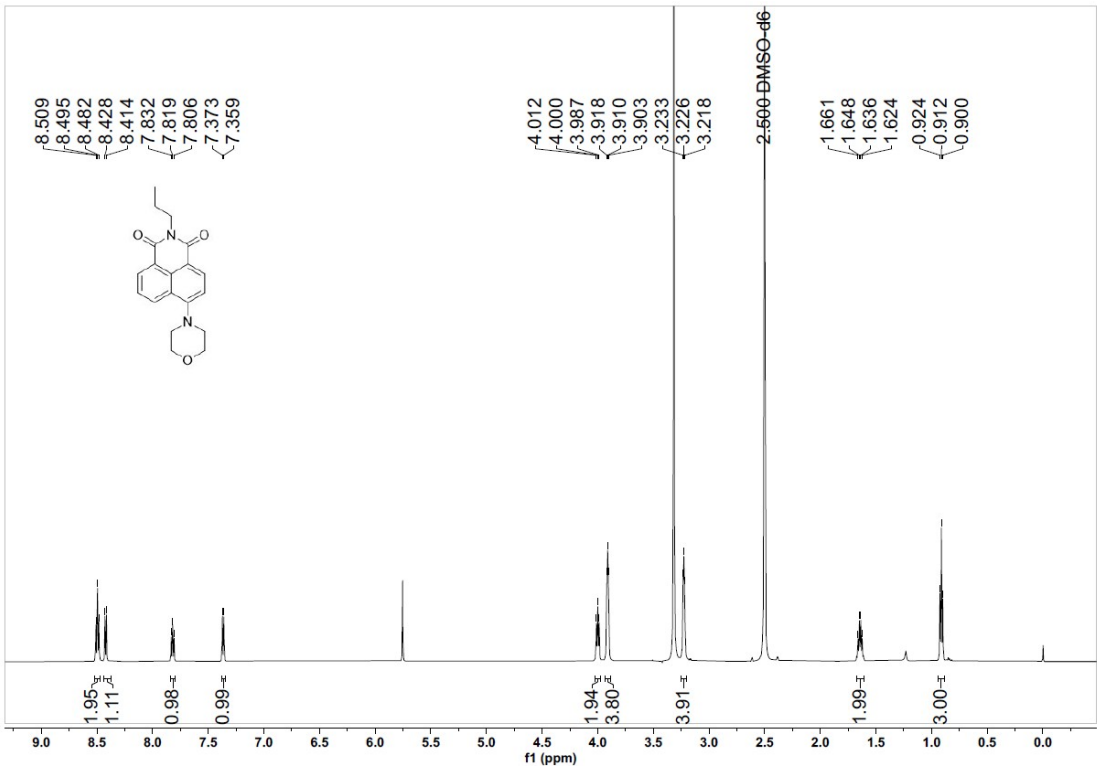

Figure S53. ^{1}H NMR Spectra of **Mor-NI-Pro** (600 MHz).

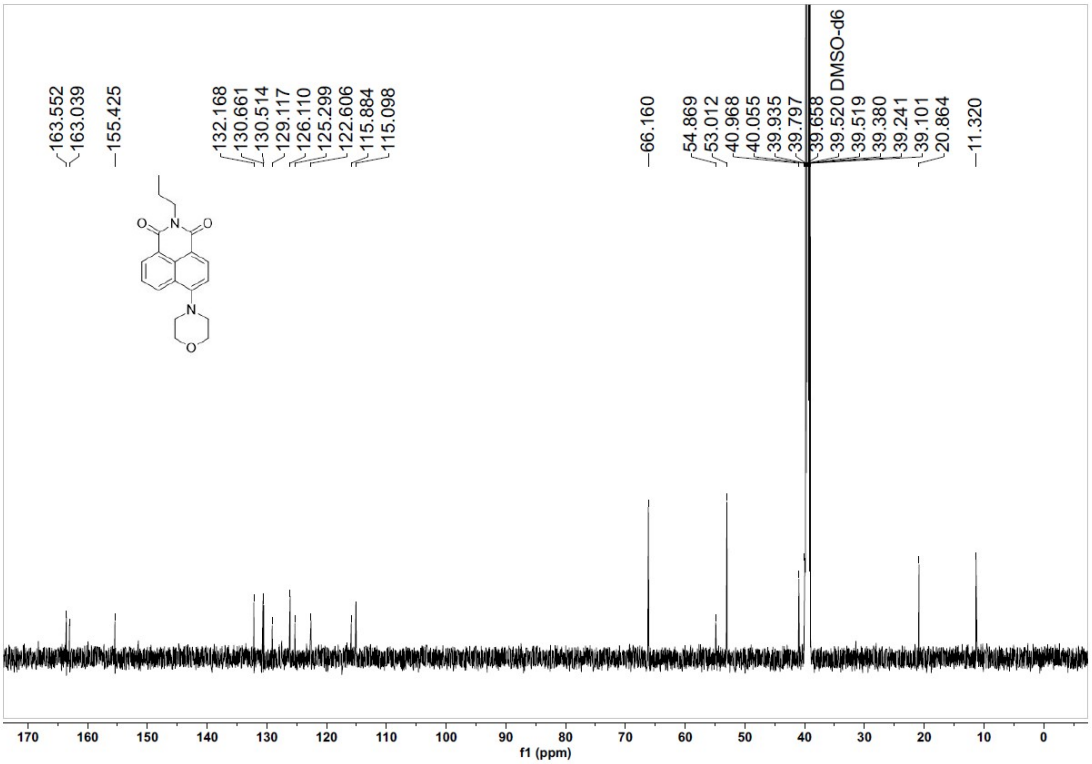

Figure S54. ^{13}C NMR Spectra of **Mor-NI-Pro** (151 MHz).

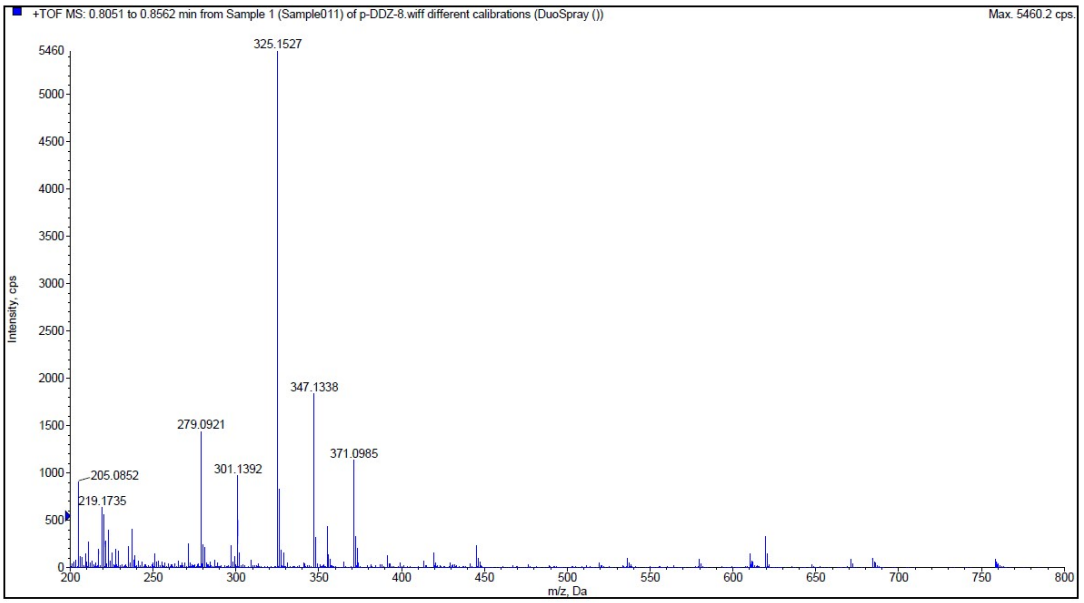

Figure S55. MS spectra of **Mor-NI-Pro**.

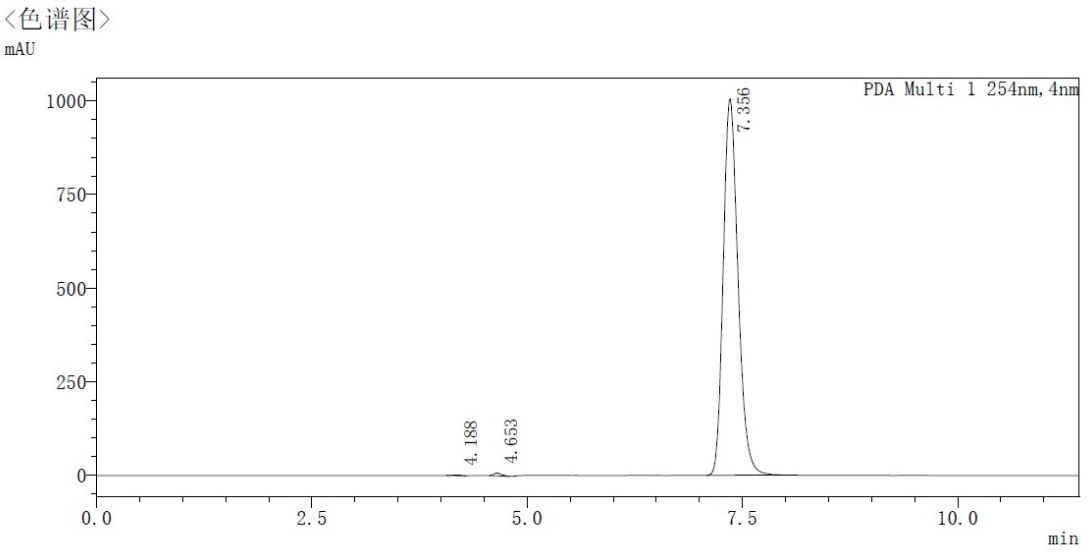

峰表

PDA Ch1 254nm

峰号	保留时间	面积	面积%
1	4.188	12795	0.106
2	4.653	46012	0.382
3	7.356	11996661	99.512
总计		12055468	100.000

Figure S56. HPLC analysis of **Mor-NI-Pro**.

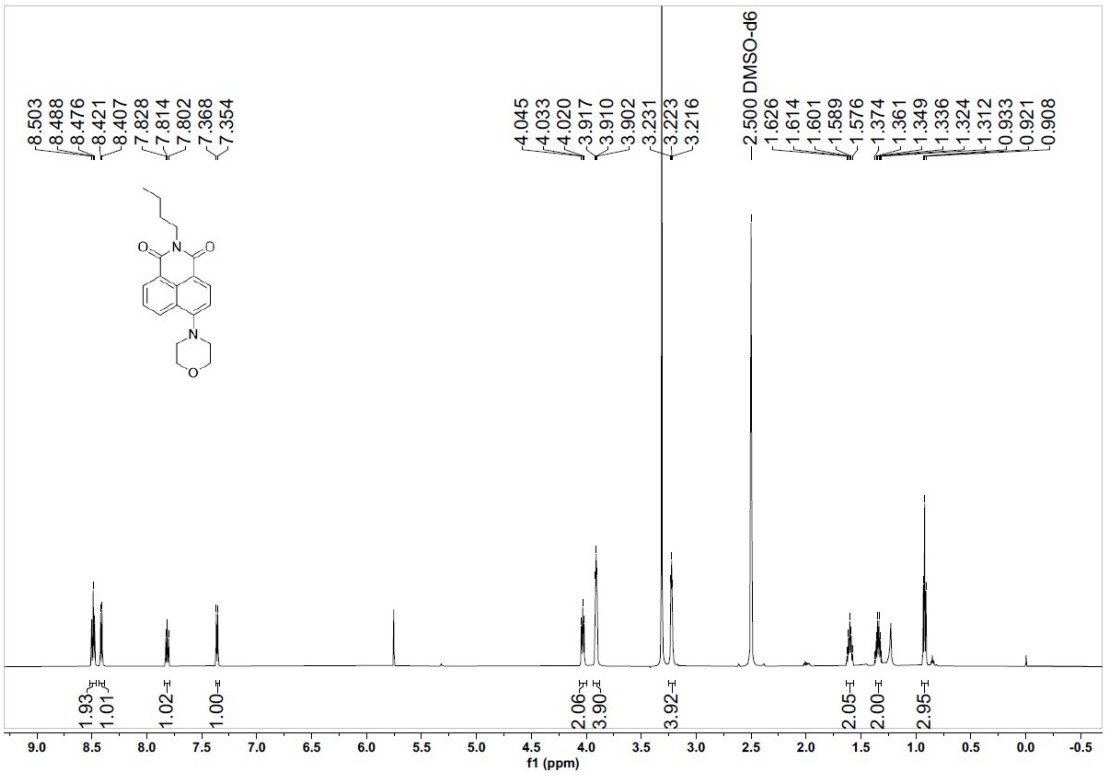

Figure S57. ^{1}H NMR Spectra of **Mor-NI-Bu** (600 MHz).

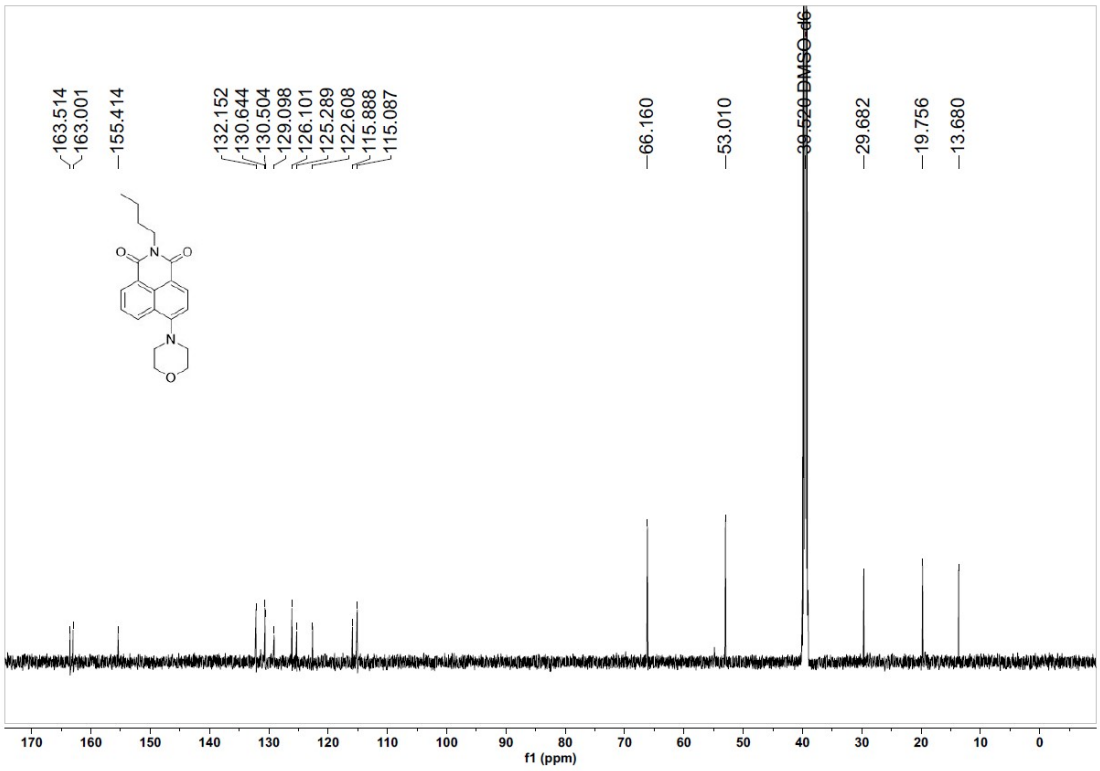

Figure S58. ^{13}C NMR Spectra of **Mor-NI-Bu** (151 MHz).

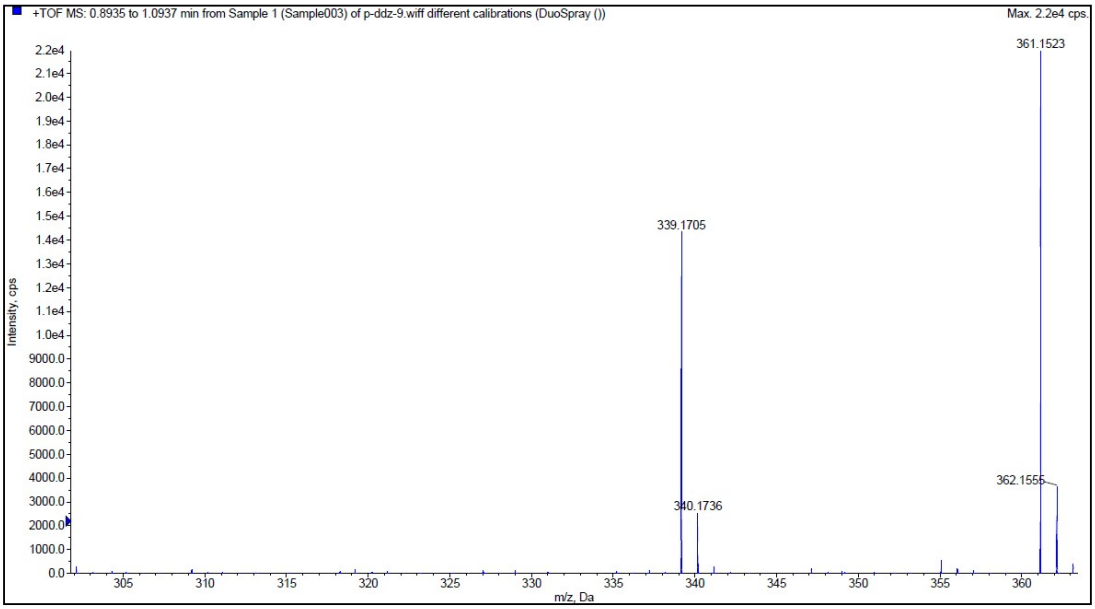

Figure S59. MS spectra of **Mor-NI-Bu**.

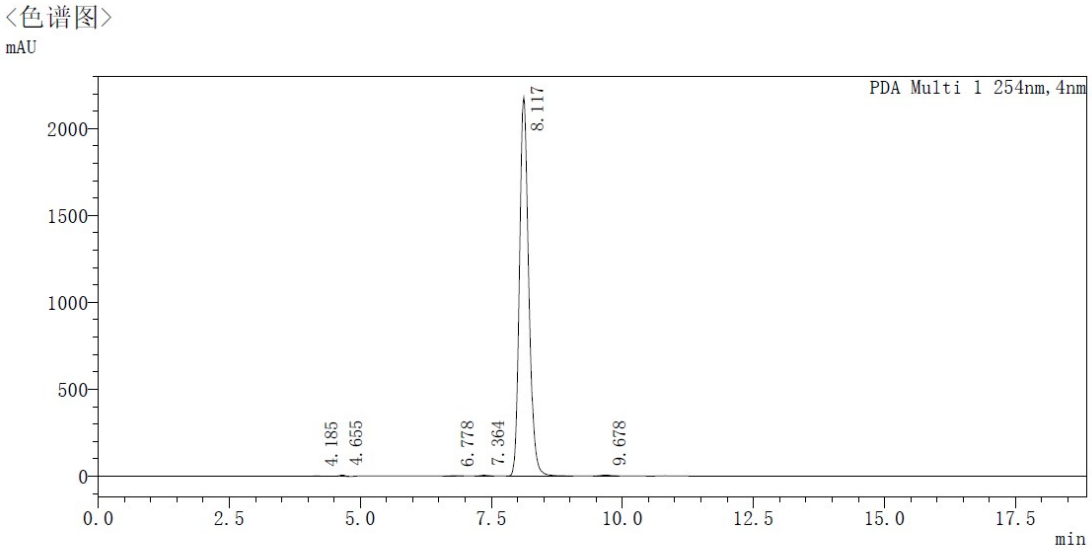

峰表

PDA Ch1 254nm

峰号	保留时间	面积	面积%
1	4.185	9353	0.035
2	4.655	41173	0.153
3	6.778	20222	0.075
4	7.364	44302	0.165
5	8.117	26738918	99.342
6	9.678	62118	0.231
总计		26916087	100.000

Figure S60. HPLC analysis of **Mor-NI-Bu**.

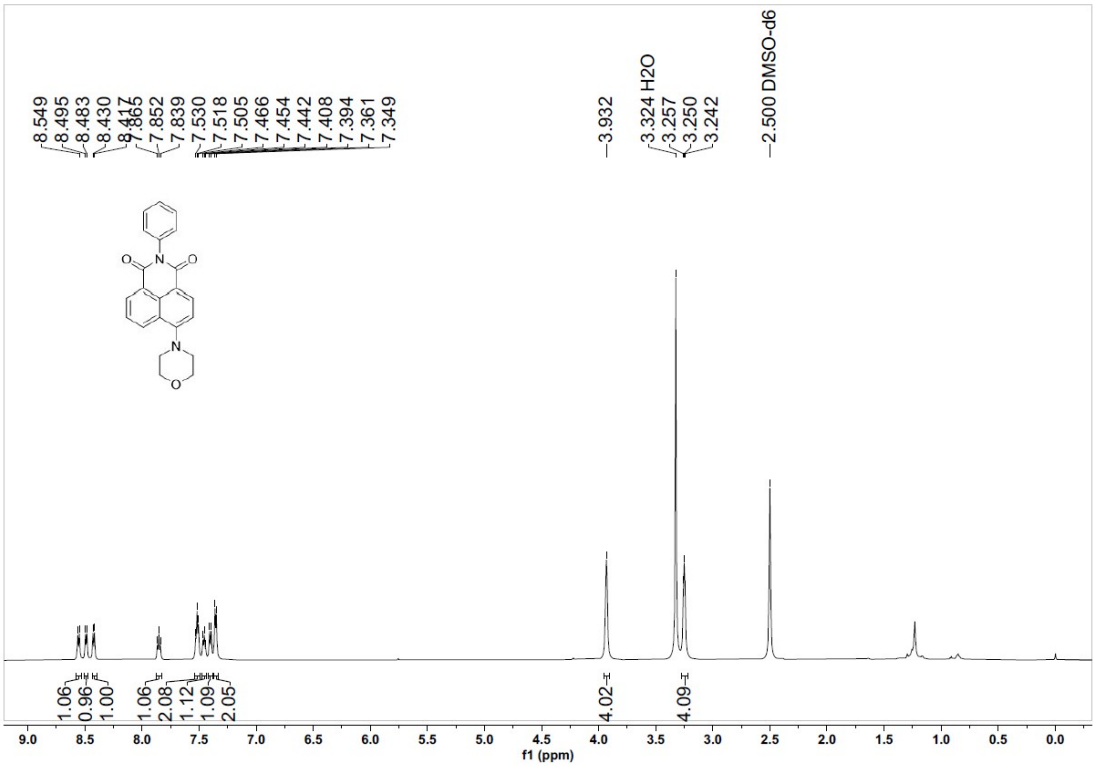

Figure S61. ^{1}H NMR Spectra of **Mor-NI-Ph** (600 MHz).

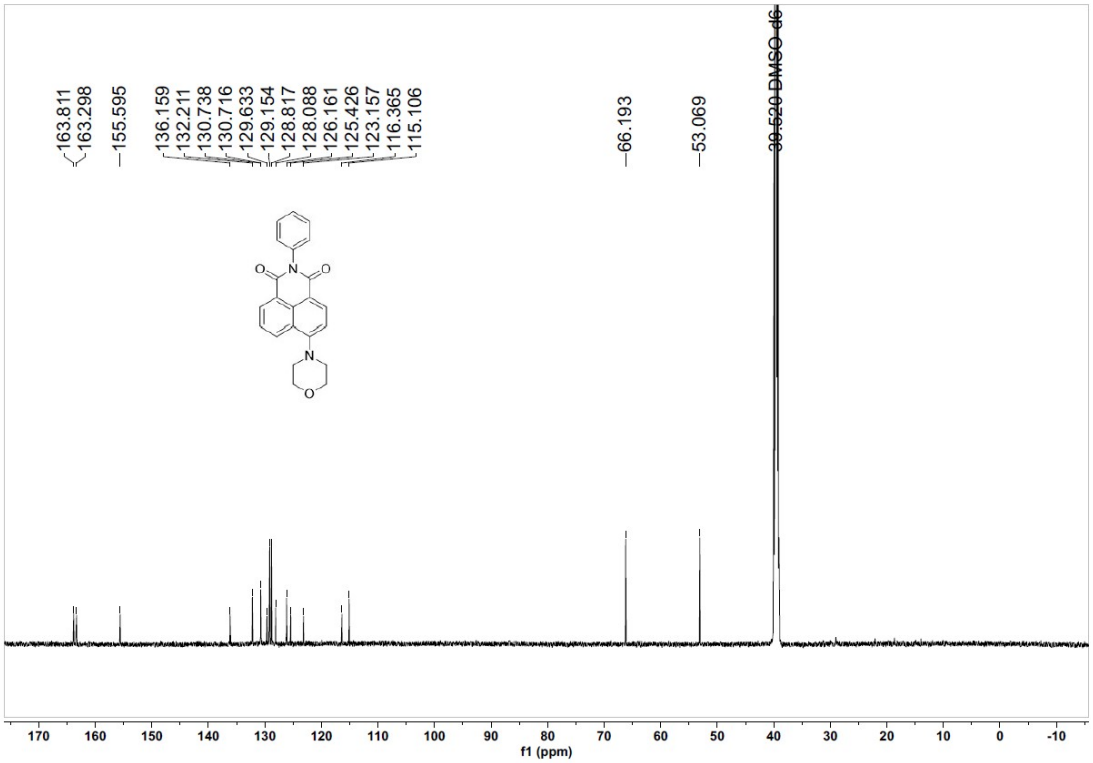

Figure S62. ^{13}C NMR Spectra of **Mor-NI-Ph** (151 MHz).

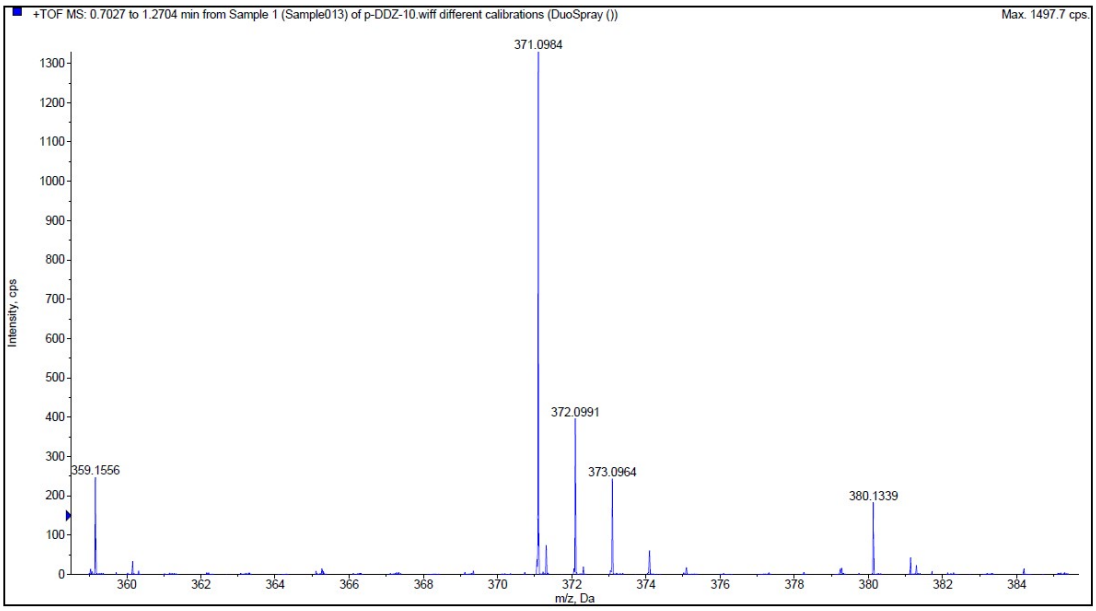

Figure S63. MS spectra of **Mor-NI-Ph**.

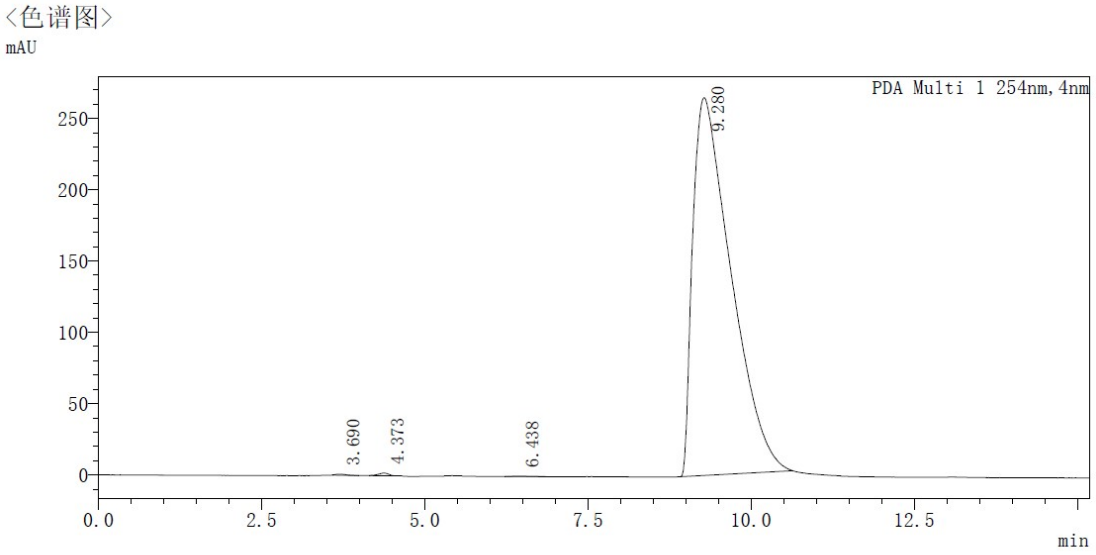

峰表

PDA Ch1 254nm

峰号	保留时间	面积	面积%
1	3.690	8029	0.074
2	4.373	20252	0.187
3	6.438	4541	0.042
4	9.280	10783785	99.697
总计		10816608	100.000

Figure S64. HPLC analysis of **Mor-NI-Ph**.

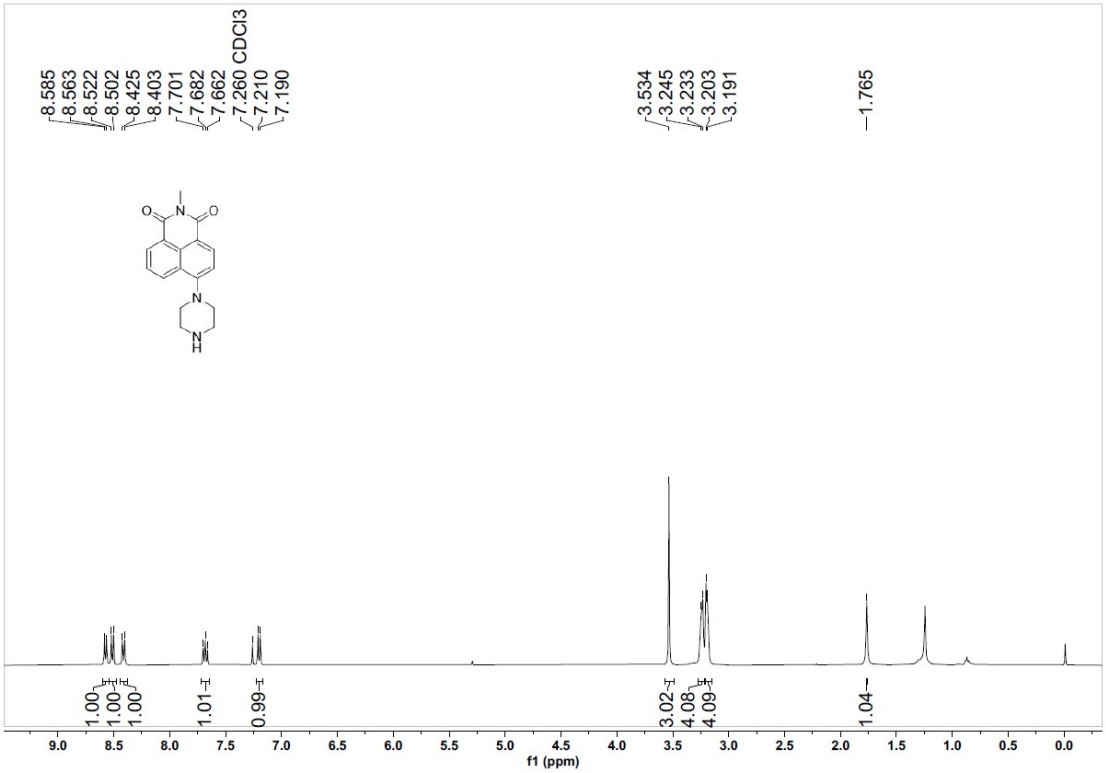

Figure S65. ^{1}H NMR Spectra of **Pip-NI-Me** (400 MHz).

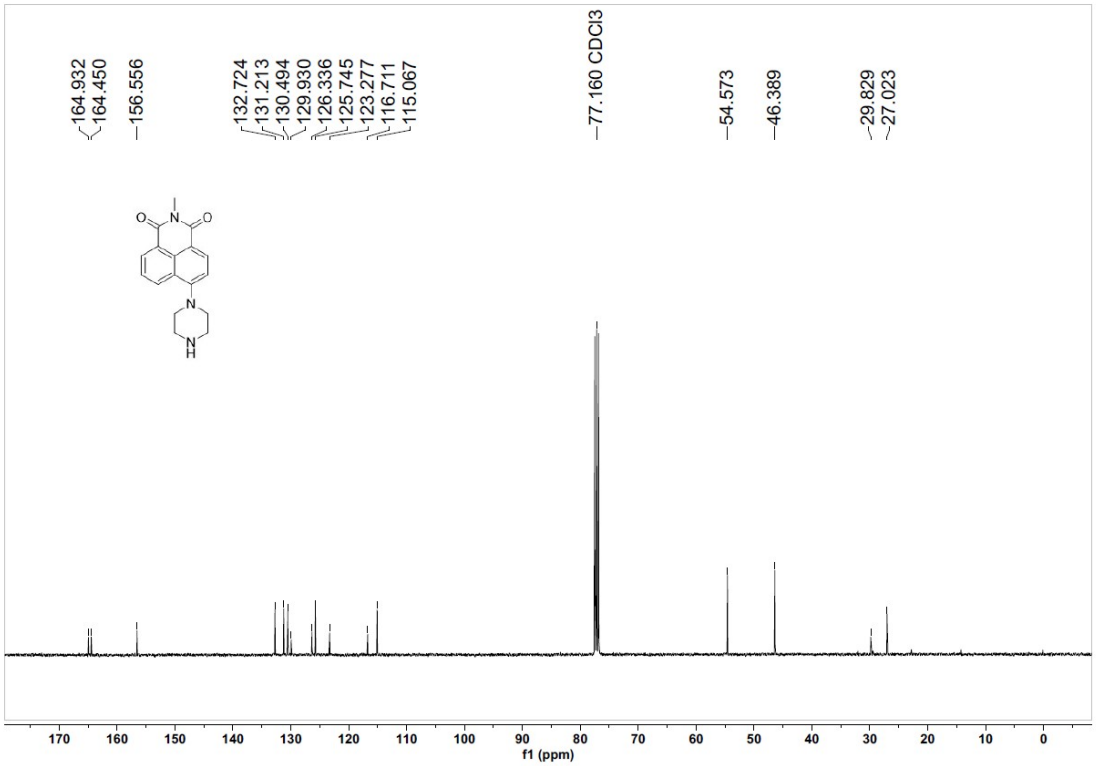

Figure S66. ^{13}C NMR Spectra of **Pip-NI-Me** (101 MHz).

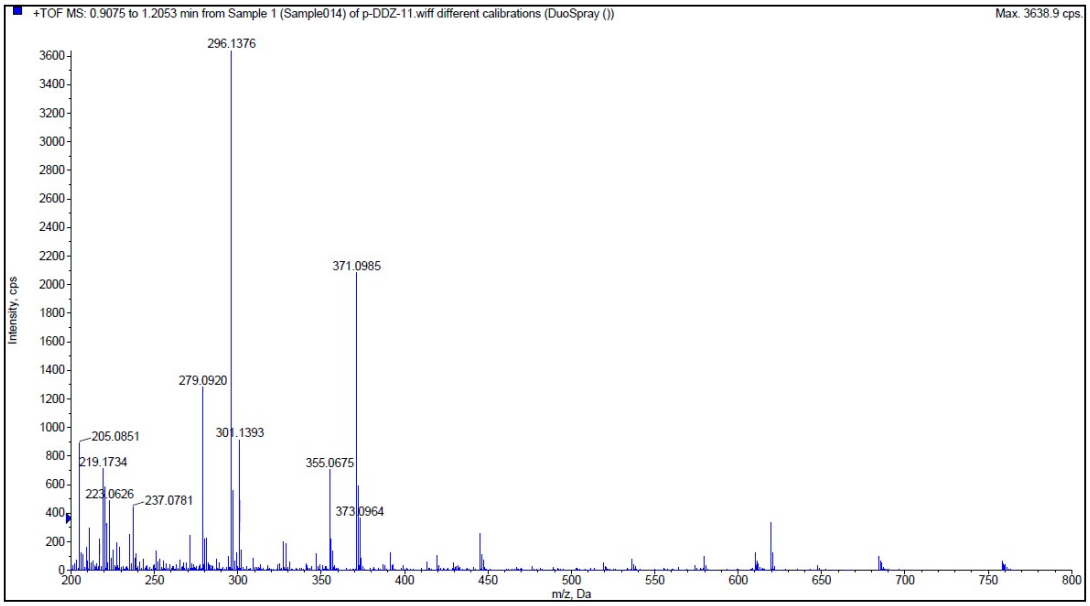

Figure S67. MS spectra of **Pip-NI-Me**.

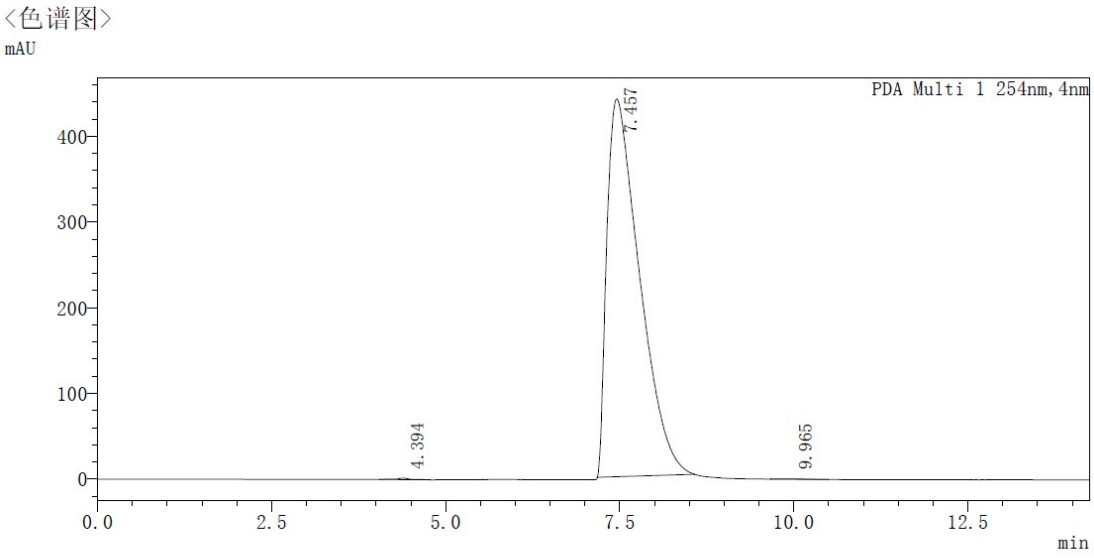

峰表

PDA Ch1 254nm

峰号	保留时间	面积	面积%
1	4.394	24325	0.169
2	7.457	14356535	99.751
3	9.965	11559	0.080
总计		14392419	100.000

Figure S68. HPLC analysis of **Pip-NI-Me**.

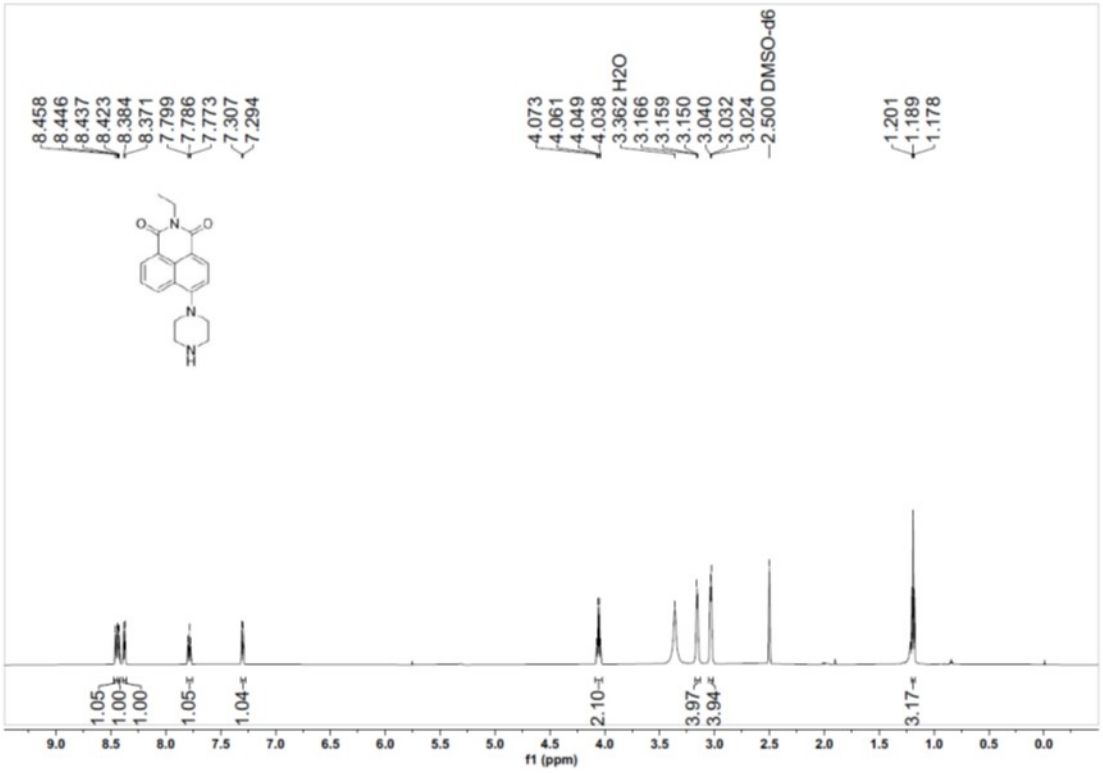

Figure S69. ^{1}H NMR Spectra of **Pip-NI-Et** (600 MHz).

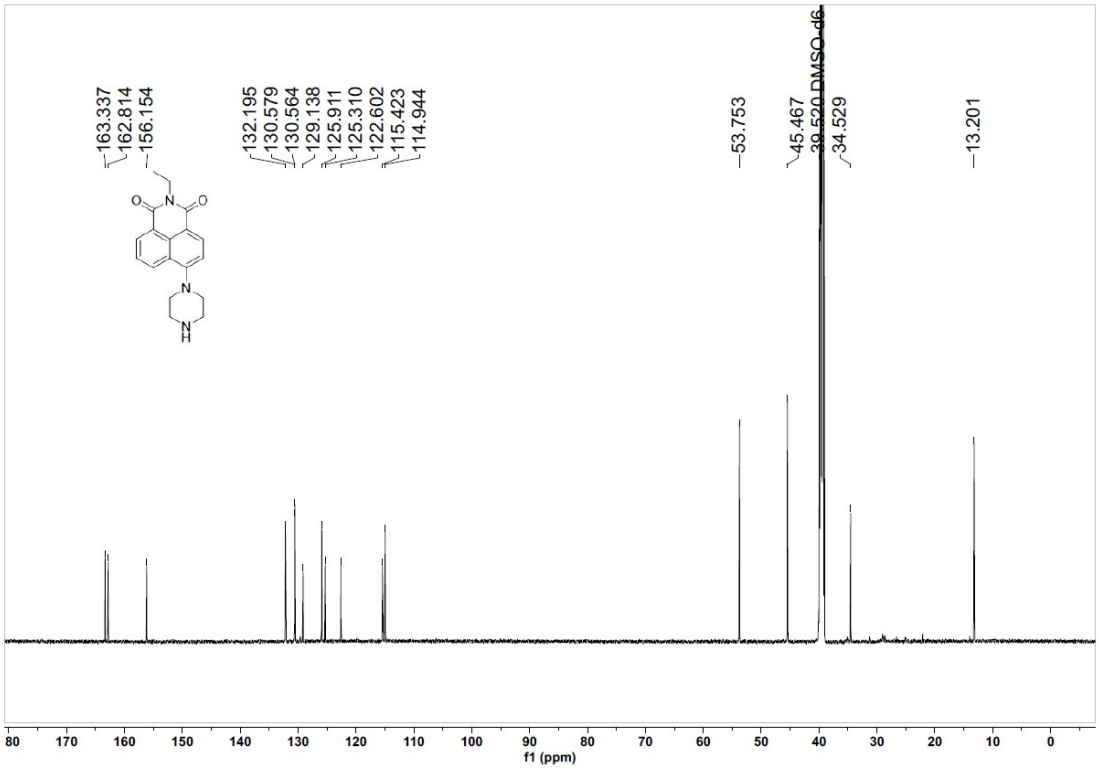

Figure S70. ^{13}C NMR Spectra of **Pip-NI-Et** (151 MHz).

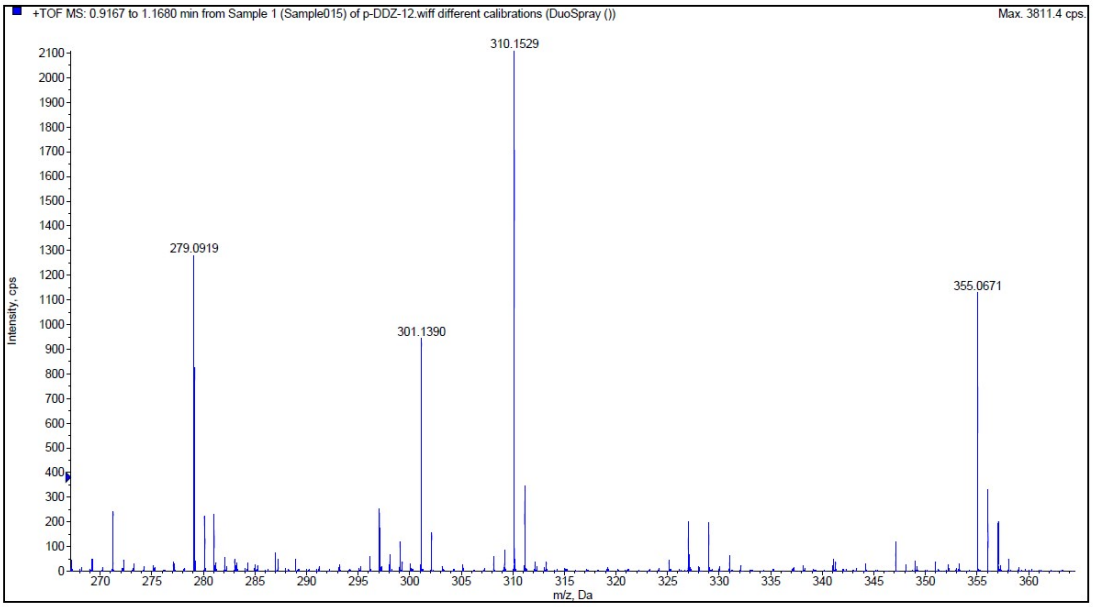

Figure S71. MS spectra of **Pip-NI-Et**.

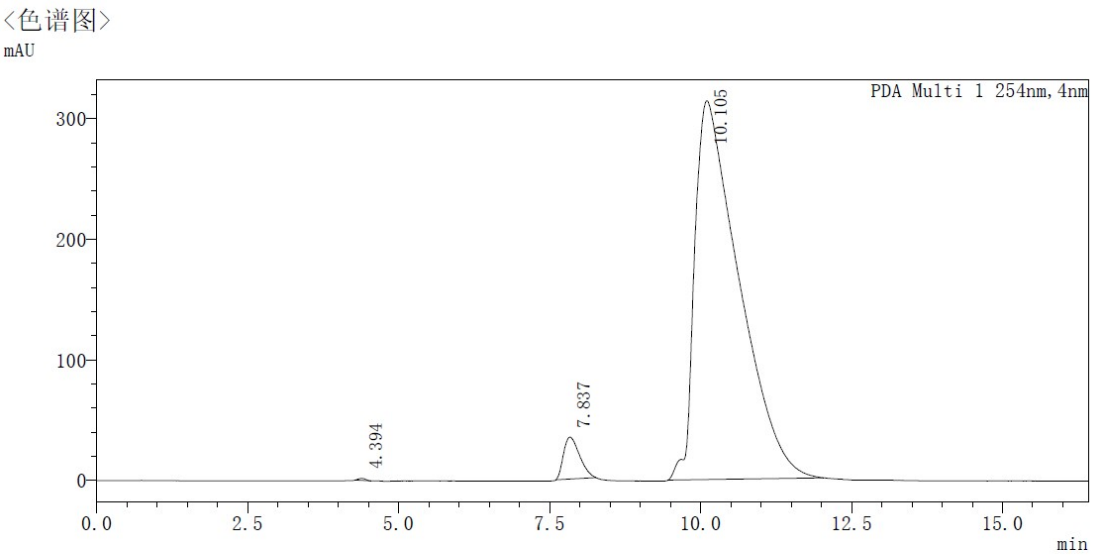

峰表

PDA Ch1 254nm

峰号	保留时间	面积	面积%
1	4.394	12874	0.077
2	7.837	642035	3.849
3	10.105	16024929	96.074
总计		16679838	100.000

Figure S72. HPLC analysis of **Pip-NI-Et**.

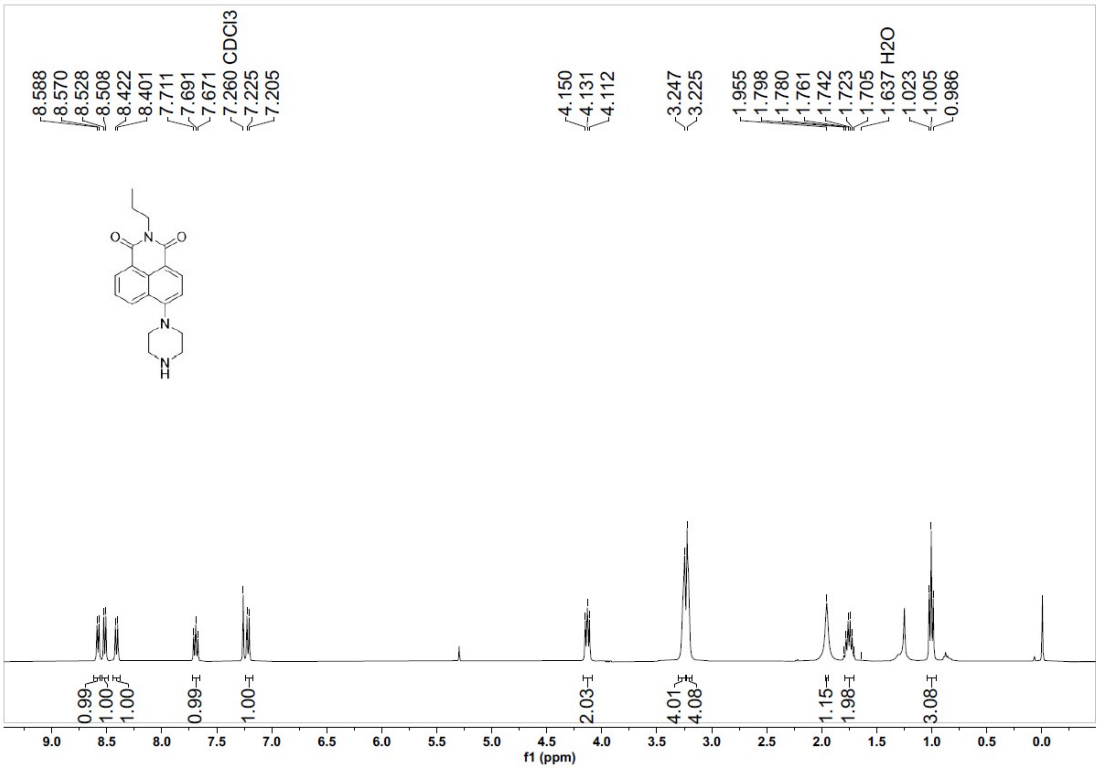

Figure S73. ^{1}H NMR Spectra of **Pip-NI-Pro** (400 MHz).

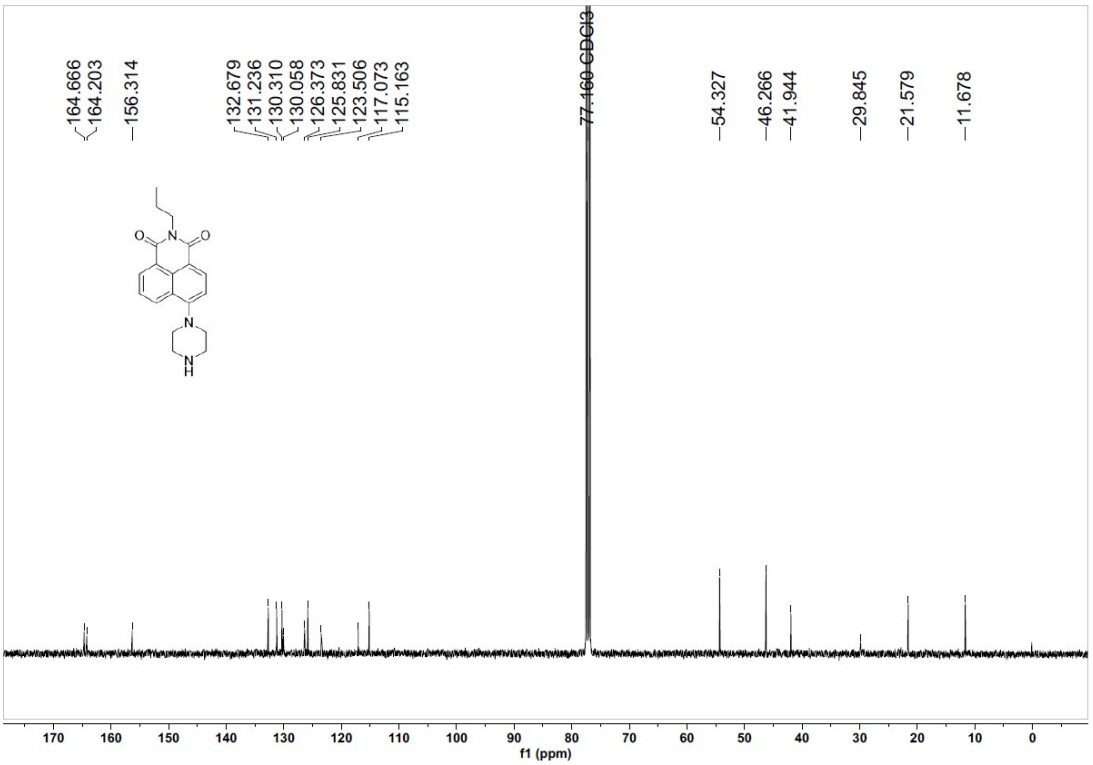

Figure S74. ^{13}C NMR Spectra of **Pip-NI-Pro** (101 MHz).

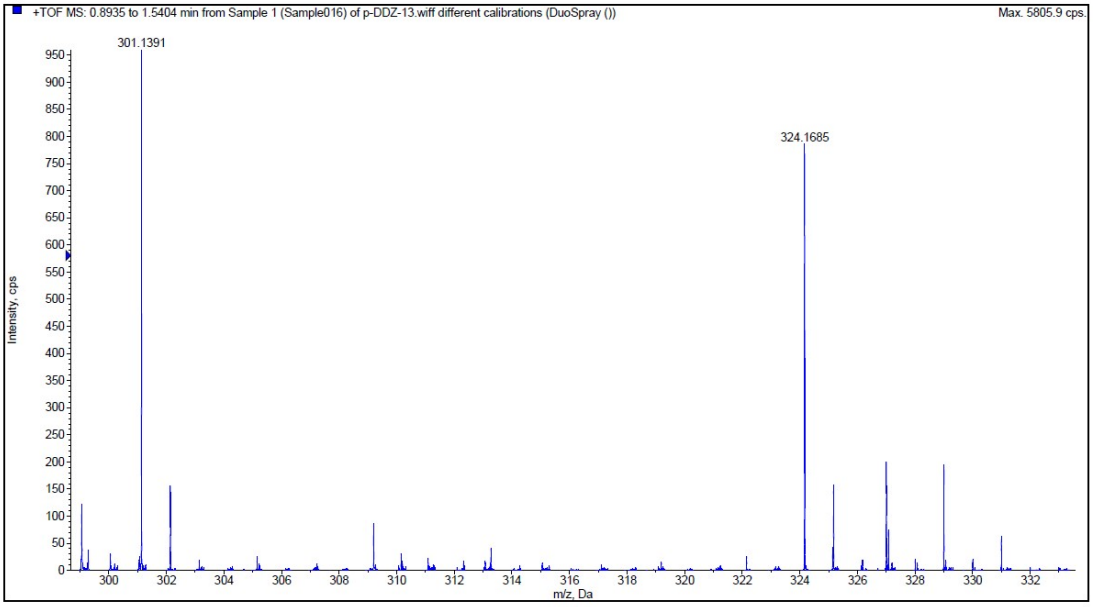

Figure S75. MS spectra of **Pip-NI-Pro**.

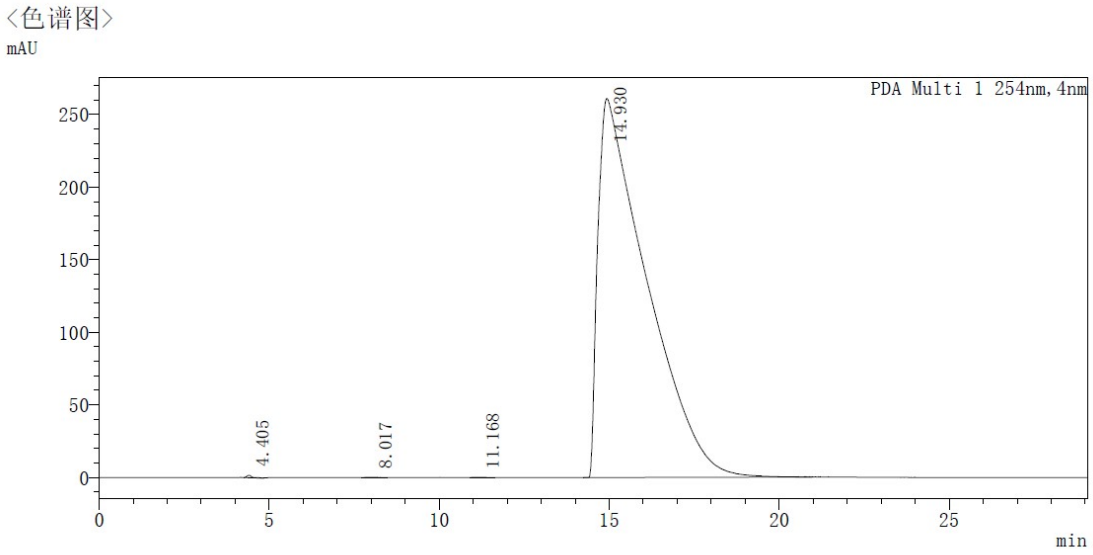

峰表

PDA Ch1 254nm

峰号	保留时间	面积	面积%
1	4.405	14568	0.056
2	8.017	5237	0.020
3	11.168	3836	0.015
4	14.930	26013442	99.909
总计		26037082	100.000

Figure S76. HPLC analysis of **Pip-NI-Pro**.

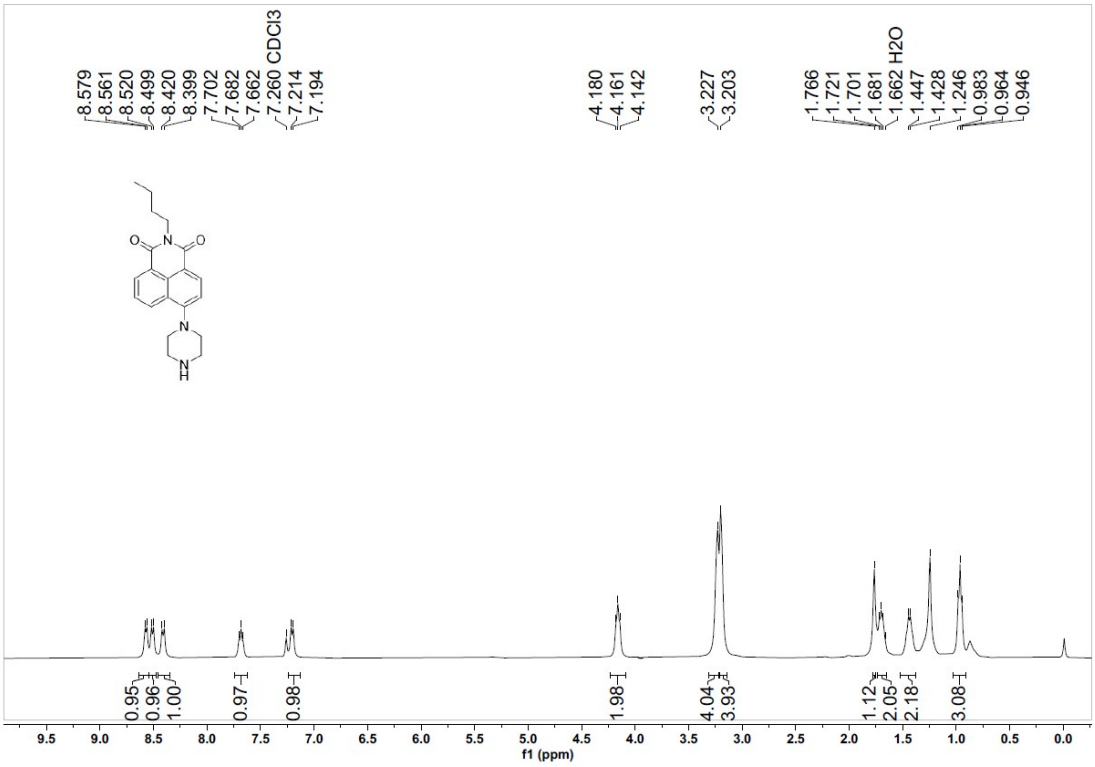

Figure S77. ^{1}H NMR Spectra of **Pip-NI-Bu** (400 MHz).

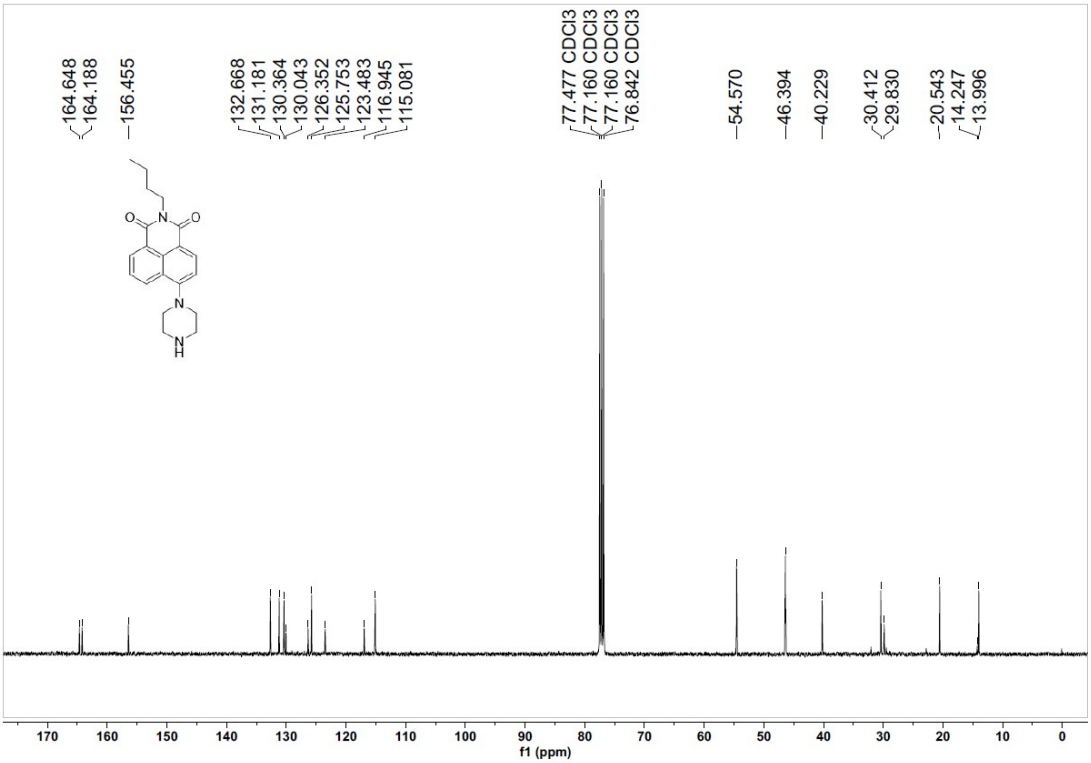

Figure S78. ^{13}C NMR Spectra of **Pip-NI-Bu** (101 MHz).

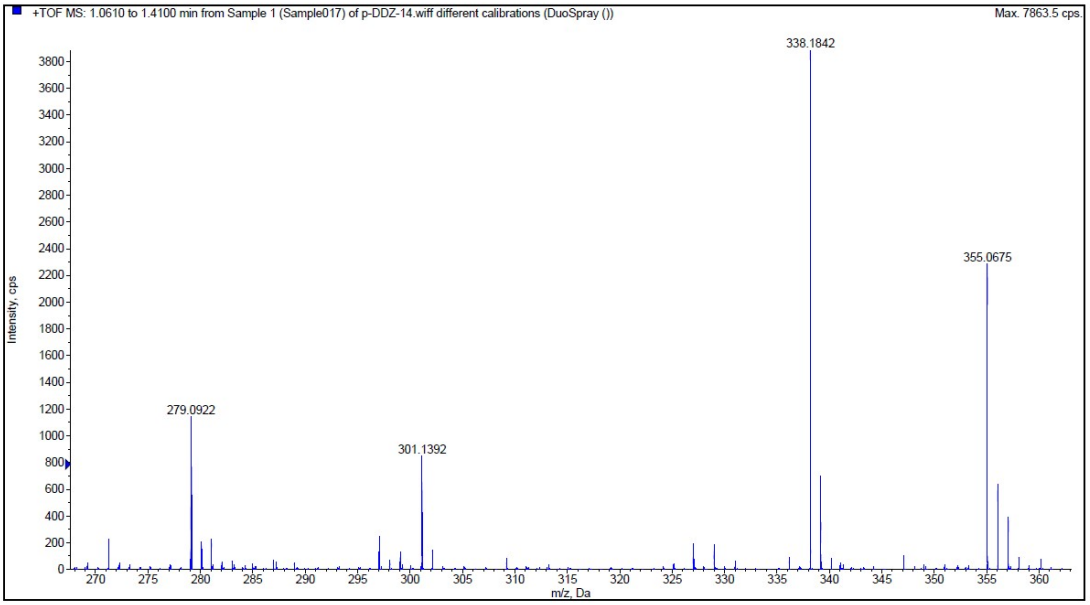

Figure S79. MS spectra of **Pip-NI-Bu**.

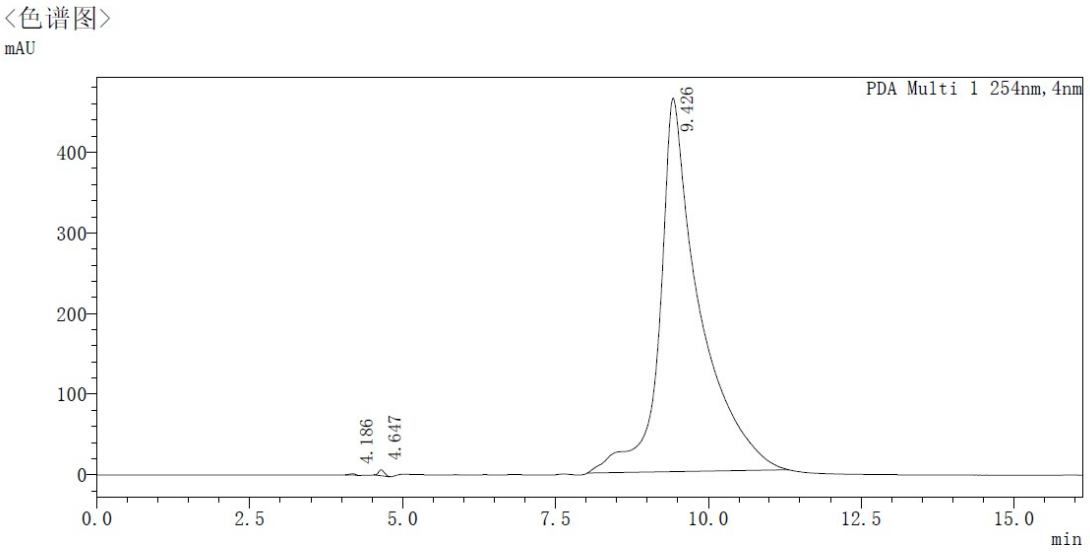

峰表

PDA Ch1 254nm

峰号	保留时间	面积	面积%
1	4.186	10845	0.052
2	4.647	48577	0.231
3	9.426	20988114	99.718
总计		21047537	100.000

Figure S80. HPLC analysis of **Pip-NI-Bu**.

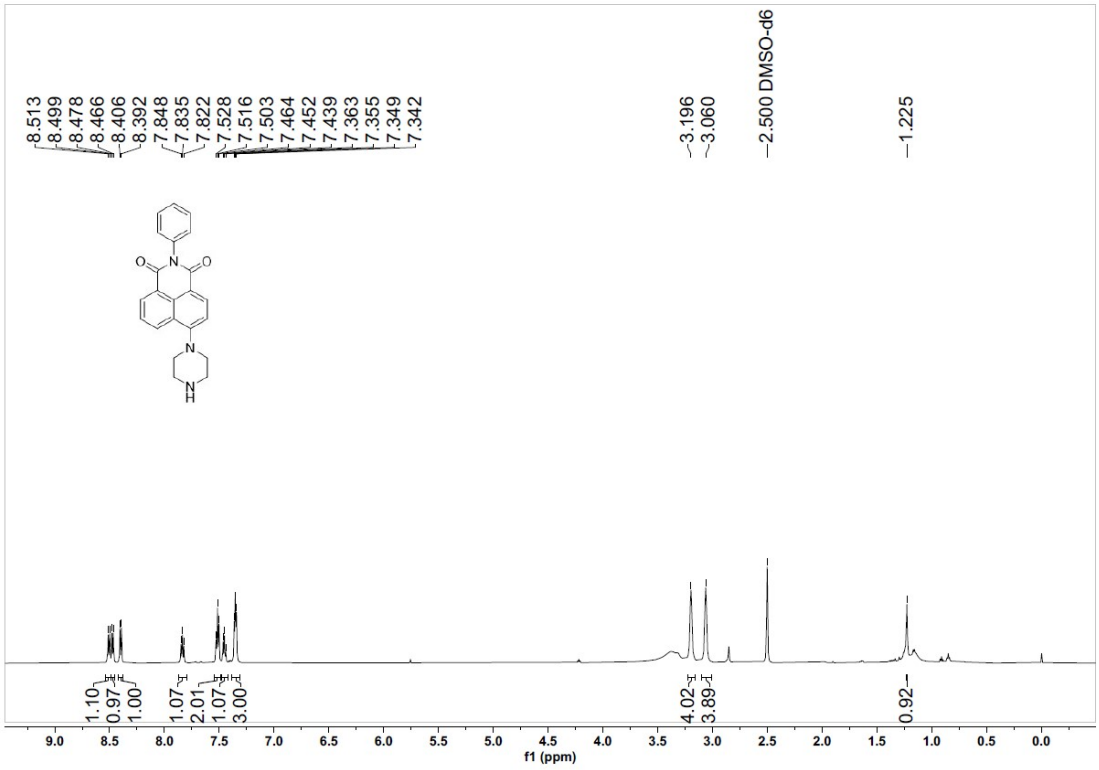

Figure S81. ^{1}H NMR Spectra of **Pip-NI-Ph** (600 MHz).

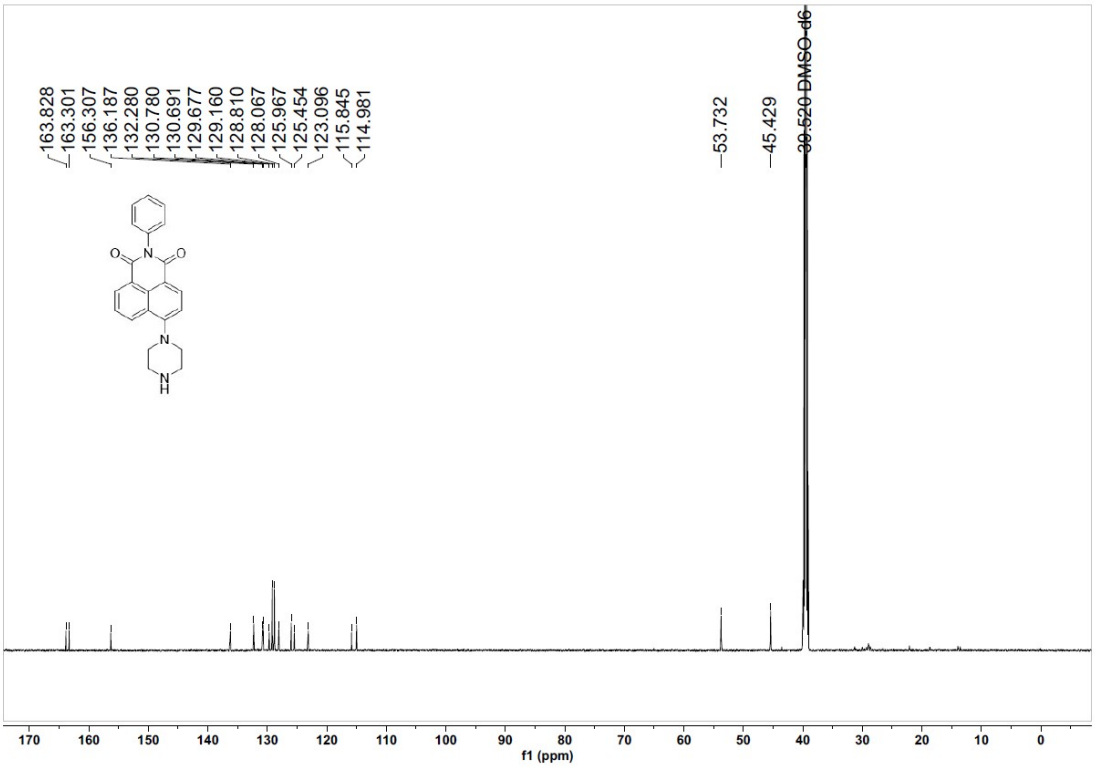

Figure S82. ^{13}C NMR Spectra of **Pip-NI-Ph** (151 MHz).

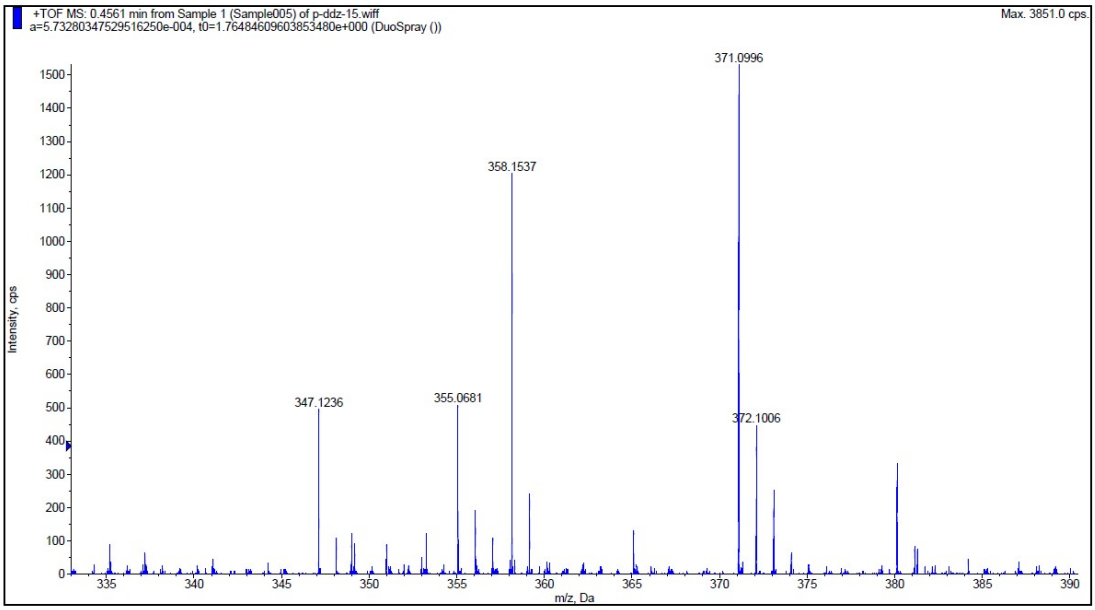

Figure S83. MS spectra of **Pip-NI-Ph**.

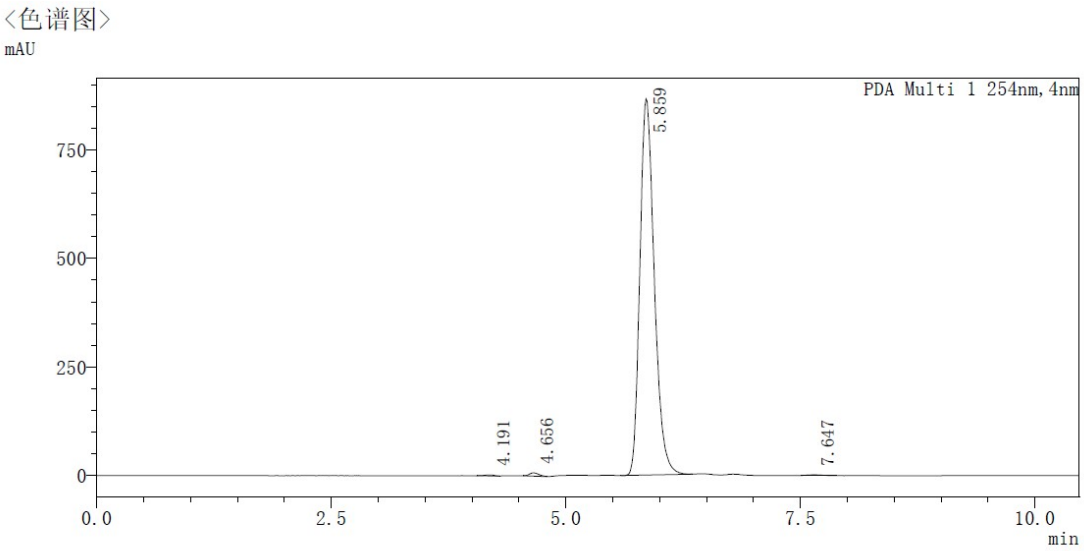

峰表

PDA Ch1 254nm

峰号	保留时间	面积	面积%
1	4.191	13942	0.149
2	4.656	49138	0.526
3	5.859	9256016	99.130
4	7.647	18137	0.194
总计		9337233	100.000

Figure S84. HPLC analysis of **Pip-NI-Ph**.

4. References

1 L. Lutkus, S. Rickenbach and T. McCormick, *Journal of Photochemistry and Photobiology A: Chemistry*, 2019, **378**, 131-135.

2 Y. Liu, D. Duan, J. Yao, B. Zhang, S. Peng, H. Ma, Y. Song and J. Fang, *Journal of Medicinal Chemistry*, 2014, **57**, 5203-5211.

3 J. Xi, L. Tian, J. Xi, D. Girimpuhwe, C. Huang, R. Ma, X. Yao, D. Shi, Z. Bai, Q. X. Wu and J. Fang, *Journal of Agricultural and Food Chemistry*, 2022, **70**, 15763-15775.

4 B. Zhang, D. Duan, C. Ge, J. Yao, Y. Liu, X. Li and J. Fang, *Journal of Medicinal Chemistry*, 2015, **58**, 1795-1805.

5 J. Zhang, Y. Chen and J. Fang, *Free Radical Biology & Medicine*, 2022, **186**, 99-109.

6 Z. Song, J. Zhang, Q. Xu, D. Shi, X. Yao and J. Fang, *Journal of Medicinal Chemistry*, 2021, **64**, 16132-16146.

7 W. Mi, H. Guan, J. Lyu, D. Zhao, Y. Xi, S. Jiang, F. Andrews, X. Wang, M. Gagea, H. Wen, L. Tora, S. Dent, T. Kutateladze, W. Li, H. Li and X. Shi, *Nature Communications*, 2017, **8**, 1088.

8 Y. Jiang, S. Huang, H. Ma, J. Weng, X. Du, Z. Lin, J. Kim, W. You, H. Zhang, D. Wang, J. Kim and H. Sun, *Journal of the American Chemical Society*, 2024, **146**, 25270-25281.